Anion binding host systems based on calix[4]arenes and nanoparticles

Filby, Maria .

Anion binding host systems based on calix[4]arenes and nanoparticles

A thesis submitted for the partial fulfilment of the requirements for the Degree of

Doctor of Philosophy

In the faculty of Science of

Durham University

by

Maria H. Filby

Durham University

Department of Chemistry

University Science Laboratories

South Road

Durham

2007

Acknowledgements

I would like to thank everyone directly and indirectly involved in this project. In particular I would like to express my enormous gratitude to Prof. Jonathan Steed for his outstanding supervision, support and encouragement. The last three years have been a wonderful experience of excitements and disappointments.

I would like to thank our collaborators: Dr. Martin Paterson of Heriot Watt University for the DFT calculations, Prof. Luca Prodi of Universtiy of Bologna for the photophysical measurements, Drs. Ritu Kataky and Jaanus Kruusma of Durham University for potentiometric titrations data.

Life in the laboratory could not be the same without all the group members both past (Dave Turner and Aled Jones), and present (Sara-Jane Dixon, Joe Lenthall, Charlotte Willans, Kirsty Anderson, Peter Byrne, Naseem-ul-Ghani Quresh and Adam Todd) to whom all my special thanks go.

I am also very grateful to all of the technical support staff of Durham University, particularly Katherine Heffernan, Ian McKeag and Dr. Alan Kenwright from the liquid state NMR, Dr. Michael Jones and Lara Turner from mass spectrometry , Judith Magee and Jarika Dostal from the analytical service.

I would also like to thank Dr. Karl Coleman of Durham University for his very useful advice on gold nanoparticles.

Finally I would like to thank my family, particularly my mother who has been tremendously helpful and supportive in difficult times.

Chapter 4

Experimental

Abbreviations

CTV Cyclotriveratrylene

UV- Vis Ultraviolet visible

IR infrared

DMSO Dimethyl sulfoxide

DABCO Diazabicyclooctane

NMR nuclear magnetic resonance

TBA tetra-n-butyl ammonium

DFT density functional theory

PET photoinduced electron transfer

PCT photoinduced charge transfer

VT variable temperature

SPP Sovent polarity/polarizability scale

DPPE 1,2-Bis(diphenylphosphino)ethane

GNP gold nanoparticles

NP nanoparticles

SPB surface plasmon band

TOAM tetraoctylammonium bromide

TEM transmission electron microscopy

EPR electron paramagnetic resonance

DHLA dihydrolipoic acid

XANES X-ray absorption near edge structure spectroscopy

GPC gel permeation chromatography

DCCI (3-dimethylamino-propyl)-ethyl-carbodiimide

HOBt (hydroxybenzatriazole hydrate)

Abstract

A range of novel host molecules with various degrees of pre-organisation for the supramolecular complexation of anionic guest species have been synthesized. Both organic core and nanoparticle-based derivatives of the ligands have been prepared and the properties of the new host ligands studied with particular reference to their anion binding behaviour.

Two types of calix[4]arene derived cationic hosts for anions with, respectively, 1,3-alternate and cone conformations have been prepared. The affinity of the tetrasubstituted calix[4]arene hosts for a variety of anions has been probed with ^{1}H NMR spectroscopic titration. The 1,3-alternate system binds dicarboxylate anions in a ditopic manner while the cone compounds have the highest affinity for bromide anion and are deprotonated by carboxylates.

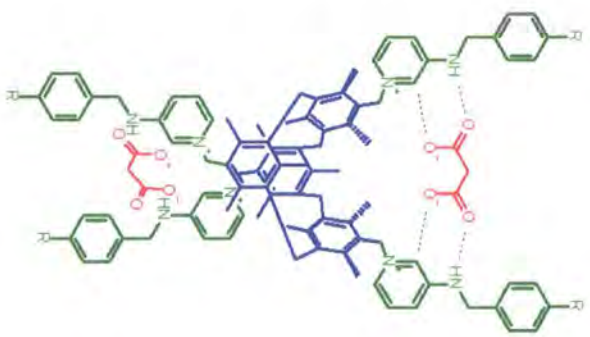

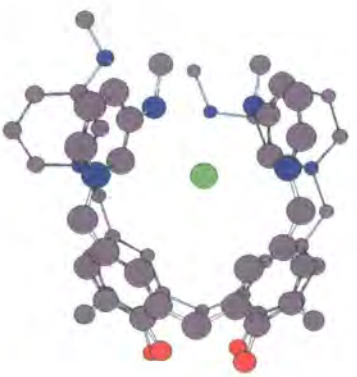

The potentially fluorescent 1,3-alternate calix[4]arene that contains a pyridinium functionality coupled *via* a methylene spacer to a pyrene group undergoes selective chloride-induced conformational change which results in strong increase in both monomer and excimer emission.

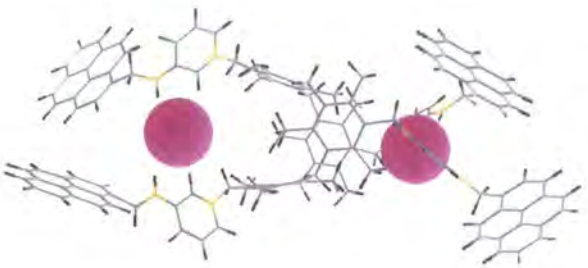

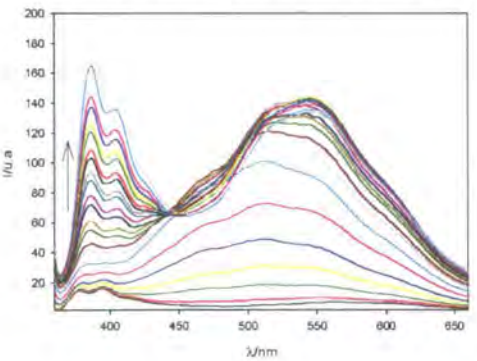

Gold nanoparticles protected with 5-[1,2]dithiolan-3yl-pentanoic acid pyridin-3-ylamide remain stable as colloidal solution in methanol and the UV aborption spectra demonstrate the nanoparticles' response to exposure of a variety of anions by red shift with concomitant decrease in intensity. Titration of the colloidal solution with silver tetrafluoroborate results in an increase in absorption indicating possible interaction of silver cations with the pyridyl nitrogen atoms

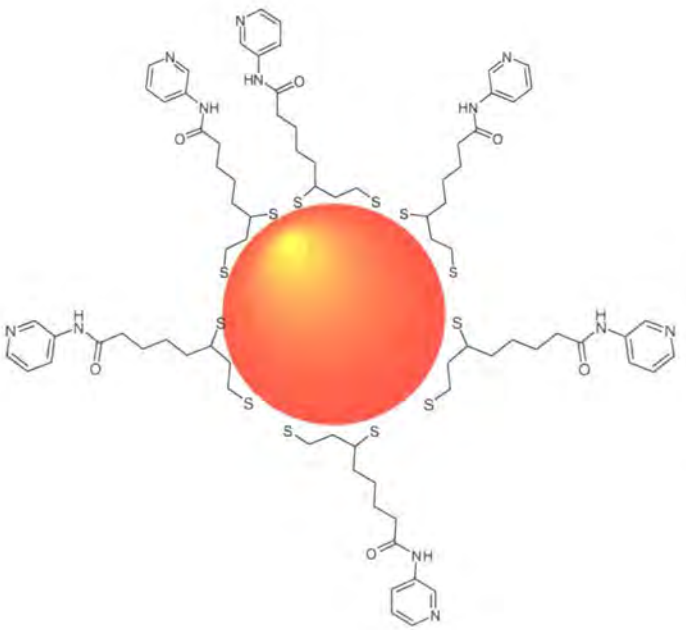

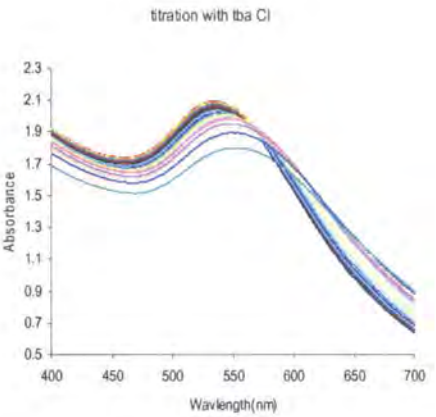

Chapter 1

General Introduction

1.1 Supramolecular Chemistry of Anions

Anion binding continues to attract growing interest among supramolecular chemists.[1-10] There is a very considerable range of possible applications of synthetically created hosts with affinities and selectivities that rival biological anion receptors,[11] particularly in a sensing context,[12] either using colourimetric methods or in systems with appended redox-active or fluorescent groups.[13-25] Attachment of anion binding groups to nanoparticles also offers a novel alternative sensing paradigm.[26] In addition, there is considerable current interest in anion transport, particularly chloride because of its biological relevance.[27, 28]

Anion binding hosts may be broadly classed as either cationic or neutral. In general, positively charged hosts offer scope for obtaining the largest binding constants. However, due to the non-directional and non-selective nature of electrostatic interactions, cationic hosts[29] are generally modulated by adding hydrogen bonding moieties. Charged hosts must also have an associated counter-anion, just as the target guest must have a counter-cation, therefore a competition situation is created which must be engineered to lie in favour of the host-guest complex. Neutral hosts[30, 31] rely solely upon the correct orientation of hydrogen-bonding or Lewis acid groups to bind guests, therefore if the fit is not exact the binding can be weak and similarly suffer from potential interference from the counter cation which is necessarily bound along with the anion.

The hydrogen bond is arguably the most important non-covalent interaction in the design of supramolecular systems, because of its strength and high degree of directionality.[32, 33] There are a number of naturally occurring building blocks that are rich sources of hydrogen bonding donors and acceptors, for example amino acids and nucleobases, and many have been incorporated into the design of anion binding hosts.[34, 35] Particularly effective donors are those in which the acidity of the donor hydrogen atom is amplified by the presence of adjacent electron-withdrawing groups. This effect occurs naturally in guanidinium system, ureas and amides. Hydrogen bond acidity may also be enhanced by remote substitution of electron withdrawing groups.[1,36] Irrespective of whether the host species is neutral or positively charged there remains a dependence upon dipole-based interactions to select and retain the guest species. Well positioned

directional interactions are essential for selectivity in such systems. Although not as strong as coordination interactions, a cumulative effect may be obtained leading to comparable binding strengths to those achieved by cation receptors in many instances.

Anion binding hosts may also be divided on the basis of their flexibility or degree of preorganisation. If the host does not undergo a significant conformational change upon guest binding it is said to be preorganised.[37] Host preorganisation is a key concept because it represents a major contribution to the overall free energy of guest complexation. During the binding process the host undergoes conformational readjustment in order to arrange its binding sites in the fashion most complementary to the guest and at the same time minimising unfavourable interactions between one binding site and another on the host. Rigidly pre-organised hosts such as anion binding cryptands[38] may quite often have high complexation activation energy and tend to exhibit slower guest binding kinetics. In contrast, conformationally mobile hosts are able to adjust rapidly to changing conditions and both complexation and decomplexation are usually fast. Although generally having less intrinsic affinity for their guest than conformationally rigid molecules, flexible hosts are potentially more useful receptors in sensing applications because of their fast response times, reversible binding and the possibility of detecting binding by means of the altered conformation.[13, 16, 20, 25, 39, 40]

The vast majority of both macrocyclic and podand anion receptors are organic compounds. Work by Beer and co-workers amongst others has resulted in a parallel body of receptors based on ferrocene, cobaltocinium, dithiocarbamate, metalloporphyrin and tris(bipyridyl)ruthenium and rhenium derived coordination compounds,[13, 41-51] all of which incorporate substitutionally inert metal centres. In the mid 1990's Steed and Atwood reported a range of calixarene and CTV-derived organometallic bowl shaped receptors.[8, 42, 52-54] More recently, parallel work by Loeb and Gale and by Steed among others has seen the introduction of more labile coordination complex anion hosts. Such systems have the potential advantage of self-assembling under anion templated conditions and can prove to be highly synthetically efficient.[24, 42, 55-59]

1.2 Pinwheel Hosts

A very elegant design introducing an array of guanidinium group functionalities situated around an aryl core was reported by Anslyn and co-workers in 1997,[60] producing a cavity that is functionalised with three hydrogen bond donor moieties in order to bind tricarboxylate anions such as citrate. The host-guest interaction is enhanced by positive charge on the guanidinium side arm.

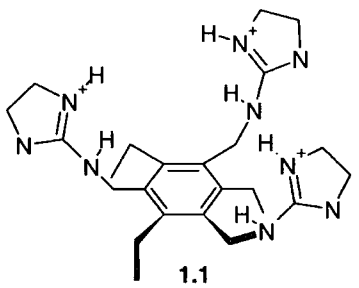

1.1

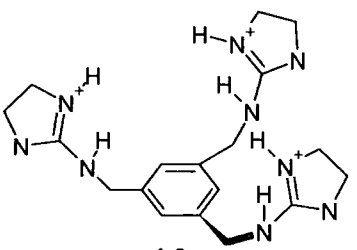

1.2

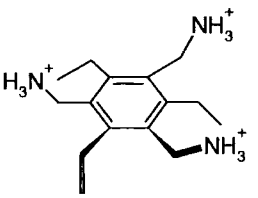

1.3

Preorganisation is achieved by incorporating these recognition groups into a trisubstituted 1,3,5-triethylbenzene core, generating a cone shape cavity where all three guanidinium arms protrude in one direction.[60] The introduction of steric bulk around the benzene-derived core predisposes the compound to adopt the preferred conformation by 3.5 kcal mol^{-1} in similar systems.[60] The concept has also been used in cation-binding hosts.[9, 61, 62] Compound **1.1** binds citrate with an association constant of $7x10^3$ M^{-1} in aqueous solution. This value is much higher than for control compounds, either without the ethyl substituents (**1.2**) to test the advantage of preorganisation, or functionalised with ammonium groups (**1.3**) to emphasize the significance of the multi-point hydrogen bonding of the guanidinium groups with the carboxylate units. However, in the presence of buffer the binding affinity of **1.1** for citrate drops by nearly two orders in magnitude. The decrease in binding of citrate probably arises due to competition from other anions present in the buffer. Anslyn has used this pinwheel core (for which improved syntheses are available[63, 64]) as the basis for a very broad range of anion hosts such as **1.4** including those containing metal centres such as **1.5**. An array of such hosts attached to polystyrene beads form the basis for a fluorescent 'electronic tongue' able to distinguish certain beverage components or bioanalytes based on their recognition signature pattern as part of a dye displacement assay.[65-67] Parallel work by Kim and co-workers has used a similar core to produce a range of CH hydrogen bond donor systems such as **1.6** that also bind effectively to anions, for example K_a = 1.1x 10^6 for Cl^-

binding by **1.6** in 9:1 MeCN: DMSO. The electron withdrawing nitro groups enhance the hydrogen bond acidity of the imidazolium CH groups.[68] This work has recently been extended by Duan and co-workers to produce functionalised derivatives useful for anion sensing applications.[40] Also, Schmuck and co-workers recently introduced guanidinio-carbonyl pyrrole binding sites with a hexasubstituted aryl core to give receptor **1.7** [16, 69]

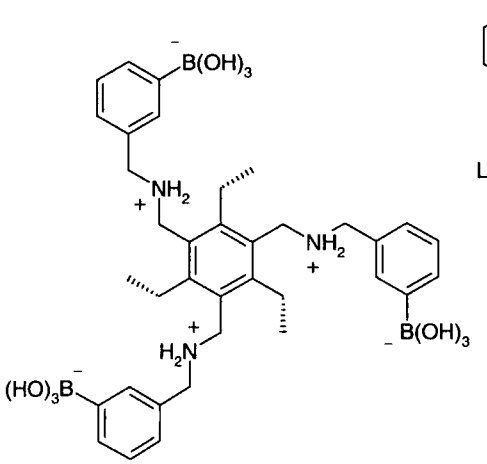

1.4

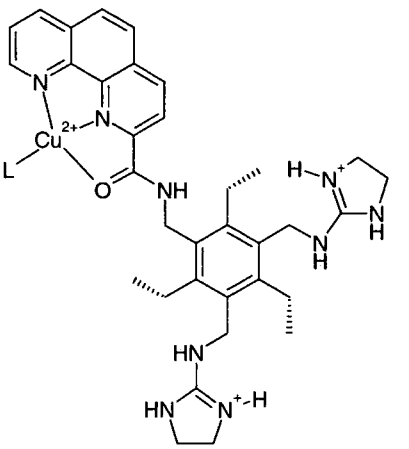

1.5

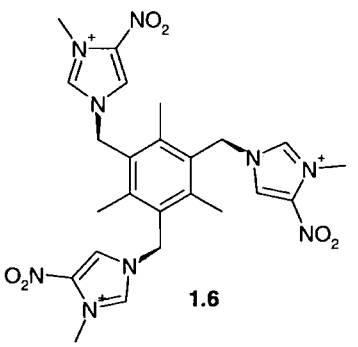

1.6

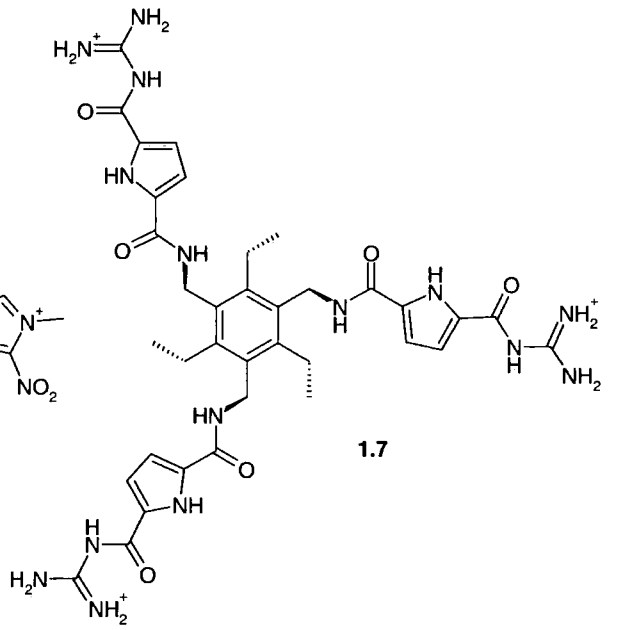

1.7

Host **1.7** contains acylated guanidinium groups which account for an increased acidity and the pyrrole amide provides an additional hydrogen bonding site. Binding between host **1.7** and carboxylates is much stronger as a result; association constants of 3.4×10^5 M^{-1} with trimesate and 1.6×10^5 M^{-1} with citrate were determined by UV-Vis spectroscopic titrations in 10% DMSO in water. These associations were confirmed by fluorescence titration in water which provided

constants of $K_a = 4.4x10^5$ M^{-1} and $2.3x10^5$ M^{-1}, respectively. Even in excess of bis-tris buffer and chloride, the binding constant for citrate only reduced to $8.6x10^4$ M^{-1}.

Garratt and co-workers, in part in collaboration with Steed group, have also examined the hexasubstituted benzene core, along with a naphthalene analogue, as the basis for a series of diazobicyclooctane (DABCO) hosts (**1.8** – **1.9**) designed to bind anions *via* electrostatic interactions.[70-73] One such tripodand (**1.8a**) can discriminate between the ferricyanide and ferrocyanide ions. An X-ray crystallographic study of the trication host with the ferricyanide trianion shows how the tripodand co-ordinates electrostatically to the anion, Figure 1.[73]

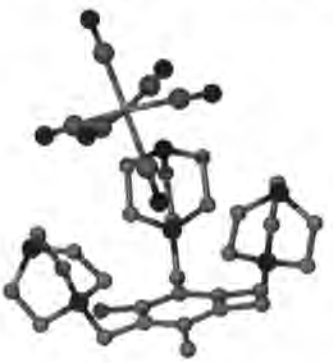

Figure 1 X-ray crystal structure of the 1:1 ferricyanide complex of receptor **1.8a**.

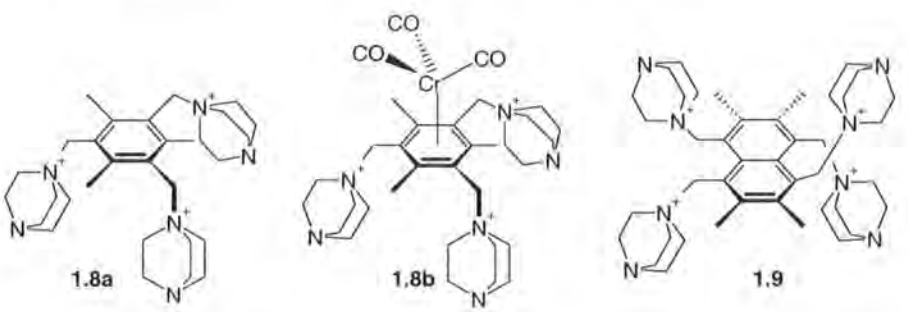

The presence of the $Cr(CO)_3$ group in the analogous tripodal species **1.8b** (and a 1,4-disubstituted analogue) as well as the three methyl substituents contributes to a marked degree of preorganisation around the core, forcing the DABCO arms to point in the same direction. ^1H NMR spectroscopic titration studies were carried out for **1.8a**·3Br$^-$ and **1.8b**·3Br$^-$ in D_2O. However, in the case of the non-complexed trication **1.8a** the binding constant with trimesate is considerably greater than for the complexed **1.8b**·3Br$^-$ (K_a = 776 M^{-1}), but the data are obtained from chemical shift changes of the anion in one case and for the host in the other which may

introduce experimental error. It was suggested that the blocking of access to one face of the host outweighs the preorganisation effect of the chromium tricarbonyl unit. The $Cr(CO)_3$ group also acts as an IR reporter group in the solid-state. The carbonyl bands of the IR spectrum in KBr of various salts of **1.8b**, namely bromide, iodide, citrate, tetrafluoroborate, hexafluorophosphate, triflate and trifluoroacetate, were recorded. An increase in ν_{CO} from halides to trifluoroacetate indicates the diminishing effectiveness in quenching the positive charge on the trimesate anion. It was also noted that IR frequencies reflected much better binding of the anion in organic solvents as water solvation properties effectively screen the polycationic host from the electron-donating effect of the guest. Acetonitrile and acetone solvents do not solvate the guest species as effectively and probably encourage tighter guest binding.[71]

Steed *et al.* began looking at organised electrostatic anion-binding cations in 1999 as a follow on from work on calixarene and cyclotriveratrylene based organometallic receptors.[8, 52-54, 74, 75] Thus reaction of 1,3,5-tris(bromomethyl)-2,4,6-triethyl benzene[60,76] with either pyridine or 4,4'-bipyridine cleanly affords receptors **1.10** and **1.11** as the bromide salts. Such a reaction represents a simple example of a much more general modular approach in which interchangeable core, binding and signalling moieties may be simply prepared from readily available building blocks. The key objective is the tailoring of inter-anion discrimination by manipulation of the dimensions and symmetry of the host structure and binding site disposition. Steed's particular interests lie in conformationally flexible anion receptors that undergo a significant anion-triggered adaptation or induced-fit upon binding. Such a strategy represents a possible route to signal amplification since the conformational change and its consequences on the redox, luminescent or refractive index properties of the host material may be more readily detected than the binding itself.

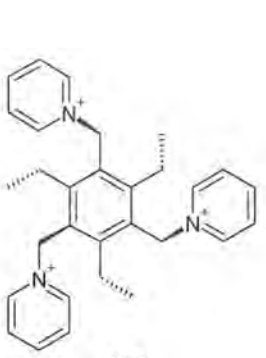

1.10

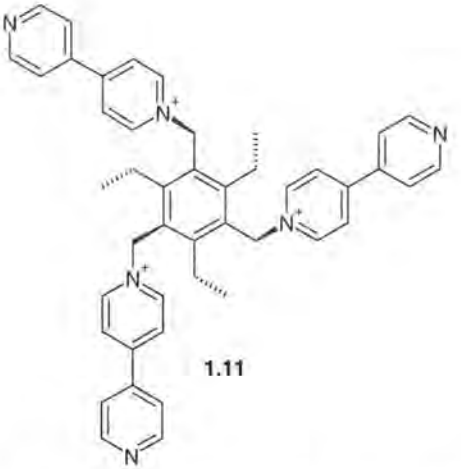

1.11

The simple design of host **1.11** contains a preorganized cavity of bipyridinium 'arms' which are linked to a triethylbenzene core resulting in a high positive charge density within the anion-binding pocket. Two different X-ray crystal structures of the bromide complex of **1.11** were obtained as disordered alternatives in the structure, a desolvated form in which host cation **1.11** acts as a first sphere ligand for bromide, interacting with the anion *via* CH···Br^- hydrogen bonds, and a solvated complex in which **1.11** acts as a second sphere ligand for hydrated bromide Figure 2. In both forms two bipyridinium arms are coplanar accounting for π-stacking interactions between pairs of cation **1.11** in the solid state, therefore, deviating from the ideal C_{3v} symmetry.

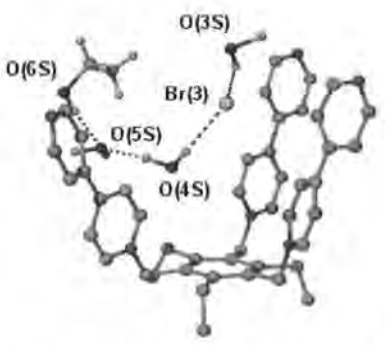

(a)

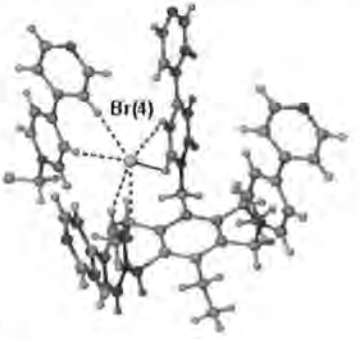

(

Figure 2 (a) Structure of solvated **1.11**·Br^{2+} showing positions of included water and ethanol. Selected O···Br distances: 3.222, 3.444 Å (b) solvent free **1.11**·Br^{2+} incorporating CH···Br interactions 2.660-2.977 Å.

Conversely a PF_6^- salt crystal obtained from water/acetonitrile adopts a threefold symmetric conformation. One PF_6^- anion is deeply included within the molecular cavity.

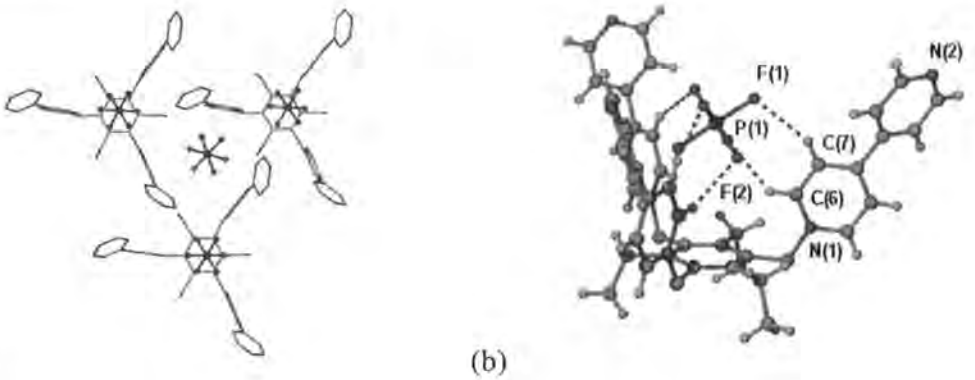

(a) (b)

Figure 3 (a) Encapsulation of PF_6^- by cation **1.11** in a threefold symmetric conformation. (b) The achiral PF_6^- induces a rigid threefold symmetric chiral structure on the lower pyridinium rings *via* CH···F interactions (H···F distances 2.39 and 2.53 Å)

The affinity of the PF_6^- salt of **1.11** for simple anions such as Cl^-, Br^-, I^-, HSO_4^-, SO_4^{2-}, $H_2PO_4^-$, $AcCO^-$ and NO_3^- in aqueous MeCN-d_3 solution was probed using ^1H NMR spectroscopic titrations, however, the spectra showed insignificant changes. When **1.11** was titrated against ATP in aqueous acetonitrile, however, it showed a moderate affinity, with $K_a = 71$ M^{-1} suggesting π-stacking with an aryl anion along with electrostatic forces as an important role in this interaction.[77]

One successful approach for preparing anion hosts has been to add hydrogen bond donor groups to an organic scaffold to yield receptors that interact with anions through hydrogen bonding. Building recognition into such hosts requires an understanding of the geometric requirements for complementary hydrogen bonding.

The behaviour of these tricationic pinwheel hosts changes dramatically when a hydrogen bonding moiety is introduced to the hexasubstitued core to give **1.12**. Further addition of redox-active or fluorescent signalling modules gives hosts **1.13** and **1.14**.[20]

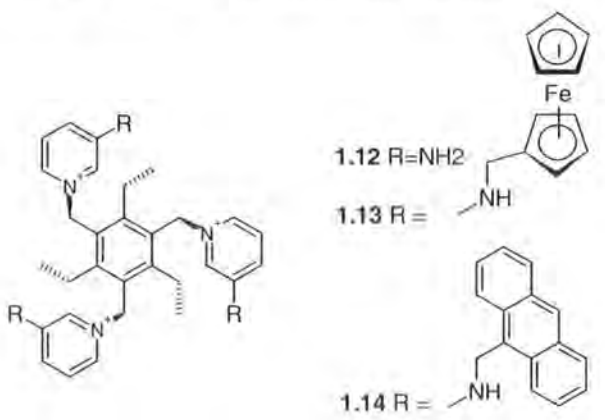

The binding constants (K_{11}) determined by ^{1}H NMR titration in MeCN-d_3 for the interaction of hosts **1.12** – **1.14** with Br^-, were 13 800, 2950 and 486 M^{-1} respectively. Compound **1.12** proved a particularly effective host for chloride with binding constants too high to measure by NMR methods. Introduction of chloride to the hexafluorophosphate salt of **1.12** also results in remarkable changes in the dynamic behaviour of the host. The conformation exchange between cone and partial cone conformations where one of the arms is on the other side of the aryl core is switched off upon addition of chloride anion which stabilises the cone conformation. Compound **1.12**·3PF_6 was shown by X-ray crystallography to adopt a non-C_3 symmetric geometry in which one aminopyridinium arm is on one side of the aryl core and the remaining two are on the other – a partial cone geometry, (Figure 4).

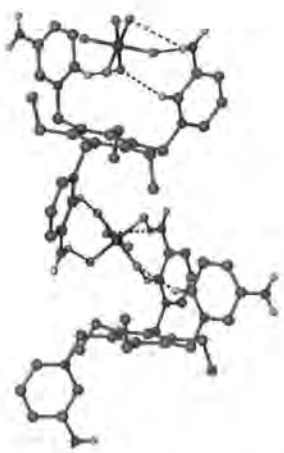

Figure 4 Partial cone conformation of **1.12**·3PF_6 from X-ray crystal structure (two repeats showing PF_6^- binding in the solid).

Podand **1.12** also proved an effective host for acetate, while nitrate is bound much less strongly despite its similar geometry. The strong binding (K_{11} = 10 500 M^{-1}) is probably due to higher basicity of acetate. Titration and variable temperature NMR studies show that the bulky **1.13** and **1.14** bind non-spherical anions such as acetate in a very different manner to halides, typically in a partial cone conformation. The increasing steric bulk of the redox or luminescent substituents in hosts **1.13** and **1.14** contributes to their decreasing affinity for halides. Titration

results of **1.13** with Cl^-, Br^- and I^- show a trend in diminishing affinity for larger anions (K_{11}=17 380, 2950 and 1860 M^{-1} respectively.) The electrochemistry of **1.13** was also explored in collaboration with Alan Bond's group. The voltammetry of **1.13**·$3PF_6^-$ in MeCN solution and ionic liquids, exhibits an overall three-electron oxidation consisting of three closely spaced one-electron-transfer steps, which implies a minimal communication between the ferrocene redox centres in the cation.[18] The solid state electrochemistry of the compound proved more complicated and highly anion-dependent. A resolved series of three oxidation waves were observed in the presence of KPF_6 with scan dependent characteristics suggesting limited solubility, (Figure 5b). However, on addition of KCl or NaCl, dissolution and re-precipitation occurred to give a voltammogram with stripping characteristics, (Figure 5a).

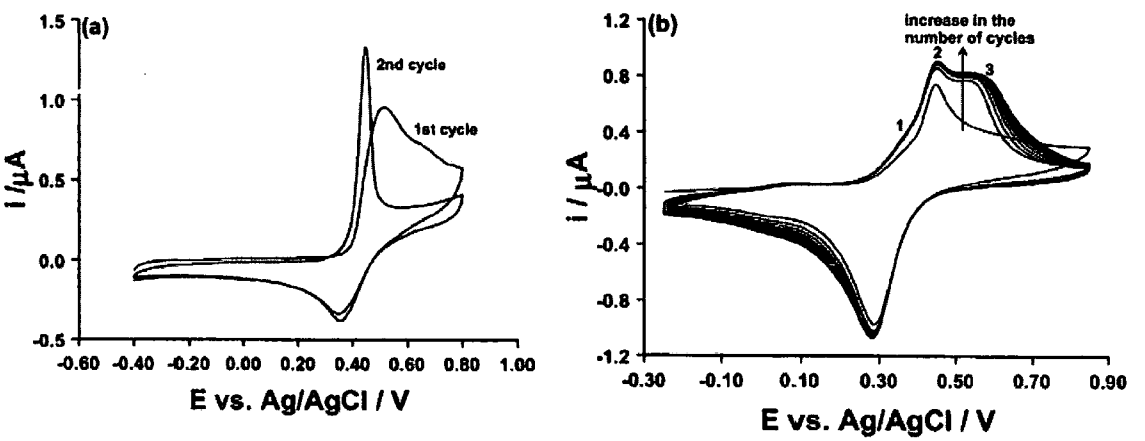

Figure 5 (a) Cyclic voltammetry of solid **12**·$3PF_6^-$ adhered to a 1 mm diameter GC electrode in the presence of 0.01 M NaCl. (b) Cyclic voltammetry (20 cycles) of solid **12**·$3PF_6^-$ adhered to a 1 mm diameter GC electrode in the presence of 0.4 M aqueous KPF_6. (Scan rates 0.1 V s^{-1}) (reproduced from ref 18).

Compound **1.14** falls into the category of the fluorophore-spacer-receptor model,[78] where an excited anthracene unit can associate with the ground state of a second fluorophore and produce an intramolecular excimer (anthracene-anthracene). The fluorescence intensity of **1.14** increases when exposed to ambient light suggesting interaction of the arms with one another. Exposure of a sample of **1.14** to UV irradiation (254 nm) for 30 min resulted in an appearance of two new peaks in the ^1H NMR spectrum suggesting a $4\pi+4\pi$ cycloaddition reaction forming cis and trans isomers of the photodimer or formation of both intra- and intermolecular addition species.[79] The

fluorescence studies of this photocoupled derivative receptor, show that the intensity decreases i.e. quenching is observed by 30% on the addition of Cl^- and 50% for I^-. This could be explained by an enhancement of electron transfer from the receptor towards the fluorophore. No significant change in fluorescence intensity occurs if anions are added to a fresh sample of receptor **1.14**·3PF_6^-.[25] The X-ray crystal structure of host **1.14** $(PF_6)_3$·MeOH·2MeCN (Figure 6) shows that the cationic host does adopt a cone conformation with alternation about the hexasubstituted core. The anthracenyl arms are splayed out, however, and the three NH groups do not converge. It is remarkable that the central anion is held solely by CH···F interactions and eschews the remaining secondary amine binding site.

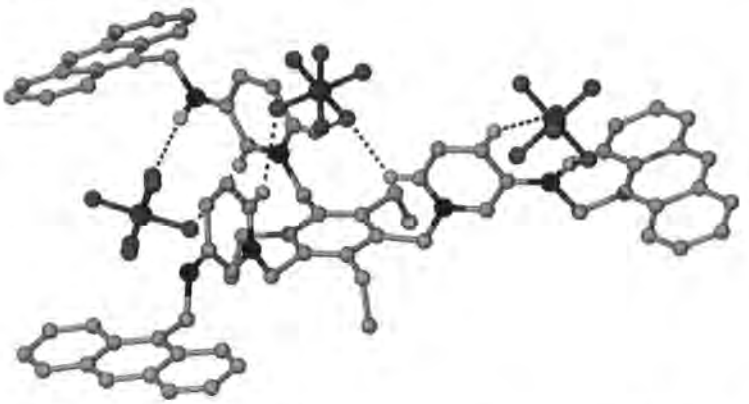

Figure 6. X-Ray structure of receptor **1.14**·3PF_6 showing cooperative anion binding of the central PF_6^- anion by weak hydrogen bonds.

Conversely an X-ray crystal structure of **1.12**·3Br^- (Figure 7),[25] shows a remarkable encapsulation of an intra-cavity bromide anion by a six-fold array of NH···Br^- and CH···Br^- interactions. Two of the three NH groups are involved in interactions to bromide, which appears to be just slightly too large for the cavity (N···Br distances are 3.35 and 3.40 Å).

Figure 7 X-ray crystal structure of **1.12**·3Br^-. Only the central Br^- anion is shown for clarity.

The modular strategy towards these cationic pinwheel receptors renders the synthesis of a range of compounds with different hydrogen bonding functionality readily accessible. Thus compounds with amide, ester, carboxylic acid and urea functionalities are all available. Urea compounds in particular are expected to exhibit stronger hydrogen bond donation and hence more effective anion complexation, particularly in more competitive solvents (the amine receptors function well in acetonitrile but exhibit little binding in DMSO, for example). The urea moiety is known to be a strong double hydrogen bond donor and, like the closely related amide group, has been utilized effectively in a number of anion binding systems.[10, 24, 43, 58, 80-82] In the case of urea, both donor hydrogen atoms may face towards the guest and the potential exists for the anion to be chelated to each arm in $R_1^2(6)$ motif, or $R_2^2(8)$ in the case of oxyanions.[83] The precursor ligands **TUP** and **OUP** are readily obtainable from the reaction of 3-aminopyridine with the appropriate isocyanates,[57] and reaction with 1,3,5-tris(bromomethyl)-2,4,6-triethyl benzene[60, 76] gives the tripodal receptors **1.15**.[84]

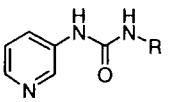

TUP R = p-tolyl
OUP R = n-octyl

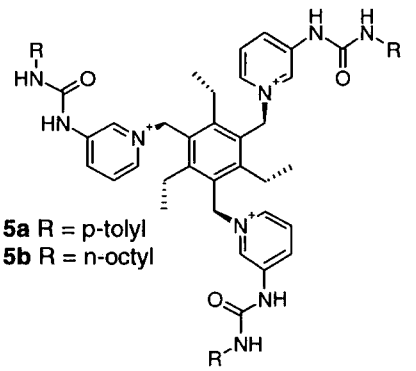

1.15a R = p-tolyl
1.15b R = n-octyl

As in previous host species **1.10 – 1.14**, counter-anion metatheses were carried out to exchange bromide for the more readily displaced hexafluorophosphate anion. These exchange reactions were carried out by stirring solutions of the bromide salts in the presence of a large excess of tba-PF_6 (tba = tetra-n-butyl ammonium). Three crystals structures of receptor **1.15a** were obtained, each containing different counter-anions resulting in dramatically altered geometries. The structure of **1.15a**·3Br$^-$ adopts an alternating 'up-down' conformation of the substituents around the central aryl core with functionalised arms on the opposite face to the ethyl groups. The pseudo-cone geometry forms a central cavity occupied by one of the bromide anions which hydrogen bonds to only one of the urea groups. The other two bromides interact with two arms facing away from the cavity (Figure 8).

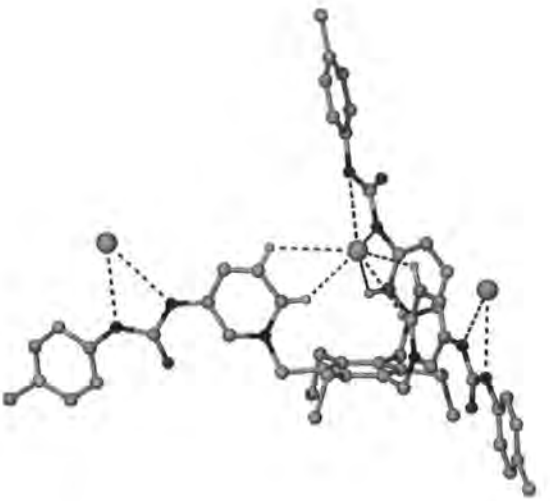

Figure 8 One independent host-guest complex from the crystal structure of **1.15a**·3Br$^-$, showing the hydrogen bonding interactions to the anions.

The structure of **1.15a**·3PF_6^- obtained from acetone does not have a central cavity. The three functional arms are situated on one face of the central aryl core but are folded inwards over it. One of the ethyl groups is also on the same face as urea groups. Only one urea group is engaged in a hydrogen-bonding to one of the PF_6^- anions. One urea proton binds the anion in a bifurcating mode, the other forms a linear NH···F interaction. The other two PF_6^- anions are incorporated in the lattice and the other two urea moieties only interact with two enclathrated acetone solvent molecules within the structure (Figure 9a).

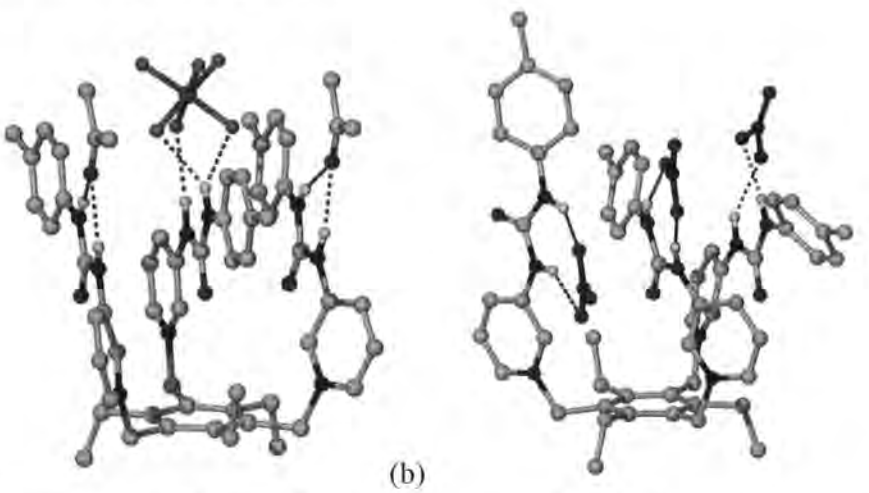

(a) (b)

Figure 9 (a) X-ray structure of **1.15a**·3PF_6^- showing the interactions between the urea protons and the PF_6^- anion; (b) X-ray structure of **1.15a**·1.5PF_6·1.5NO_3 showing interaction of the urea protons with two NO_3^- anions.

The third structure exhibits a mixture of nitrate and hexafluorophosphate as the counter anions in a 1: 1 ratio. The structure is related to that of the PF_6^- complex but the substituents unfold somewhat in this case to accommodate the hydrogen bonding between the nitrate and the urea moiety (Figure 9b). The solution studies of **1.15a** confirmed the strong bonding to bromide in particular, as seen in the crystal structure. Binding constants of **1.15a**·$3PF_6^-$ with Cl^-, Br^-, I^- and NO_3^- obtained from ^1H NMR titrations in the very competitive solvent DMSO-d_6 were as follows K_{11} = 437, 2884, 41 and 347 M^{-1}. The highly basic acetate was also strongly bound, K_{11} = 1622 M^{-1}.[84]

The **TUP** derivative **1.15a** is an effective host in DMSO but it is limited by solubility constraints. The more lipophilic analogue **1.15b** was developed to overcome these limitations and was studied in MeCN by both ^1H NMR titration and variable temperature NMR spectroscopy. These experiments revealed a very different behaviour to the amine analogues (such as **1.12**) with an unsymmetrical partial-cone chloride-binding low temperature structure. There is a considerable conformational change from this 1:1 complex upon addition of excess chloride with a series of anion binding and conformational equilibria quite different to those observed for the very similar amine analogues **1.12 – 1.14** (Figure 10a). This conformer was also found to be the most stable *in silico* in the gas phase by DFT methods (Figure 10b). In contrast, for the tolyl complex **1.15a**, calculations suggest a cone conformer. While the neglect of solvation effects in these gas phase calculations renders them only loosely applicable they are highly consistent with the NMR results and provide a starting point for understanding the solution phase data.

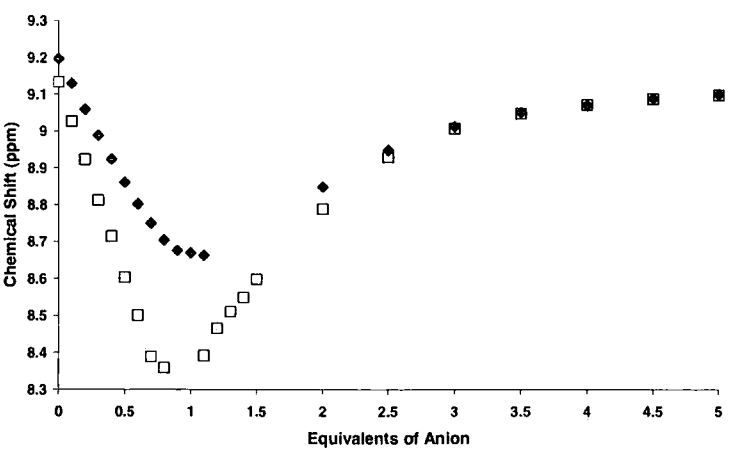

(a)

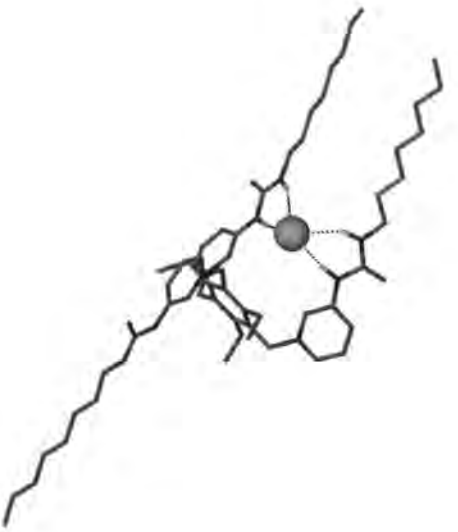

(b)

Figure 10 (a) ^{1}H NMR titration curve for Cl^- (squares) and Br^- (diamonds) binding by **15b** in MeCN-d_3; (b) Lowest energy conformer of **1.15b**·Cl^- from DFT methods (reproduced from ref 84).

A host incorporating thiourea motif with adjacent pyrene or anthracene as signalling groups has been reported by Sasaki *et al.* [85] Receptor **1.16** falls into a category of neutral podands. Having a six-fold substituted benzene ring as a rigid spacer, host **1.16** proved to be effective for recognition of the tetrahedral dihydrogen phosphate anion.

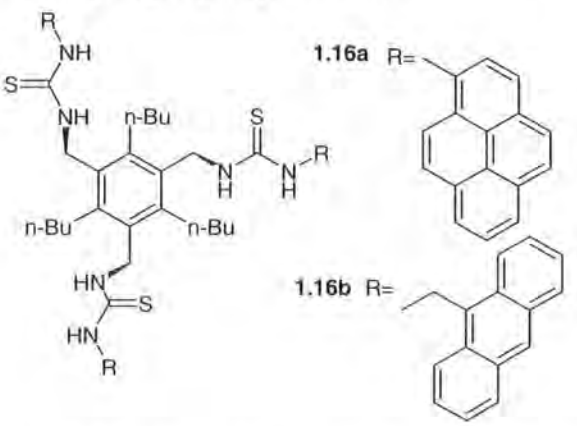

Indeed fluorescence study of **1.16a** showed long-wavelength emission upon addition of guest anions in acetonitrile (Figure 11).

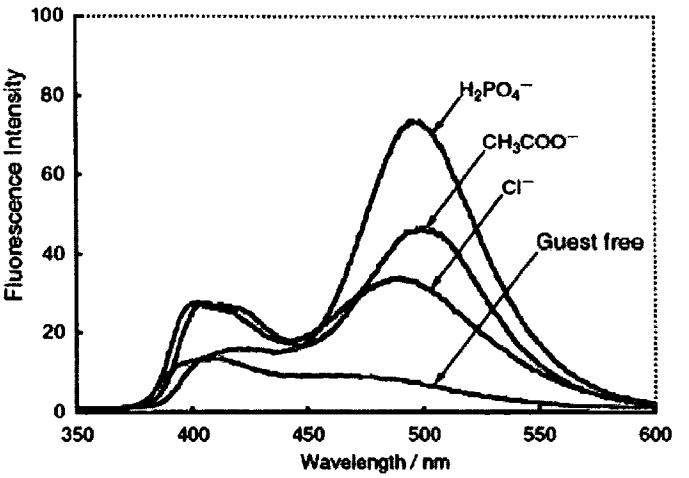

Figure 11 Fluorescence spectra of receptor **1.16a** with several guest anions in acetonitrile. [**1.16a**] = 2.0×10^{-6} M. [Anion] = 4.0×10^{-4} M. Excitation wavelength: 310 nm. All anions were used as their tba salts (reproduced from ref 85).

On the other hand, a tripodal thiourea receptor **1.16b** connected to anthracene groups *via* methylene units showed a decrease in fluorescence intensity upon addition of anions. In both cases, the degree of the change in emission intensity was in the order of $H_2PO_4^- > AcO^- > Cl^- \gg ClO_4^-$, which is different from the basicity of the guest anions. The anthracene unit in **1.16b** is connected to the thiourea group *via* a methylene spacer, therefore it is thought that the emission quenching in **1.16b** is due to a photoinduced electron transfer (PET) process. The photoinduced transfer has been reported in anion binding host systems by several others.[86-88] It can be either switched "on" or "off" depending on the charge on the adjacent anion binding group (Figure 12).

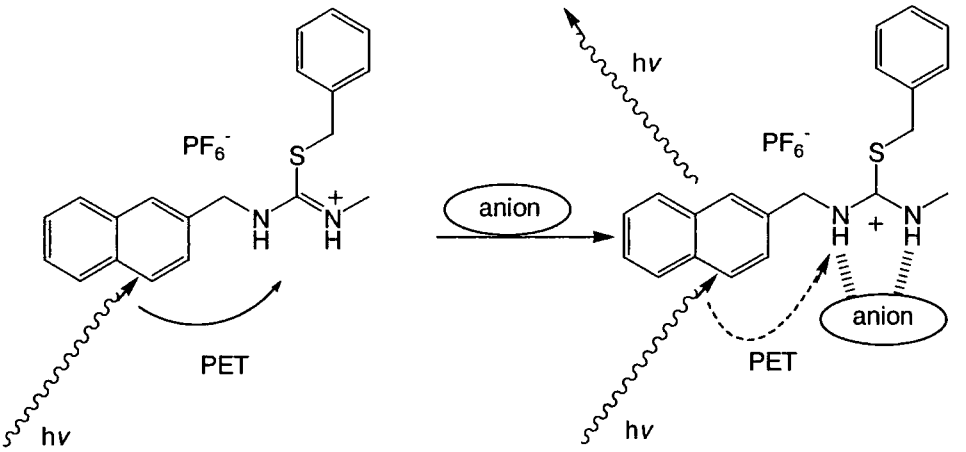

Figure 12 PET observed in a simple receptor with maximum enhancement (ca. 1600%) in the emission reached upon addition of 3 equiv. of AcO^-, compared to that with no anion bound (reproduced from ref 88).

The conformational induced switching concept has also been utilised recently by Meng *et al.* [89] Host **1.17** incorporates benzoimidazolium hydrogen bonding moieties and naphthalene signaling units into the benzene ring tripodal core. The host adopts cone conformation upon binding chloride anions selectively over bromide and the change results in an excimer.

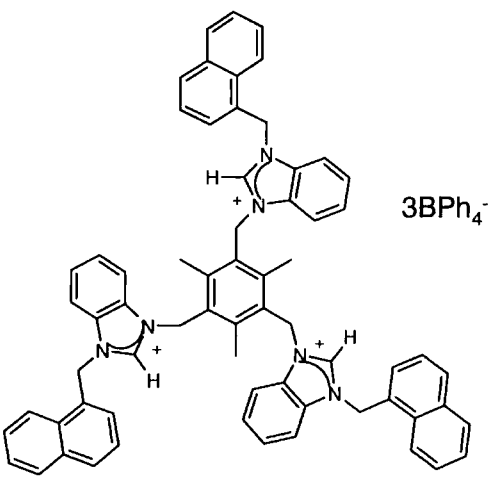

1.17

Chapter 2

Calixarene Based Hosts

2.1 Aims of this project

The aim of this project is to expand the triethylbenzene work (discussed in section 1.2) to much larger and more pre-organised organic scaffolds such as the one of calix[4]arene. The reaction routes to the target molecules are depicted in Scheme 1.

We began with an introduction of bromomethyl group to the cone and 1,3-alternate calix[4]arene scaffolds. Bromide is a good leaving group and on the addition of neutral nucleophiles, such as pyridine derivatives, an S_N2 reaction takes place to produce pyridinium compounds as the bromide salts.

The design of the cationic molecular receptors incorporates side arms that have a directional hydrogen-bonding site, introduced by the presence of secondary or primary amine functionalities, as well as the weaker directionality imparted by pyridinium CH···anion interactions. The overall four-positive charge of the host is produced during the reaction between the aryl-bromide and the aminopyridine derived pendant side arms.

The degree of pre-organisation and flexibility as a response to an anion binding event will be probed by ^{1}H NMR and photophysical techniques such as UV-vis absorption and spectrofluorometry.

The choice of building blocks for the modular assembly was guided by previous relevant results such as fluxionality of calix[4]arene hosts,[90] solubility trends of particular functional groups in common solvents[19] and photophysical properties of the reporter moieties.[25, 91] 3-Aminopyridine was initially chosen for the substitution reaction, as it is the simplest pyridine derivative that contains a hydrogen-bonding functionality for anion-binding. The primary amine of 3-aminopyridine can be also easily reacted with aldehydes, ketones or carboxylic acids to produce pyridine-derived compounds. It was also expected that the orientation of the amine groups around the pyridine ring would influence the binding of the anion. The *meta* isomer

previously proved to be the best candidate for anion recognition as the hydrogen atoms can point into the centre of the cavity and bind an anion by an array of NH···X and CH···X (X=anion). The *ortho* and *para* isomers are not in the correct orientation for anion binding as the NH functionalities proved in previous work to point away from the host's cavity.[20]

Adding long aliphatic chains such as R=$CH_2C_6H_4(CH_2)_4CH_3$ to the functional amine groups, improves overall solubility of the hosts in organic solvents, whereas hosts with R=H are more likely to crystallise. It was anticipated that the event of interaction with the guest molecule would result in modulation of the flexible appending groups to accommodate the best fit. Some preorganisation can be achieved through a choice of particular conformation of calix[4]arene to bind anions of specific geometric shape.[92]

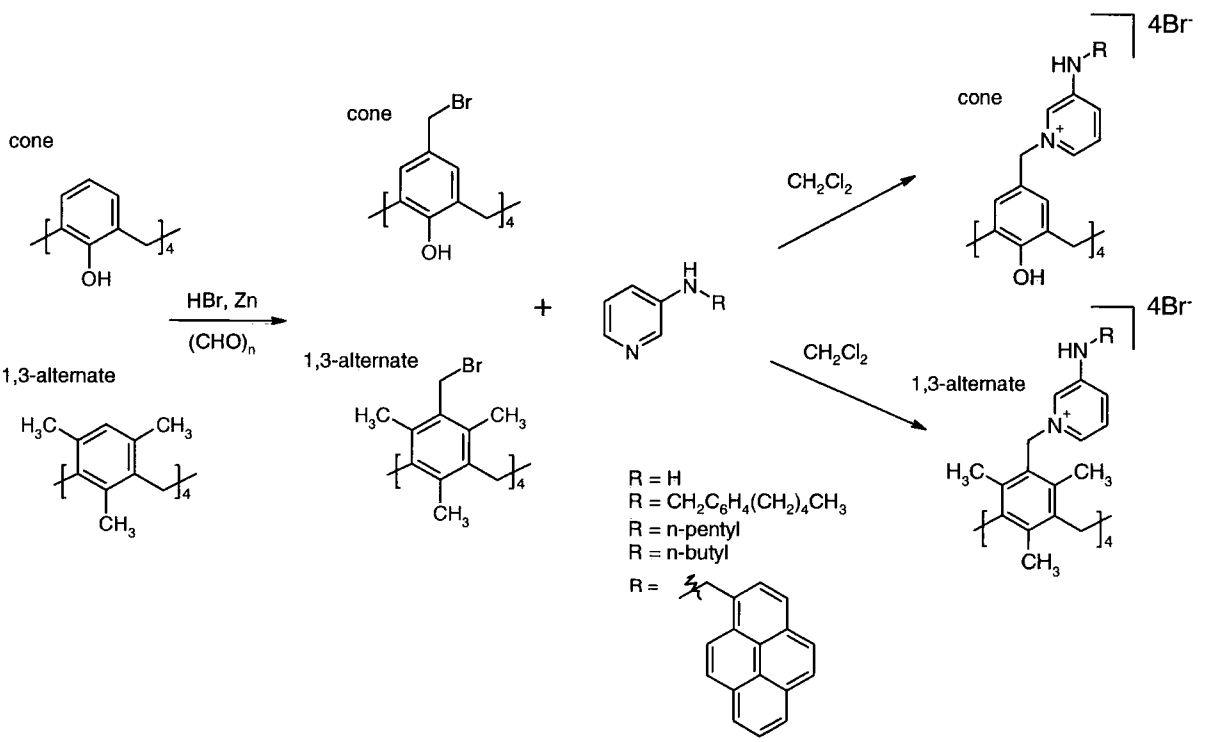

Scheme 1 Reaction paths to the target molecules.

2.2 General Introduction

Utilising the fluxional behaviour of hosts such as the pinwheel[14, 20, 73] has proved an excellent concept for the design of future array of signalling receptors. The degree of conformational flexibility of an anion binding host has a large impact on the binding constant. A small change in the conformation however, can bring about a large response and ultimately signal generation. Where there is certain geometrical pre-organisation for binding specific anions, very high binding constants may be achieved. The binding constant, however does not always reflect the best geometrical fit of anions. The basicity and charge distribution play an important role in the final association energy. The majority of fluxional receptors reported contain some type of scaffold, organic or inorganic, to which flexible appendages incorporating anion binding groups and reporter moieties are attached. Previous work within the group has investigated the properties of aminopyridinium binding groups with or without redox or fluorescent reporter groups based on the triethylbenzene core. Inter-anion discrimination depends primarily on the structural characteristics of the hosts and thus a wide range of building blocks may be used in order to achieve the general design.

The high synthetic versatility of the calixarene platform offers a unique opportunity of tuning geometry, solubility and functionality by introducing various groups to either lower or upper rim. The selectivity for a particular analyte can be accomplished through the design of spatial distribution of non covalent bonding moieties incorporating a combination of hydrogen bonds, electrostatic attraction or π-π stacking. In addition to the fluxional nature of the calix[4]arene's scaffold or the possibility of locking it into a particular conformation, there is also an additional flexibility between the functional groups. Occurrence of such behaviour allows even more sophisticated recognition of binding event and transducing it to some observable signal. The greater complexity and variety of non-covalent interactions, the more specific analyte recognition can take place. One could take an example from nature and compare with the specificity of binding sites in proteins, induced fit model or allosteric regulations.[93, 94] Many synthetic host designs have been modelled on naturally occurring receptors. Utilization of calix[4]arene platforms allows a significant control over the steric properties in addition to the possibility of varying functional and reporter groups.

There is a whole plethora of synthetic calixarenes both neutral and cationic for binding anions, a modest percentage of which display fluxional behaviour and/or report binding events.[95] The most relevant examples from literature are included in this chapter. One should take a careful approach to how to evaluate the design as many factors determine the subtlety of anion recognition. In some cases the binding may be very clearly seen even with a 'naked eye' but with a closer examination the event only happens for the most basic anion, often associated with the deprotonation of NH groups.[96] The magnitude of complexation constants very often follow the basicity trend of the anions which is size/polarity related in simple spherical halides with the most basic anion being F^-. Oxo-anions and carboxylate anions are generally most basic. The high complementarity and selectivity can be best achieved for anions of complexed geometry where various binding sites are available although it is often difficult to control the selectivity and sensitivity. It is worth noting that both host and guest can undergo a readjustment to lower their complex formation energy.

Examples included in this chapter display the synthetic flexibility of the scaffold where either upper rim or lower rim of the calix[4]arene functionalization can be achieved. The conformation of the calix[4]arenes can be synthetically preselected, the choice of functional groups of known affinity for particular anions also singled out and a number of appending "arms" stoichiometrically controlled. Both compounds **2.1** and **2.2** have been synthesised previously and constitute very important precursors to a variety of receptors designed for binding both anionic and cationic species.[97-99]

Calixarene chemistry is well developed and the conformational properties of the calixarenes are subject to control and indeed locking by appropriate choice of functional groups.[100-102] It is well known that the unmodified calixarenes p-*tert*-butyl calix[4]arene **2.1** and de-*tert*-butylated calix[4]arene **2.2** adopt cone conformations because of strong hydrogen-bonding interactions among the OH groups, whereas introduction of acyl or alkyl substituents suppresses conformational freedom because of steric hindrance (i.e., inhibition of oxygen-through-the-annulus rotation) and results in conformational isomers.[103]

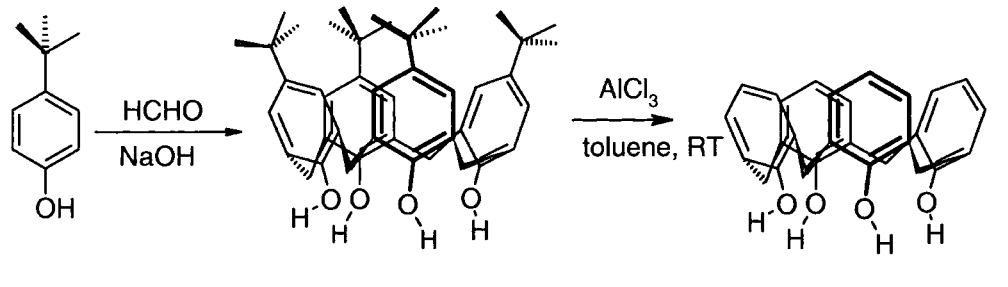

2.1 **2.2**

Scheme 2 Synthetic route to calix[4]arene cores (ref 101).

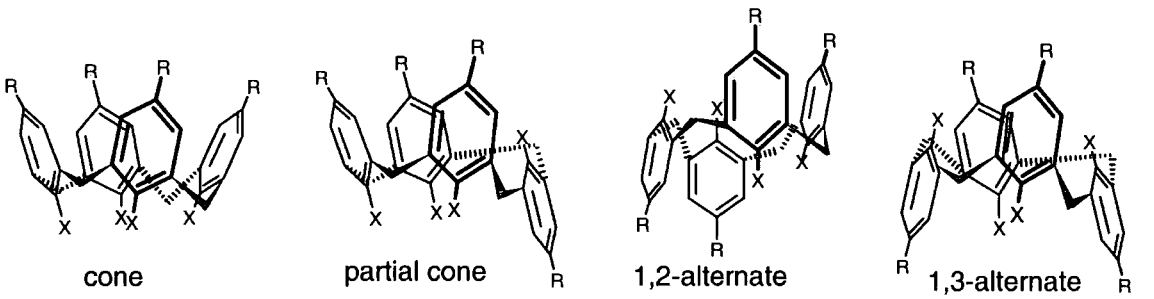

x=OH, OR'
R'=Me,n- Pr, n-Hexyl
R=H
R=Bu^t

Figure 13 Four different conformers observed following alkylation at the OH position

Changing the nature and the length of the alkyl substituents on the phenolic OH groups at the lower rim of **2.1** results in **2.3**,[31] cone, **2.4**,[104] 1,3-and 1,2-alternate/partial cone and **2.5**,[95, 105] mobile calixarene conformers. It is known that methyl group is not, whereas n-propyl and longer alkyl groups, are bulky enough to suppress the oxygen-through-the-annulus rotation therefore tetra-O-propylation and longer chain tetra-O-alkylation results in conformationally immobile calix[4]arenes. Shinkai *et al.*[104] noticed that upon alkylation of **2.1** using n-PrBr and NaH, product **2.4** results in cone and partial-cone conformers in a ratio of approximately 1: 1. When n-PrI was used the proportion of partial cone conformer increased to 81% probably due to the preferred reduced steric hindrance in partial cone against the more bulky n-PrI. It was also noted that when de-*tert*-butylated calix[4]arene **2.2** was alkylated by n-PrBr in presence of NaH as opposed to the *tert*-butyl calix[4]arene **2.1** the yield of cone conformer product **2.4** decreased and that of 1,3-alternate was increased. This preferred isomer results from reduced crowding of the hydrogen atoms and propyl groups on the edges of calixarene. However when the temperature is raised to 75 °C and reaction (i) (Scheme 3) is stirred for 18 hours, the

tetrapropoxycalix[4]arene **2.4** could be obtained exclusively in the cone conformation in 66% yield. When Cs_2CO_3 was used as base for abstracting protons from the OH groups the main products were partial cone and 1,3-alternate calixarenes (Scheme 3). Hence the conformer distribution is also affected by alkali metal cation, which acts as template metal in the step where the conformation is immobilized. [104, 106, 107]

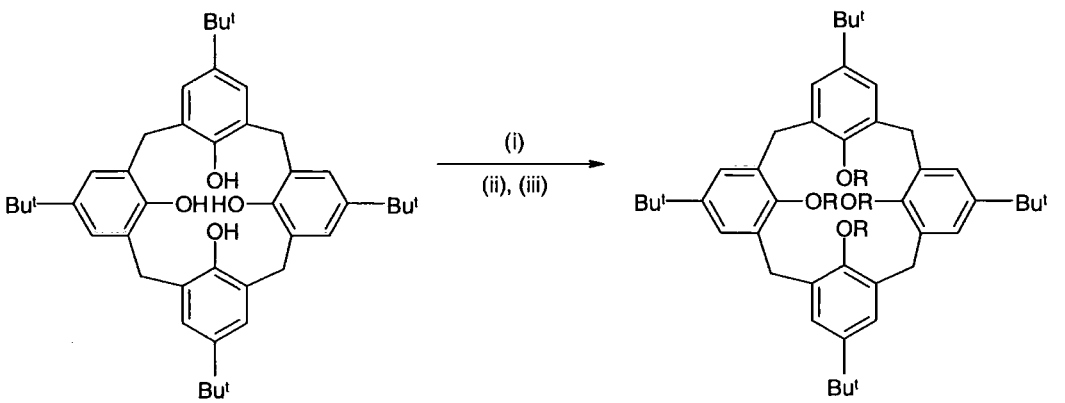

2.1

2.3 R=hexyl; cone
2.4a R=propyl; cone (4%), partial cone (81%) and 1,3-alternate (18%)
2.4b R=propyl; 1,3-alternate (67%), 1,2-alternate (9%) and partial cone (24%)
2.4c R=propyl; cone (66%)
2.5 R=methyl; mobile

Scheme 3 Synthetic route to the various conformers of calix[4]arene. (i) RI, NaH in DMF, r.t. (to obtain compounds **2.3**, **2.4a**, **2.5**,), (ii) RI Cs_2CO_3 in CH_3CN, reflux (to obtain compound **2.4b**) or (iii) RI NaH in DMF, 75°C for 18 h (to obtain compound **2.4c**). The yield percentage was confirmed by HPLC analysis.

2.2.1 Lower rim functionalized calix[4]arenes

Yong-Bing He has recently reported two-armed neutral receptors **2.6** and **2.7**. The difunctionalized calix[4]arene **2.7** is soluble in chloroform, methanol, ethanol, acetone and DMSO, but **2.6** is only soluble in DMSO.[92]

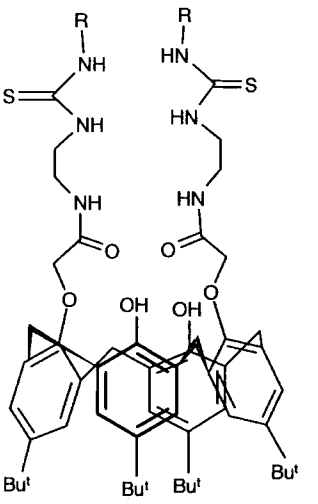

2.6 R= p-nitrophenyl
2.7 R=1-naphthyl

The recognition properties of receptors **2.6** and **2.7** for various anions such as malonate, succinate, glutarate, adipate, acetate, dihydrogen phosphate and the halide (Cl^-, Br^-, I^-) anions as tba salts have been monitored by UV-vis spectroscopy. With the addition of adipate anion to the solution of receptor **2.6** in DMSO (5.0×10^{-5} mol L^{-1}), the characteristic absorption peak of the host at 359 nm increased gradually with a slight red shift and a new peak at 487 nm was observed. This new peak was also observed in case of addition of increasing amounts of dicarboxylates, in particular, malonate, succinate, glutarate, adipate, resulting in the change in colour of the solution of **2.6** from yellow to red, which can be observed by the naked eye. When a protic solvent such as methanol is added the colour changes back to yellow. The solvent is thought to interfere with the hydrogen-bonding between **2.6** and the dicarboxylates. Upon addition of increasing amounts of dicarboxylate to the solution of **2.7** in DMSO(5.0×10^{-5}molL^{-1}), the characteristic peaks at 260 nm and 289 nm of the host change. The peak at 289 nm decreases while the intensity of the 260 nm absorption increases, and a new absorption band appeares at 340 nm. Similar phenomena have been observed when other, α,ω -dicarboxylate anions e.g. malonate, succinate, glutarate are added to a solution of **2.6** or **2.7**. Upon addition of acetate (AcO^-), dihydrogen phosphate ($H_2PO_4^-$) or the halide anions to a solution of **2.6** or **2.7** in DMSO, the UV-vis absorption spectra of **2.6** or **2.7** do not change indicating no interaction. The continuous variation method has been used to determine the stoichiometric ratios of the receptor **2.6** or **2.7** and the anion guests. The job's plot (Appendix 1) method indicates a 1: 1 ratio. The same method was applied to deduce stoichiometric ratios between **2.6** and **2.7** and other dicarboxylate anions (malonate, succinate, glutarate) which also formed 1: 1 complexes. The

NMR spectroscopic study confirms strong bonding with the thiourea protons of **2.7** shifting on formation of 1:1 with adipate complex from 8.42 to 10.98 and 9.61 to 12.19 ppm, whereas the thiourea protons of **2.6** disappear. This behaviour previously observed by Nam[108] and recently reviewed by Fabbrizzi [109] is ascribed due to deprotonation of the acidic thiourea NH. When acetate (AcO^-), dihydrogen phosphate ($H_2PO_4^-$) or the halides (Cl^-, Br^-, I^-) was added to solutions of **2.6** or **2.7** in DMSO-d_6, no change the ^1H NMR spectra was detected.

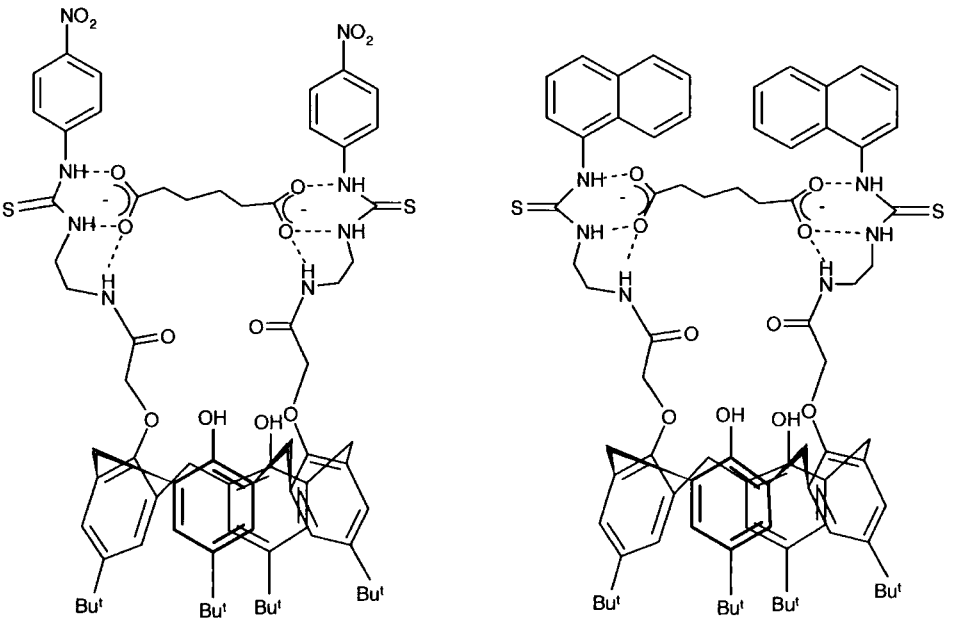

Figure 14 Possible binding models for the interaction of **2.6** and **2.7** with adipate anions.

Addition of adipate to **2.7** results in an increase in fluorescence intensity following excitation at 344 nm. A new broad band with long-wavelength fluorescence emissions from ~410 nm to 600 nm was observed. Similar phenomena were also observed for other dicarboxylate anions. The anion-induced fluorescence enhancement might be due to the efficient fluorescent retrieval upon interaction between the anion guest and the receptor unit of **2.7**. In the absence of anion, the fluorescence intensity of receptor **2.7** is quenched by a PET (photo-induced electron transfer) process to some extent. As the anion is introduced into the solution of receptor **2.7**, the interaction between the receptor unit and anion could diminish the efficiency of the PET process. In contrast photoinduced charge transfer (PCT) has been scarcely used for anion sensing,[110] although examples in cation recognition are abundant.[111] The PCT requires a cation binding entity which is linked to a fluorophore via another group which enhances conjugation of the charge. When a fluorophore contains an electron-donating group (often an amino group)

conjugated to an electron-withdrawing group, it undergoes intramolecular charge transfer from the donor to the acceptor upon excitation by light. The consequent change in dipole moment results in a Stokes shift that depends on the microenvironment of the fluorophore. It can thus be anticipated that cations in close interaction with the donor or the acceptor moiety will change the photophysical properties of the fluorophore because the complexed cation affects the efficiency of intramolecular charge transfer. One other phenomenon in which fluorescence of a molecule is enhanced arises due to formation of an excimer. An excimer (a dimer) can occur when an electronically excited moiety such as flat delocalized π system as in pyrene interacts with a second pyrene in its ground state. If the pyrenes are sufficiently far apart from each other, upon light absorption only one of the pyrene units experiences locally this excitation which in turn gives rise to "monomer" emission. The observation of excimer emission indicates that diffusive encounter between the pyrenes has occurred (dynamic excimer). Quite often an excimer-like emission is observed (static excimer) if the units are also associated in the ground state. [112] In a time-resolved experiment, the difference between the static and the dynamic eximer can be established, where the growth of the dynamic but not of the static excimers as a function of time can be observed. An alternative distinction between dynamic excimers and those formed from (pre)associated pyrenes is that in the latter case the pyrenes are sufficiently close that they exhibit perturbed absorption and excitation spectra. Excitation spectra provide evidence for ground- state interaction of the pyrene groups monitored at the monomer emission and at the excimer emission. While the monomer and excimer emission spectra have similar overall features, they cannot be superimposed.

These concepts were recently applied to anion binding by Kim *et al.* [91] A 1,3-alternate calix[4]arene conformation was locked by a methodology previously reported by Shinkai[104] and Collins.[113] The calixarene-based fluorescent chemosensor **2.8** contains two fluorogenic pyrene units conjugated to amide groups as the guest recognition. Among the anions tested, (F^-, Cl^-, Br^-, I^-, AcO^-, HSO_4^-, and $H_2PO_4^-$ as their tba salts in MeCN) only F^- causes a red shift of the absorption band of **2.8** to 400 nm ($\Delta\lambda$=54 nm) (Figure 15).

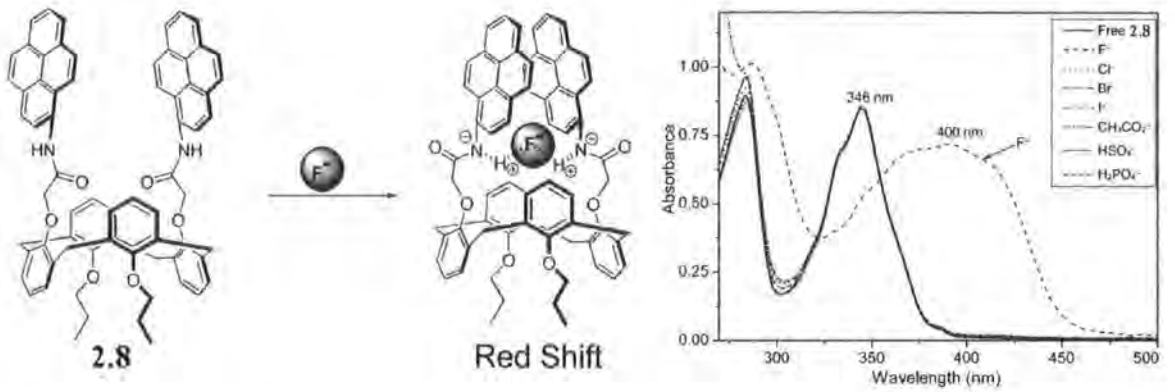

Figure 15 UV-vis spectra of **2.8** (0.20 mM) upon addition of tba salts of F^-, Cl^-, Br^-, I^-, AcO^-, HSO_4^-, and $H_2PO_4^-$ (60 mM) in MeCN (reproduced from ref 91).

With excitation at 346 nm, **2.8** exhibits monomer and excimer emissions at 385 and 482 nm, respectively, due to dynamic excimer formation.[114] Addition of F^- to **2.8** induces a drastic change in its fluorescence spectrum, in which the monomer emission is strongly quenched and the excimer emission is blue-shifted by 12 nm. The blue-shifted excimer emission is attributed to a pyrene dimer formed in the ground state, the static excimer. The spectrum monitored at the excimer emission is red-shifted compared to the spectrum monitored for the monomer, and the bands in the spectrum monitored for the excimer are broadened (Figure 16).

In contrast, other anions gave only a slight change in fluorescence intensities with no wavelength changes. When F^- is added up to 600 equiv, both excimer and monomer emissions of **2.8** are gradually quenched. This is due to a photoinduced electron transfer (PET) from F^- to the pyrene units, as well as to the wavelength shift for the UV absorption band (Figure 15). On the other hand, addition of more than 600 equiv of F^- resulted in a new band at 470 nm with a steady decrease of the monomer emission at 385 nm. Noticeably, upon excitation of **2.8** at 400 nm, the intensity of the peak at 470 nm is remarkably enhanced with increasing F^- concentration (Figure 17). These observations suggest that the chemical species absorbing the energy at 400 nm are such that their pyrene fluorophores form a static dimer in the ground state, caused by hydrogen bonding between F^- and amide protons. This proposal can be clarified by characterizing the nature of the blue-shifted emission to 470 nm and the original emission at 482 nm.[114]

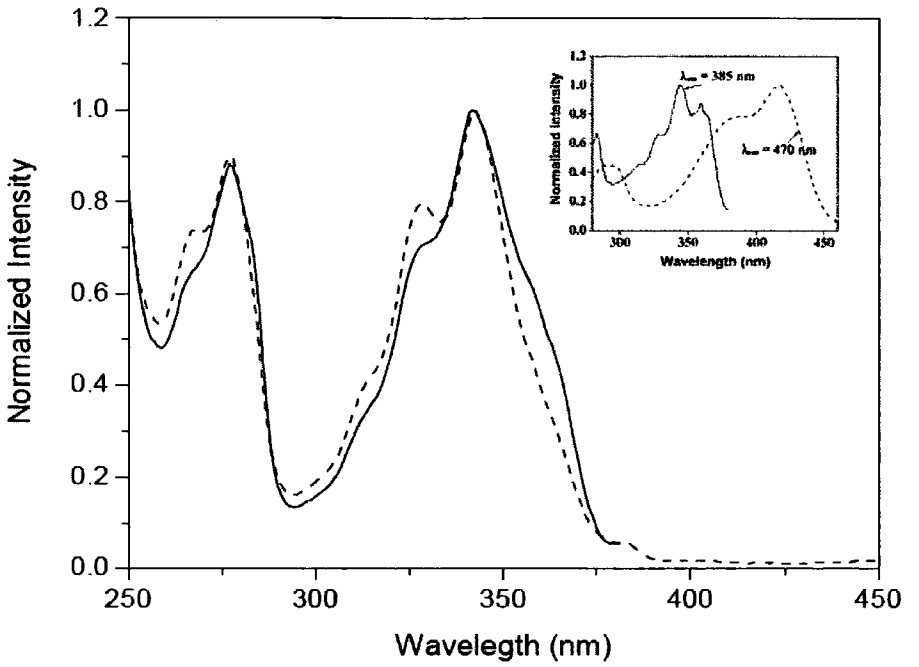

Figure 16 Excitation spectra (normalized) of free **2.8** monitored at 385 nm (solid line) and 482 (dashed line). Inset: excitation spectra (normalized) monitored at 385 (solid line) and 470 nm (dashed line) in the presence of 1000 equiv of $Bu_4N^+F^-$ (reproduced from ref 91).

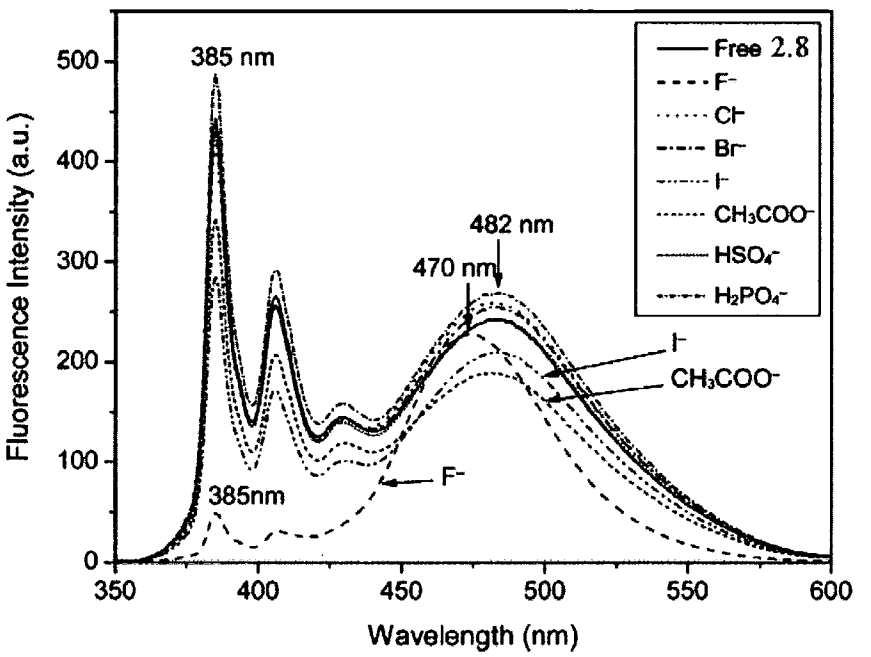

Figure 17 Fluorescence spectra of **2.8** (6.0 μM, excitation at 346 nm) upon addition of tba salts of F^-, Cl^-, Br^-, I^-, AcO^-, HSO_4^-, and $H_2PO_4^-$ (6.0 mM) in MeCN (reproduced from ref 91).

A more recent example of an optically sensing calix[4]arene has been reported by Diamond *et al.*[115] Tetrasubstituted 1,3-alternate calix[4]arene **2.11** provides a preorganised scaffold for binding chloride anions. The neutral host with urea functional groups is bridged with single methylene spacers to pyrene moieties. Interestingly during the synthesis of **2.11** the calix[4]arene **2.2** upon reaction with **2.9** adopts the 1,3-alternate conformation which can be observed in the ^{1}H NMR spectrum by the appearance of a proton resonance for the methylene groups of the calix[4]arene annulus. This resulting conformation is due to the attachment of four sterically bulky appendages derived from **2.9**. It was also noted that **2.2** doesn't react with **2.10** under the same conditions as in the reaction with **2.9**. This was suggested to occur due to bromide being a better leaving group in substitution reactions. The ditopic preorganisation of **2.11** does not only contain anion binding urea but also the reporter pyrene groups between which there is a degree of overlap. The resultant excimer emission of 452 nm (λ_{max}) is significantly blue shifted in comparison to other intramolecular pyrene excimer systems, which are typically around 480 nm. This shift can be explained by partial overlapping of the pyrenes and identified as static due to interactions between urea groups inducing this overlap as oposed to the dynamic excimers in which the pyrene moieties are free to fully overlap.[116] Upon binding of chloride anions the intramolecular pyrene excimer system is disrupted due to conformational changes. The excimer emission of **2.11** is quenched, with a concomitant rise in the monomer emission. This behaviour is only observed upon addition of chloride anions.

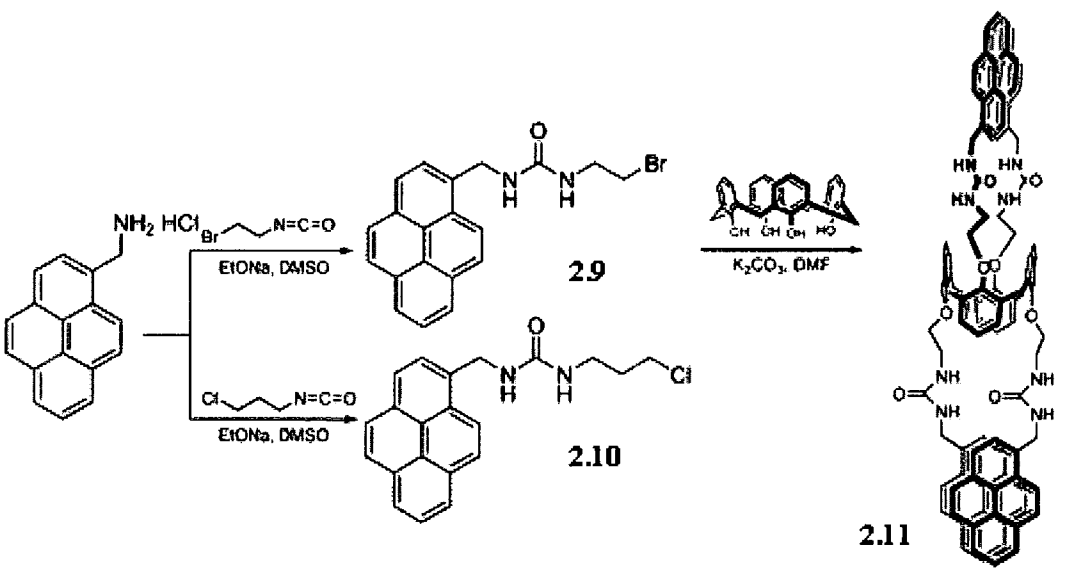

Scheme 4 Synthetic routes to precursors **2.9** and **2.10** and calix[4]arene **2.11** (reproduced from ref 115).

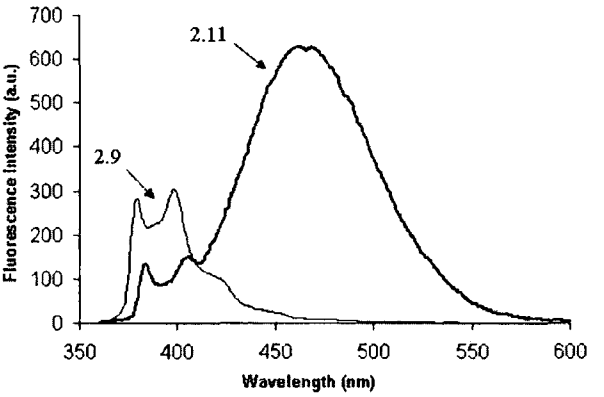

Figure 18 Emission spectra of **2.9** and **2.11** ($1x10^{-6}$M) in acetonitrile-chloroform (95:5v/v) showing monomer maxima at 376 nm and 398 nm. Only **2.11** shows an additional large band at 452 nm due to excimer formation. (The excitation wavelength was 340 nm) (reproduced from ref 115).

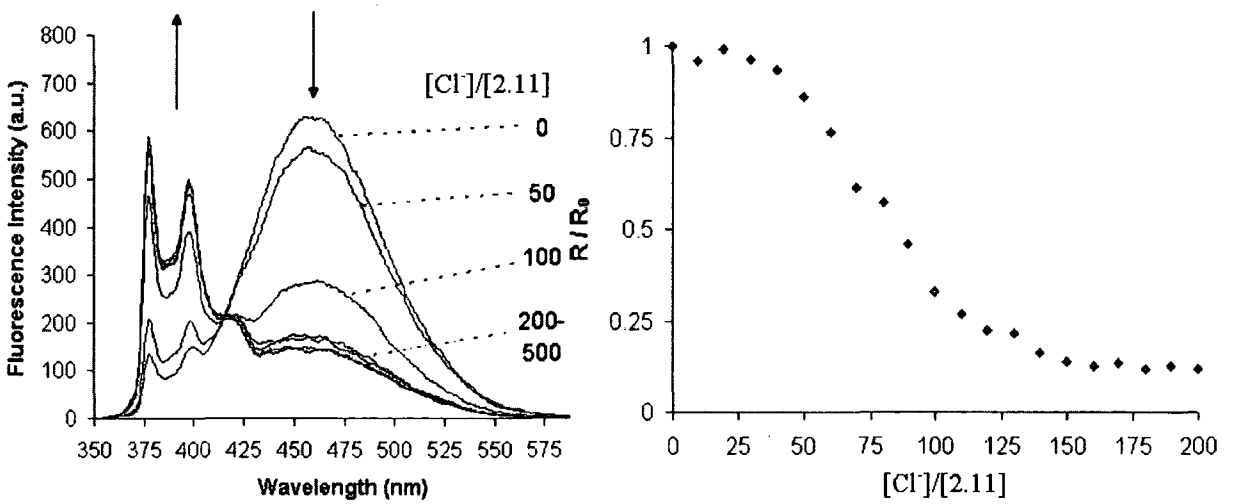

Figure 19 Changes of the fluorescence spectrum of a 1x 10^{-6}M molar solution of **2.11** in acetonitrile-chloroform (95:5 v/v) upon addion of the specified number of equivalents of chloride ([Cl^-]/[**2.11**]. R_0: Ratio of excimer (λ_{em}=452 nm) to monomer (λ_{em}=398 nm) of free **2.11**. R: Ratio of excimer to monomer with varying [Cl^-]. (The excitation wavelength was 340 nm) (reproduced from ref 115).

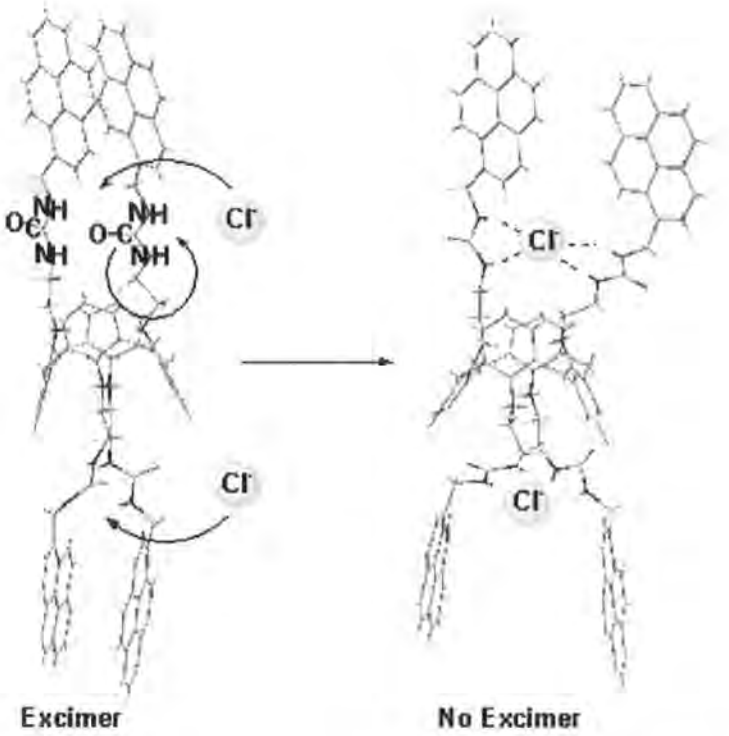

Scheme 5 Binding of chloride ions by **2.11**. Quenching of Excimer Emission (452 nm) caused by a perturpation of the pyrene π-π interaction by the change in conformation of the pyrene moieties (reproduced from ref 115).

Due to the size of the bulky pyrene moieties, which face each other through π-π interaction, there is a confined space for an appropriately sized anion to coordinate with the urea proton. The binding event of chloride anion causes the pyrene moieties to unstack, hence reducing the excimer emission. This behaviour is not observed on addition of F^-, Br^-, I^-, NO_3^-, ClO_4^-, AcO^-, SCN^-, HSO_4^-, $H_2PO_4^-$. This exemplifies the importance of size complementarity which is necessary for an event of binding and signalling. An association constant of $K_{Cl} = 2.4 \times 10^4\ M^{-1}$ was obtained from the change in excimer-to-monomer ratios (by non-linear regression analysis). The isoemissive point at 412 nm indicates that there is only one type of complexing mechanism which is equivalent in both cavities of **2.11**. There was no change in the absorption spectra upon addition of an excess of chloride anion hence the absorption and emission process is confined to the aromatic planar pyrene portion of the receptor (monomer) and the association of two such moieties (excimer). ^1H NMR spectroscopy titration was not carried out to obtain comparable binding constants for Cl^- and the remaining anions.

2.2.2 Upper rim functionalised calix[4]arenes

Whilst the above examples of calixarenes demonstrate their photophysical signalling by either enhanced or decreased photoluminescence upon anion binding, others have proved useful to be effective electrochemical sensors. Beer *et al.* have incorporated successfully ferrocene reporting unit onto the upper-rim of calix[4]arenes through either urea or amide hydrogen bonding units.[43]

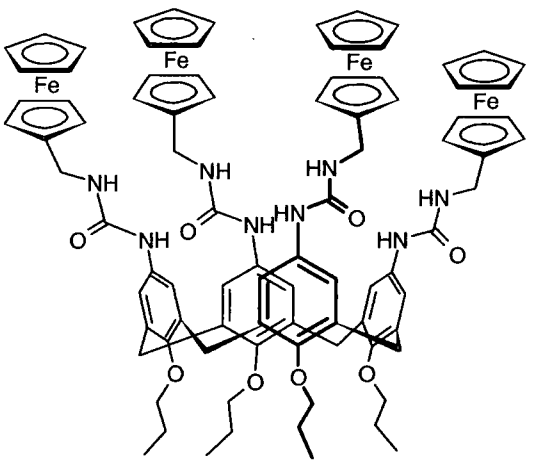

2.12

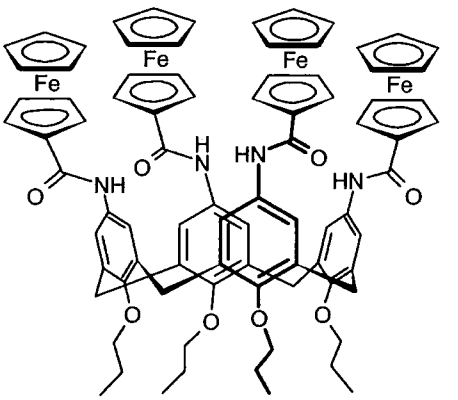

2.13

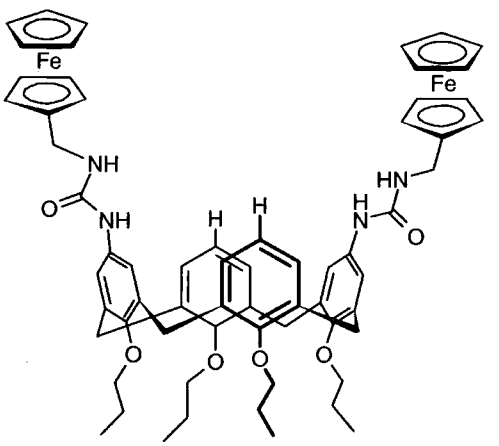

2.14

The ^{1}H NMR spectra of **2.12** in non-polar solvents such as C_6D_6, reveal the formation of solvent-containing dimers which dissociate in polar solvents such as d_6-DMSO. A ^{1}H NMR spectroscopic titration study of **2.12**, **2.13** and **2.14** with chloride, benzoate and dihydrogen

phosphate, added as their tba salts in CD_3CN: d_6-DMSO (1: 1) demonstrates the highest binding constants for **2.13** (K_a=30, 150 and 130 M^{-1}) respectively. The association constants of the disubstituted receptor **2.14** and tetrasubstituted **2.12** with chloride and benzoate are comparable. However host **2.12** binds dihydrogen phosphate six times more strongly than **2.14** due to extra binding sites available for the most basic anion. Interestingly, the introduction of ureas does not result in larger association constants compared to the amide receptor despite the higher acidity and increased anion binding ability of the urea NH protons. With regards to the hosts' electrochemical capabilities as sensors all receptors display a single quasi-reversible oxidation for the ferrocene/ferrocenium redox couple indicating that the ferrocene moieties act independently and are all oxidised at the same potential. Their voltammetric behaviour in the presence of increasing concentrations of anionic guest solutions show significant cathodic perturbations of the ferrocenes' oxidation potential E_{pa}, concomitant with the disappearance of the reduction wave E_{pc}. These cathodic shifts can be attributed to the binding of an anionic guest by the NH protons of the urea and amide groups in close proximity to the ferrocene redox centres, facilitating oxidation to ferrocenium. The disappearance of the reduction wave on anion addition indicates either that the complexed anion–ferrocenium cation interaction is disfavouring reduction back to ferrocene or that an EC mechanism is in operation. [117]

$R \rightleftharpoons Ox + ne$ E step

$Ox \rightleftharpoons P$ C step

The EC mechanism above illustrate oxidation of species R to form species Ox, and Ox undergoing chemical reaction to form product P. If the C step is significantly fast so that Ox is being removed to form P, there will be less Ox remaining near the electrode and the reduction wave E_{pc} disappears.

2.3 Functionalised Cone Calix[4]arenes

2.3.1 Synthesis of starting materials

P-tert-butylcalix[4]arene **2.1** was easily prepared in good yield by the base-induced condensation of *p-tert*-butylphenol and formaldehyde. Aluminium chloride catalysed removal of the *tert*-butyl groups resulted in calix[4]arene **2.2** (Scheme 2), a readily available starting material for the introduction of functional groups onto the upper rim.[118] Bromomethylation of **2.2** was achieved in a single step using a simplified version of the literature procedure (Scheme 6).[119]

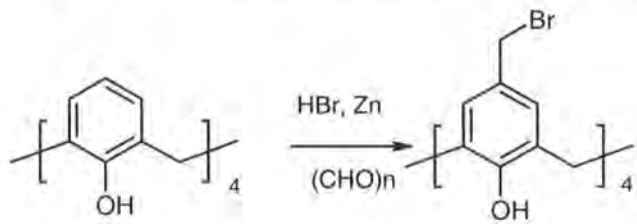

2.2 **2.15**

Scheme 6 Bromomethylation of calix[4]arene.

The characteristic appearance of downfield shifted methylene protons adjacent to bromo substituents was observed at δ 4.26 in the ^{1}H NMR spectrum of the product. A first attempt to recrystallize the product **2.15** from hot methanol resulted in a nucleophilic substitution of the bromide with a methoxy group. The crystals obtained were suitable for X-ray diffraction and the structure is depicted in Figure 20a.

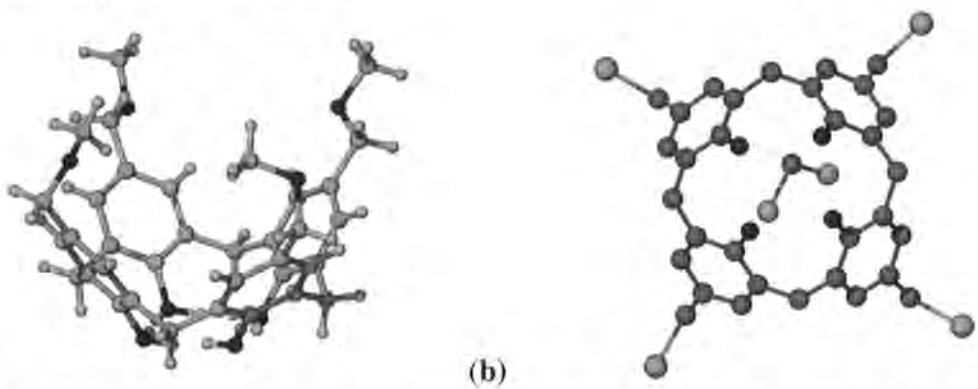

(a) **(b)**

Figure 20 X-ray crystal structures of the methoxy ethyl calix[4]arene a) and bromomethylated calix[4]arene **2.15** with a dichloromethane molecule included in the cavity. The position of protons could not be resolved due to poor quality of the crystal b).

Recrystallisation of **2.15** from much less polar solvent such as hot dichloromethane resulted in the desired pure product as crystals which were suitable for X-ray analysis. The crystals proved to be multiple and were very difficult to solve. However the structure confirms identity of product. It was possible to determine the connectivity of the host's atoms and a presence of one molecule of dichloromethane within the cavity (Figure 20b). The dichloromethane molecule interacts with the π electrons of the aryl rings and the shortest distances are between chlorine atom and the centre of the aryl ring and between hydrogen atom and the centre of the aryl ring. The structure without the dichloromethane has almost four fold symmetry, however, the bromine atoms which point away from the centre of the cavity deviate from this symmetry and the structure as a result falls in monoclinic space group $P2_1/c$ (No. 14). The crystal structure of methoxy ethyl calix[4] arene Figure 20 a) adopts similarly the typical four fold symmetry of the calix[4]arene's main scaffold, the pendant methoxy groups however deviate from the four fold symmetry and crystallise in different orientations with respect to the main scaffold. The cavity contains the methoxy group of neighbouring calixarene. The shortest interactions occur between the methyl hydrogen atoms and the centres of the aryl rings (Figure 21).

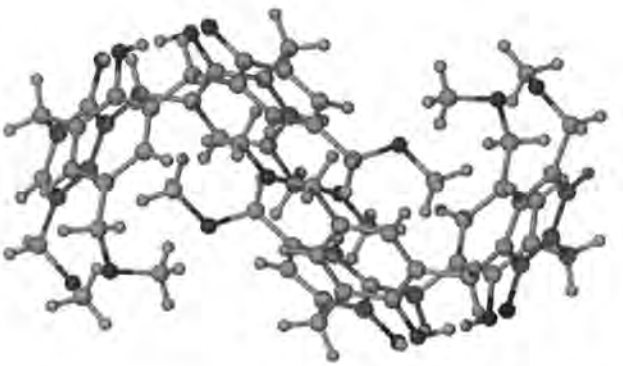

Figure 21 X-ray crystal structure of methoxy ethyl calix[4]arene showing an inclusion of the methoxy groups within the neighbouring host's cavity.

Pendant arms of the general form **2.16** are readily prepared from 3-aminopyridine and the appropriate choice of aldehyde *via* a Schiff-base condensation, followed by the reduction of the imine product with sodium borohydride, (Scheme 7).

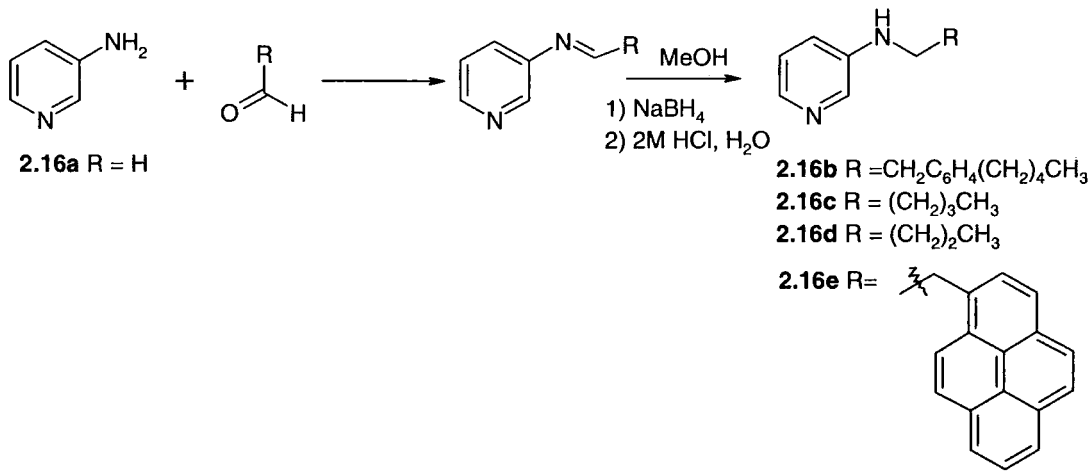

Scheme 7 Preparation of anion-binding "arms" (**2.16b - e**).

The isolation of the intermediate imines for analysis was omitted due to their relatively low stability. The stability of imines is higher for compounds with aromatic rings adjacent to either the amine or the aldehyde group. The equilibrium of the Schiff-base condensation reaction is shifted to the right when water removing agent is present such as $MgSO_4$ or molecular sieves. However, full conversion to imine never occurs (monitored by ^1H NMR). Only in the final step of reduction of imine to amine upon the addition of $NaBH_4$ are the starting materials not detected. Excess aldehyde is used to ensure that no 3-aminopyridine is present in the final product. Column chromatography was avoided as the only reactive reagent towards the bromomethyl group on calix[4]arene in the next step is the lone electron pair on the pyridine. Product **2.16b** can be recrystallised from dichloromethane and n-hexane to produce pure solid at room temperature whereas **2.16c** and **2.16d** only solidify as crystals in the fridge. The only pure intermediate that was possible to isolate as a solid was the imine of **2.16e** due to the aromaticity.

2.3.2 Synthesis of aminopyridine-based receptors.

The reaction of **2.15** with **2.16b** and **2.16c** results in the formation of hosts **2.17b** and **2.17c** in good yield as the tetrabromide salts. The amines shown in Scheme 7 are used in excess and the soluble product is precipitated out by adding diethyl ether. Any unreacted material remains in solution as both **2.16b** and **2.16c** are diethyl ether soluble. The ^1H NMR spectra of compounds **2.17b**·$4Br^-$ and **2.17c**·$4Br^-$ in $CDCl_3$ are consistent with their structure (see experimental section). The CH_2 group adjacent to the nitrogen on the pyridinium moiety shows a distinct singlet, which

is typically observed at 5.29 and 5.36 ppm, whereas the NH proton occurs as broad triplet in the regions of 7.39 and 6.90 ppm, respectively. The position of the resonance assigned to the NH proton depends on the concentration of the sample and it disappears due to exchange with deuterium on addition of D_2O. Compounds **2.17a**·3Br$^-$ and **2.17d**·3Br$^-$ precipitate out of reaction mixture almost immediately and are only soluble in DMSO and CH_3CN : H_2O (1: 1) ratio. All ^1H NMR resonances are very broad and difficult to assign due to fluxionality. Methanol solutions of bromide salts **2.17b**·4Br$^-$ and **2.17c**·4Br$^-$ upon addition of KPF_6 precipitate as the hexafluorophosphate analogues, any excess reagents or impurities remain in the solution. The metathesis hence is a purification step. Compounds **2.17a**·4Br$^-$ and **2.17d**·4Br$^-$ can be converted to the hexafluorophosphate analogues in acetonitrile/water mixture (1: 1) ratio, the products precipitate after 1 h of adding KPF_6. Compounds **2.17b**·4PF_6^- and **2.17c**·4PF_6^- are soluble in acetonitrile and acetone, whereas **2.17a**·4PF_6^- and **2.17d**·4PF_6^- only in acetonitrile. In the hexafluorophosphate salts all of the amine NH resonances are shifted upfield and occur between 6.17 and 5.45 ppm. The NH_2 resonance of **2.17a**·4PF_6^- occurs at 4.20 ppm. The position of the resonance assigned to CH_2 protons adjacent to nitrogen on pyridinium moiety is neither significantly affected by the solvent nor counter cation and remains in the region between 5.20-5.35 ppm.

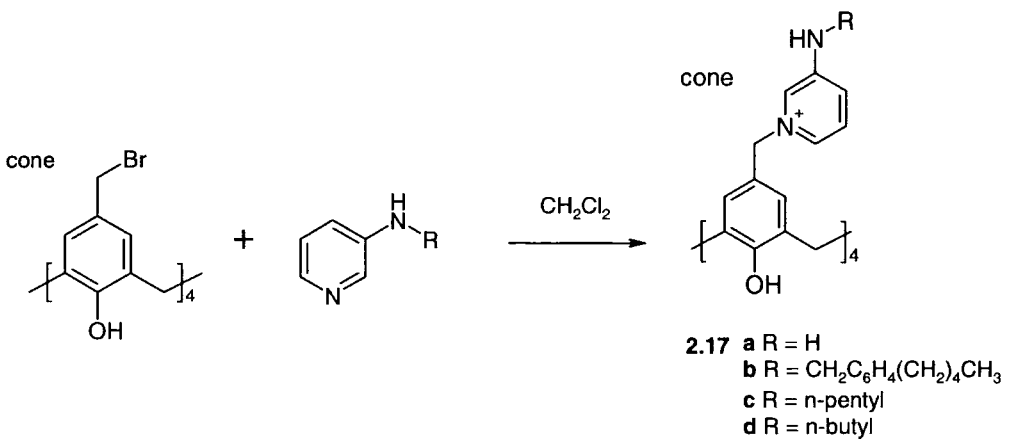

2.17 **a** R = H
b R = $CH_2C_6H_4(CH_2)_4CH_3$
c R = n-pentyl
d R = n-butyl

Scheme 8. Synthesis of bromide salts of hosts **2.17a-d.**

2.3.3 ^1H NMR spectroscopic studies of host-guest association

Due to solubility restrictions only compounds containing long aliphatic chains i.e. **2.17b**·4PF_6^- and **2.17c**·4PF_6^- were studied by ^1H NMR titrations. The binding constants for receptor

2.17b·$4PF_6^-$ and **2.17c**·$4PF_6^-$ with various anion guests were analysed from the least squares fitting program HypNMR[120] and were modelled on the best fit stoichiometry of 1:2, table 1.

Anion	Host K/M^{-1}			
	2.17b·$4PF_6^-$		**2.17c**·$4PF_6^-$	
	K_{11}	K_{12}	K_{11}	K_{12}
Cl^-	6.30×10^3	724	3.98×10^3	23
Br^-	2.45×10^4	1.9×10^3	5.34×10^4	5.61×10^3
NO_3^-	5.13×10^4	912	1.24×10^4	513

Table 1 Binding constants K/M^{-1} for **2.17b**·$4PF_6^-$ and **2.17c**·$4PF_6^-$ with various anions analysed from the least square fitting program HypNMR[120]. Errors (<5%).

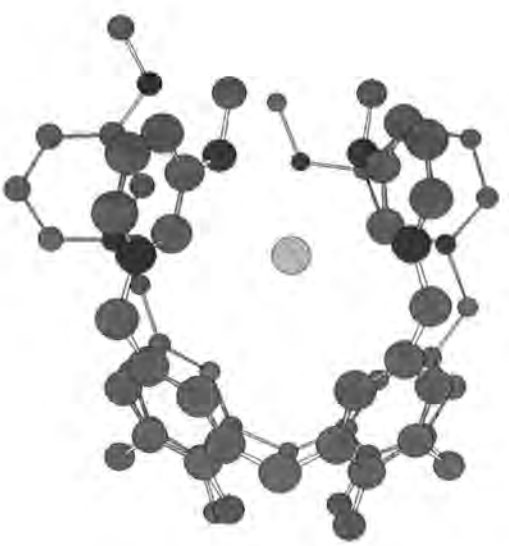

Figure 22 3D model of possible encapsulation of chloride anion within cavity of Tetra[(3-(methylamino)pyridinium-methyl) tetrahydroxyl]calixarene.

The magnitude of binding constants clearly demonstrate the size and geometry relation between the calix[4]arene's cavity and the anion. Both receptors show the highest affinity amongst halides for Br^-. This represents a reverse selectivity compared to that observed for the tripodal analogues and may be linked to the larger cavity of the calixarenes. Receptor **2.17b**·$4PF_6^-$ has significantly higher K_{11} for Cl^- than its analogue **2.17c**·**4**PF_6^-. The presence of more bulky benzyl groups in compound **2.17b**·$4PF_6^-$ may aid some conformational change to accommodate the

chloride anion. Interestingly the host which does not possess the benzyl groups i.e. **2.17c**·$4PF_6^-$ has higher affinity for the larger bromide anion. The binding constants may be related to the ease of entering the cavity by anions and hence to the fluxionality of the host. The presence of benzyl groups may impede such movement. Bulky benzyl groups may interfere with incoming anions such as bromide with diameter larger than that of chloride. The presence of benzyl groups however accounts for much stronger binding of **2.17b**·$3PF_6^-$ with NO_3^- possibly due to the π-π interaction and a good fit of large anion within the cavity. It was noted in all the titrations that upon addition of first equivalent of anion the cone calixarene becomes less fluxional. The ^1H NMR resonance assigned to methylene protons is very broad at room temperature in CD_3CN. Addition of one equivalent of NO_3^- to **2.17c**·$4PF_6^-$ causes the broad resonance to split into two resonaces which is indicative of two nonequivalent protons in the cone calix[4]arene (inside and outside)(Figure 23). The splitting may also be a result of displacing of solvent from the cavity.
The anion-receptor interaction is expected to produce two general phenomena: 1) an increase in the electron density on the host pyridine rings by through-bond propagation, which causes shielding effect and should promote an upfield chemical shift of the C-H resonaces; and 2) polarization of the C-H bonds, induced by a through-space effect, of electrostatic nature resulting in partial positive charge on the C-H bond hence deshielding it (downfield shift). The second effect ceases with a distance and only the C-H bonds close to the interaction site are affected.[96] A 3D model generated by molecular mechanics in Chem3D (Figure 22) gives some indication how the pyridine units are spatially arranged around chloride anion in the cone calix[4]arene with a general structure of **2.17** . The model can be further supported by ^1H NMR titrations following the pyridyl resonances. The resonances assigned to the pyridyl protons closest to the NH binding site 1) and 2) upon addition of anions undergo a downfield shift whereas pyridyl protons that are the farthest from the binding site such as 3) and 4) undergo a slight upfield shift.

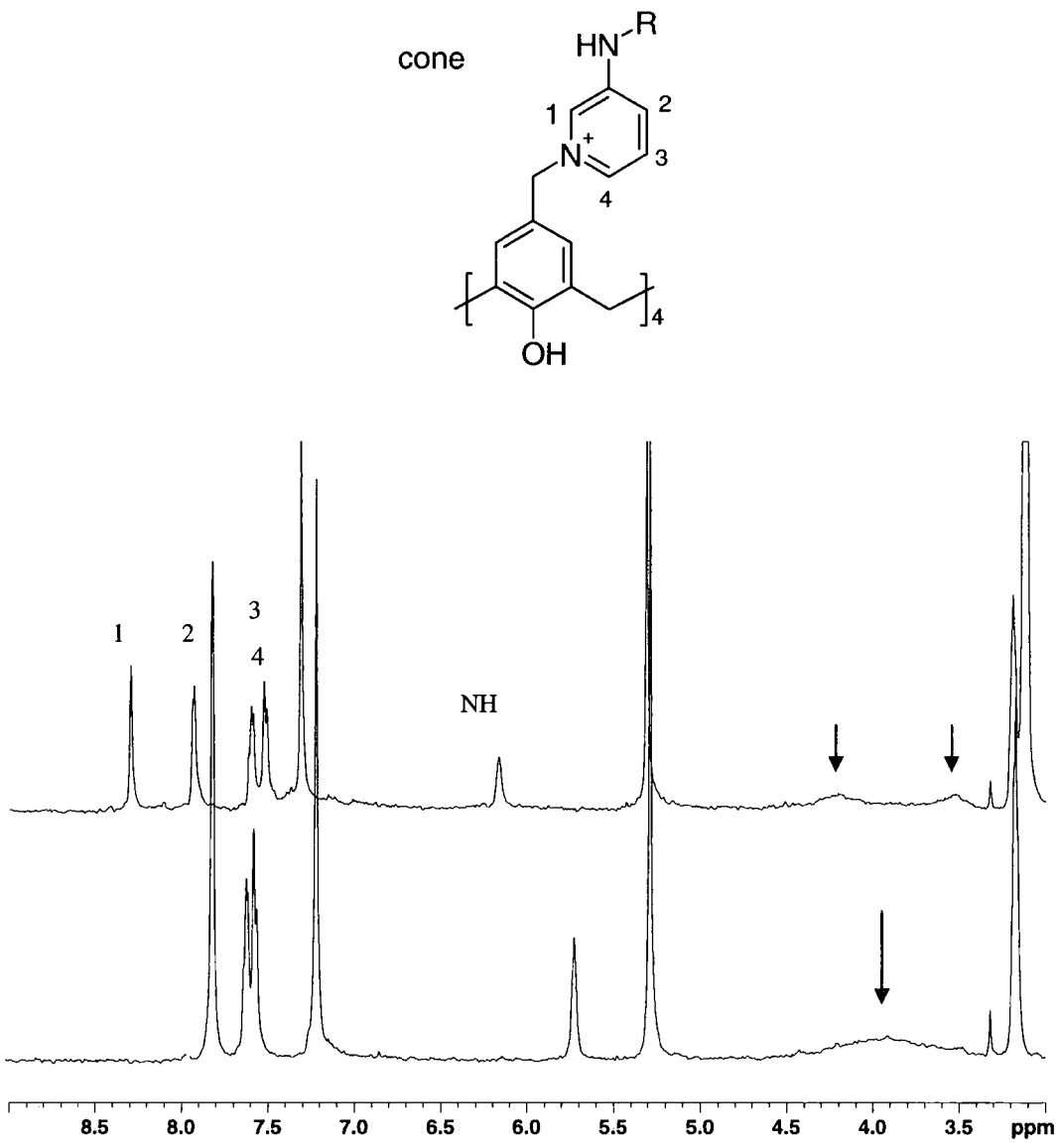

Figure 23 ^{1}H NMR plots of pure host **2.17c**·4PF_6^- in CD_3CN (bottom plot) and upon addition of one equivalent of tba NO_3^- (top plot). The arrows point at the resonances assigned to the methylene protons which become nonequivalent (top plot).

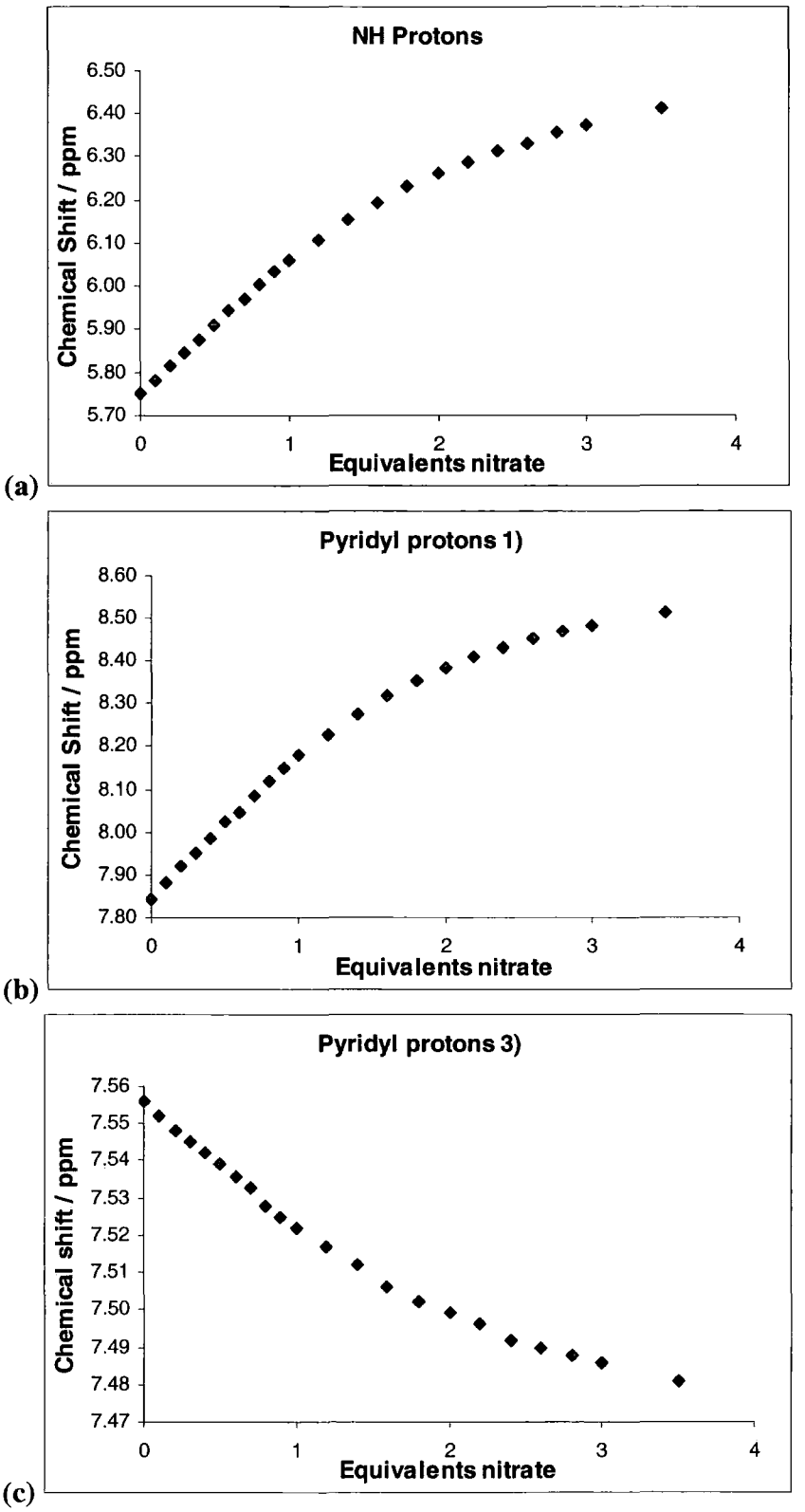

Figure 24 ^{1}H NMR titration plots for **2.17c**·4PF_6^- with tetrabutyl ammonium nitrate following the resonance of NH protons **a)** pyridyl protons 1) **b)** and pyridyl protons 3) **c)** in CD_3CN-d_3.

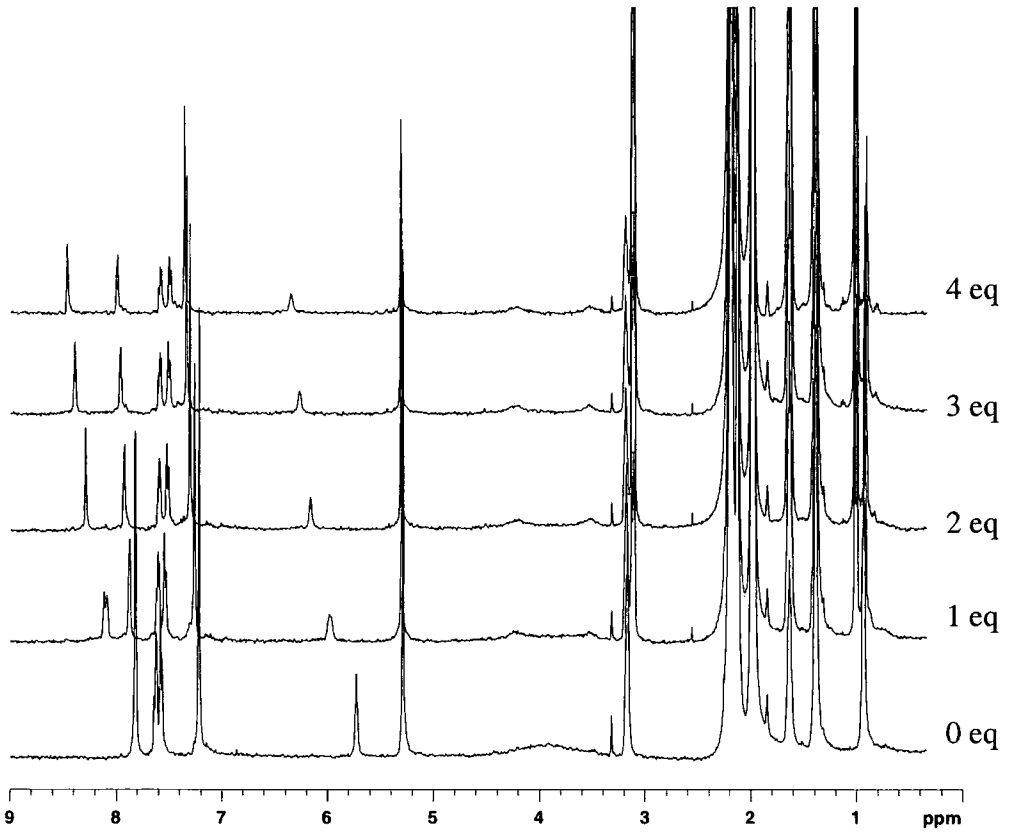

Figure 25 Stack plots showing the chemical shift of the NH and PyH protons of receptor **2.17c**·$4PF_6^-$ titrated with 0, 1, 2, 3 and 4 equivalents of tba nitrate in CD_3CN-d_3.

In all the cases the K_{12} values are much lower than K_{11} which results from charge quenching on addition of the first equivalent. On titration with acetate and dicarboxylates, there was little change in the chemical shift of the NH resonances until after one equivalent of acetate, or 0.5 equivalents of the dicarboxylates had been added, at which point binding commenced. This behaviour was interpreted as deprotonation of one calixarene OH proton by these relatively basic anions. Related behaviour has been observed for deprotonation by F^- by Gale *et al.* in a series of pyrrole clefts,[121] and remarked upon for $H_2PO_4^-$ by Beer *et al.*[46] This enhanced acidity presumably arises from the stabilisation of the phenolate anion by the pyridinium moiety. Indeed, over time, elimination was observed accompanied by the formation of free **2.16b** and **2.16c** consistent with the good leaving group character of the pyridinium group. The acidity of

2.17c·$4PF_6^-$ was probed by potentiometric titration with tba acetate in 90% DMSO-water solution (following rigorous calibration of the pH electrode in DMSO-water mixtures and taking adequate precautions to eliminate CO_2 interference) in collaboration with Drs. Ritu Kataky and Jaanus Kruusma. The resulting titration curve gave a good fit to a single deprotonation process with pK_a 4.4(5), consistent with the NMR results.

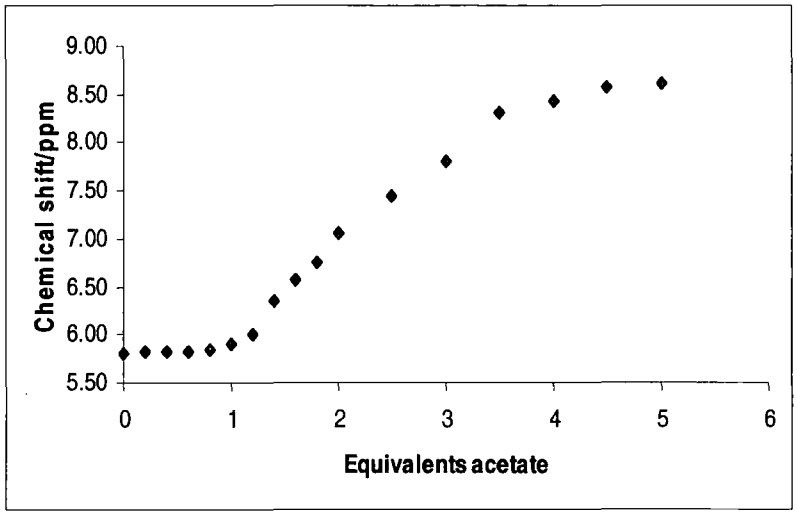

Figure 26 ^{1}H NMR titration plot of **2.17c**·$4PF_6^-$ with tba acetate in CD_3CN-d_3, following the NH resonance.

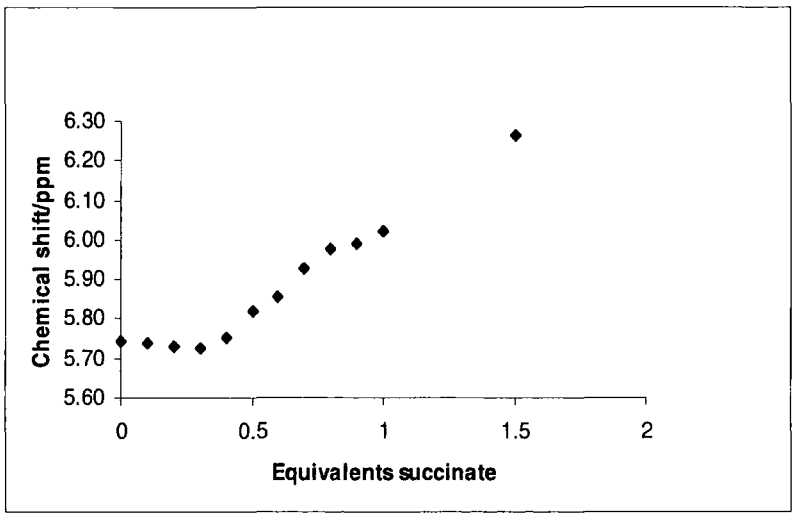

Figure 27 ^{1}H NMR titration of **2.17c**·$4PF_6^-$ with tba succinate in CD_3CN-d_3, following the NH resonance.

2.3.4 ^{1}H NMR (VT) Variable Temperature Experiments

Hosts **2.17b**·4PF_6^- and **2.17c**·4PF_6^- were both subjected to variable temperature ^{1}H NMR experiments as pure compounds and also with presence of one equivalent of chloride anion in d_6-acetone. The resonances generally sharpened at temperatures around -40°C and broadened at the lowest temperature of -70 °C. The low temperature broadening is attributed to slow exchange on the NMR time scale between various conformers of the host. The presence of one equivalent of anions at room temperature in CD_3CN-d_3 reduces the fluctionality in comparison to the host with none (Figure 23), however this phenomena can not be observed in d_6-acetone as strong hydrogen bonding within the array of hydroxide protons prevails in this solvent at all times and the methylene resonances always appear as either two sets of sharp doublets or very broad doublets at low temperatures. When the hydroxide protons do not hydrogen bond between each other the OH protons exchange with water, this phenomena is concomitant with the appearance of broadness of the methylene hence increase in calix[4]arene fluxionality.

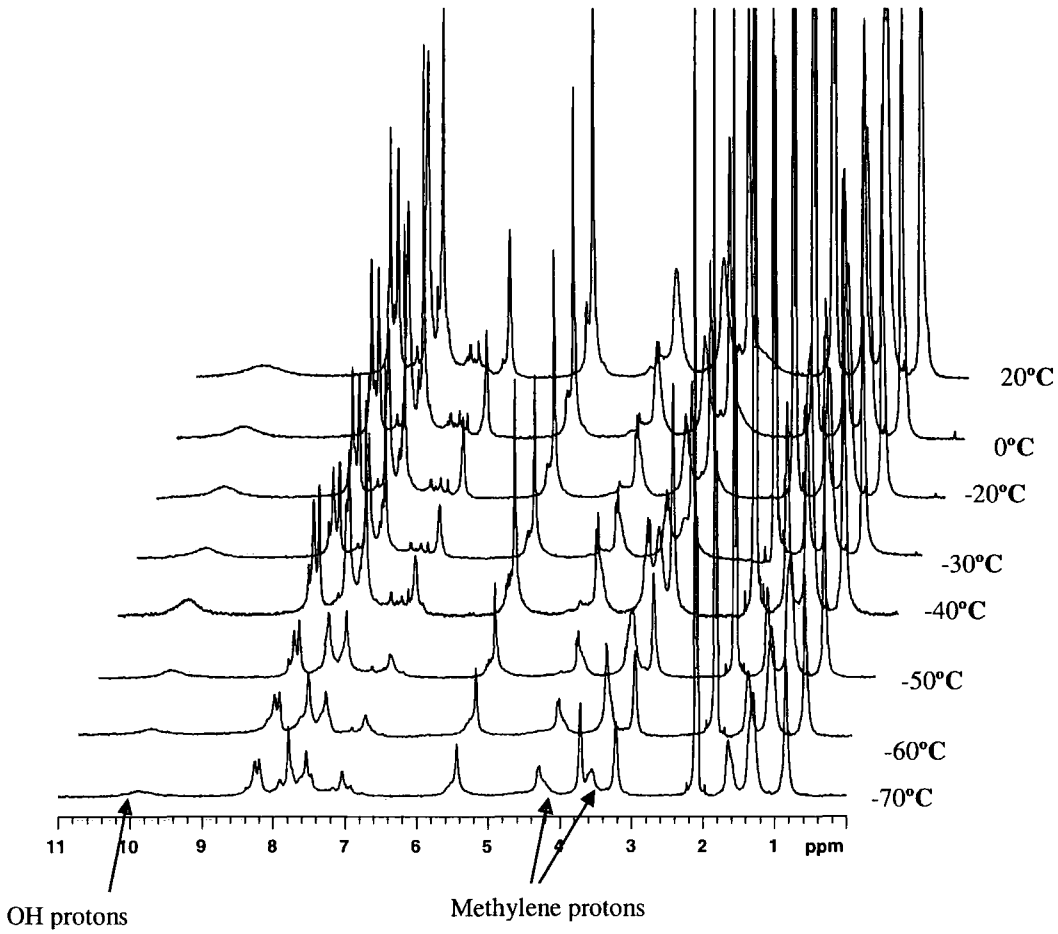

Figure 28 ^{1}H NMR VT experiment of **2.17c**·4PF_6^- in d_6-Acetone.

2.4 A ditopic receptor based on a 1,3-alternate calix[4]arene

2.4.1 Synthesis of 1,3-alternate calix[4]arene

The tetrakis hydroxyl derived from **2.18** cone calix[4]arene scaffold can be substituted by a 1,3-alternate mesityl calix[4]arene which adopts a fixed conformation. A beneficial feature of this compound is the lack of hydroxy groups para to the pyridinium cations. The hydroxy groups are relatively acidic and become deprotonated upon addition of basic anions such as dicarboxylates, thus reducing the stability of the complex (section 2.3.3 p. 45). The mesityl hydrocarbon calix[4]arene **2.18** is readily prepared from α'-chloroisodurene.[35, 122] It is locked into a 1,3-alternate conformation of the aryl rings with very little flexibility around the methylene linkers. This limited flexibility arises from the presence of three bulky methyl groups on the aryl rings. The scaffold has been used previously for organometallic units,[54] as a nitrile or pyridyl derivative, and as a ligand in the formation of coordination arrays.[123, 124] Reactions of **2.18** with formaldehyde in the presence of Zn-HBr results in a facile bromomethylation of the aryl rings to give **2.19**.[125]

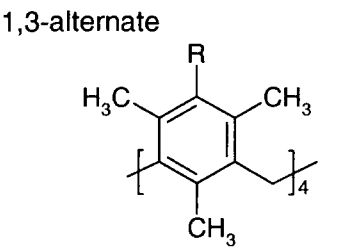

2.18 R=H
2.19 R=CH_2Br

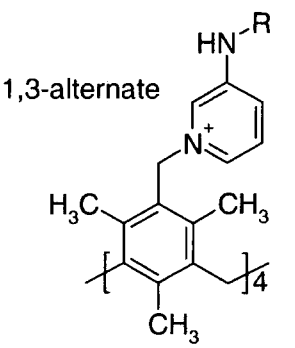

2.20a R = $CH_2C_6H_4(CH_2)_4CH_3$

e R =

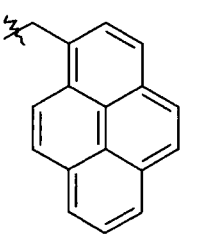

Reaction of **2.19** with 3-aminopyridine derived ligands **2.16b** and **2.16e** results in the corresponding hosts **2.20a** and **2.20e**. Ion exchange metathesis as previously demonstrated for the cone calix[4]arenes in section 2.3.1. convert the bromide salts **2.20a** and **2.20e** into the hexafluorophosphate analogues. Both **2.20b**·$4PF_6^-$ and **2.20e**·$4PF_6^-$ are acetonitrile and acetone soluble. Characteristic resonances assigned to the CH_2 protons adjacent to pyridinium peaks occur at 5.50 and 5.30ppm and NH proton peak occur at 6.20 and 6.40 ppm respectively in CD_3CN. A singlet for the methylene linkers confirms 1,3-alternate structure for all four compounds **2.18, 2.19, 2.20a** and **2.20e**. The X-ray crystal structure of **2.20a**·$4Br^-$ (Figure 29)[125] obtained by Mr. T. D. Humphries, shows that the four pyridinium arms are splayed out and bent backwards from the calixarene. Each of the arms interacts *via* a single NH unit with Br^- anion via NH···Br^- and longer CH···Br^- interactions as seen in related triethylbenzene based systems. The calixarenes are arranged in pairs about a cavity that appears to contain two CH_2Cl_2 solvent molecules, two bromide anions and the unresolved alkyl chains of the host.

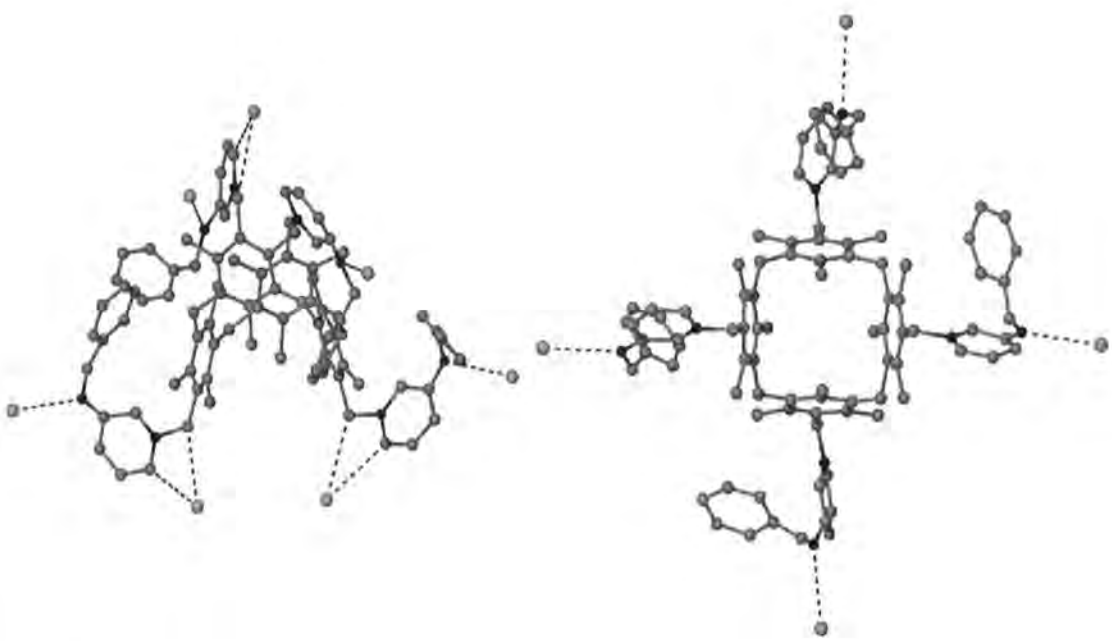

Figure 29 X-ray crystal structure of the pentylbenzyl species **2.20a**·$4Br^-$ showing the splayed conformation of the pyridinium arms, each interacting with a single Br^- anion. The *n*-pentyl chains are disordered and were not located experimentally (ref 125).

2.4.2. ^{1}H NMR spectroscopic studies of host-guest association.

The ^{1}H NMR titration study of **2.20a**·4PF_6^- in CD_3CN-d_3 confirms the lack of cooperativity between the arms in Br^- and Cl^- binding with K_{11} of only 646 M^{-1} and 1.78 x 10^3 M^{-1}, respectively (Table 2) consistent with the crystal structure. Much stronger interactions were observed between **2.20a**·4PF_6^- and carboxylate anions with K_{11} reaching 5.88 x 10^4 M^{-1} for malonate^{2-} despite more competitive solvent being used (CD_3CN-d_3: DMSO-d_6 60: 40) due to reduced solubility. The stoichiometry, determined by Job Plot method (see appendix 1 in experimental section), is consistent with the titration curves for malonate^{2-} as a 1: 2 host: guest ratio. Unfortunately the job's plot could not be completed due to solubility constrain. It is not possible to observe the relative resonances at host to guest ratios of 1: 9, 2: 8 and 3: 7 as the dilutions are very high, but had to be used to avoid precipitation. Because of this uncertainty there may be other modes of binding with ratios of host to guest being 1: 1 or possibly 1: 4. The postulated ditopic behaviour of is depicted in Figure 30. The malonate^{2-} anions are chelated by pairs of pyridinium arms *via* NH···O and CH···O interactions.

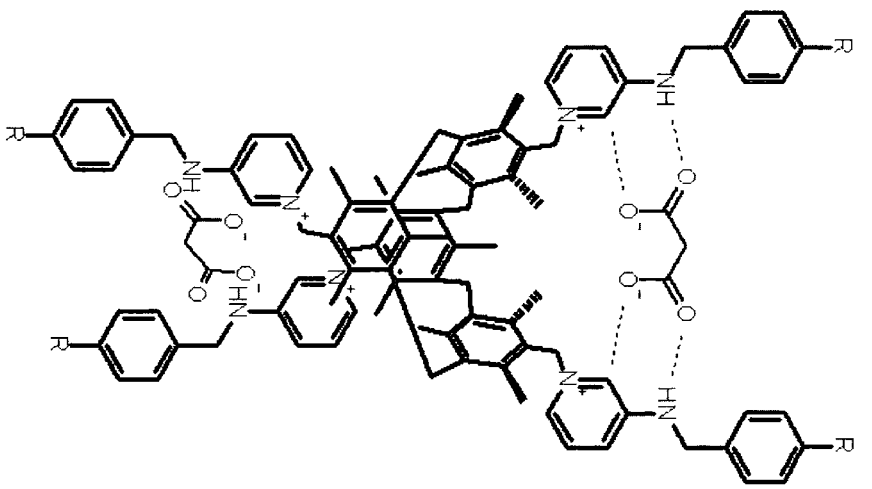

Figure 30 Model for 1: 2 ditopic anion binding.

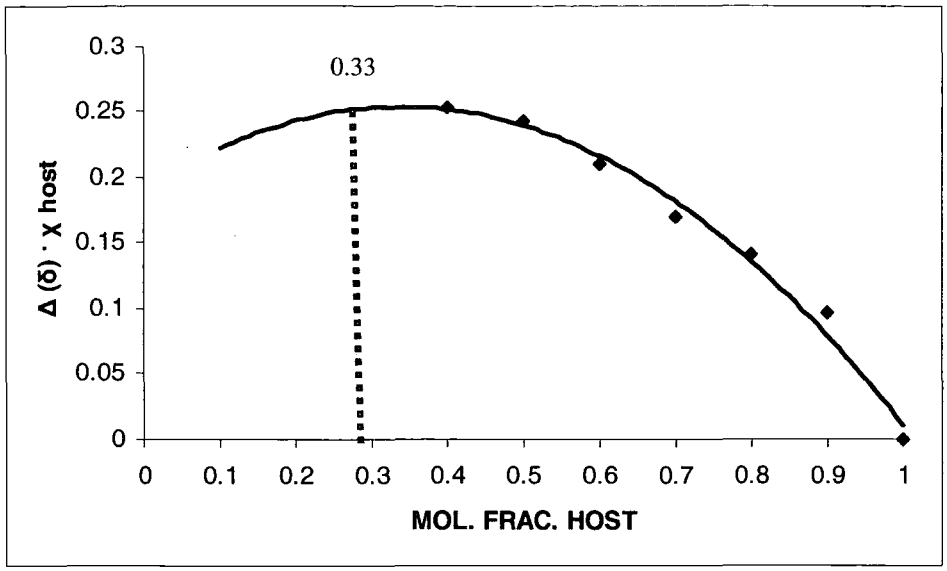

Figure 31 Job plot of **2.20a**·$4PF_6^-$ in CD_3CN-d_3 with malonate following the NH resonance. The maximum chemical shift occurs when the ratio of host to guest is 1:2 pointed by the dotted line at 0.33. See appendix 1.

Anion	Host K/M^{-1} **2.20a** ·$4PF_6^-$	
	K_{11}	K_{12}
Cl^-	1.78×10^3	355
Br^-	646	467
NO_3^-	3.09×10^3	302
AcO^-	9.55×10^3	9.33×10^3
$Malonate^{2-}$	$5.88 \times 10^{4\,b}$	83^b
	$2.72 \times 10^{3\,c}$	15^c
$Succinate^{2-}$	$2.69 \times 10^{3\,c}$	37^c

Table 2 Binding constants in MeCN-d_3 for **2.20a** ·$4PF_6^-$ host with various anions.

[a] Anions added as $N^nBu_4^+$ salts, host concentration 0.5-1.5 mM depending on solubility. [b] In MeCN-d_3:DMSO-d_6 60:40. [c] In DMSO-d_6 at 60°C. Errors (<5%).

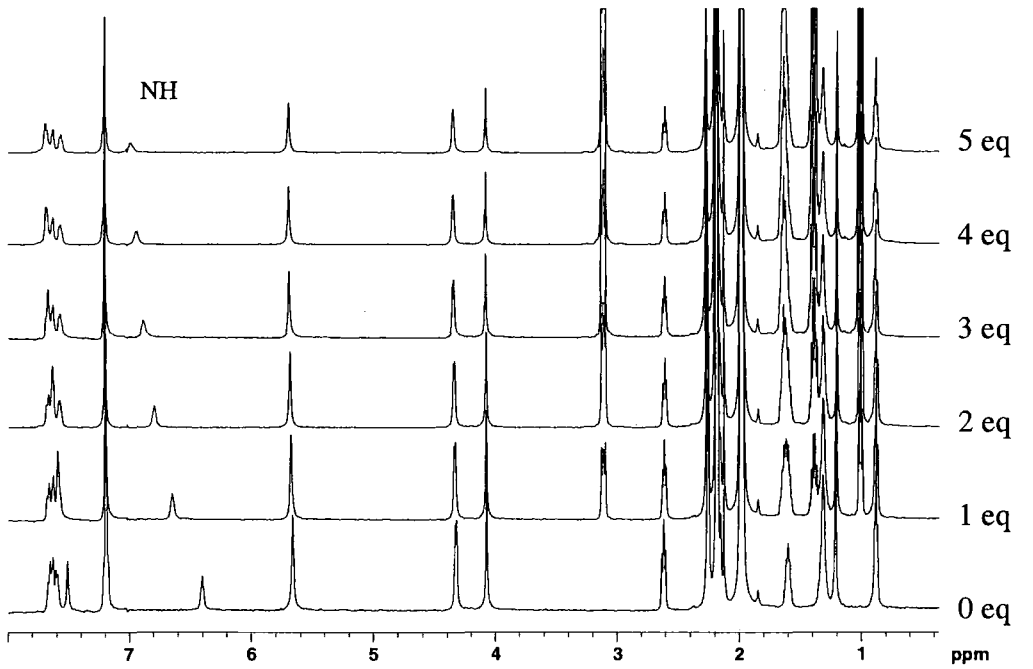

Figure 32 Stack plots showing the chemical shift of the NH and PyH protons of receptor **2.20a**·$4PF_6^-$ titrated with 0, 1, 2, 3, 4 and 5 equivalents of tba nitrate in CD_3CN-d_3.

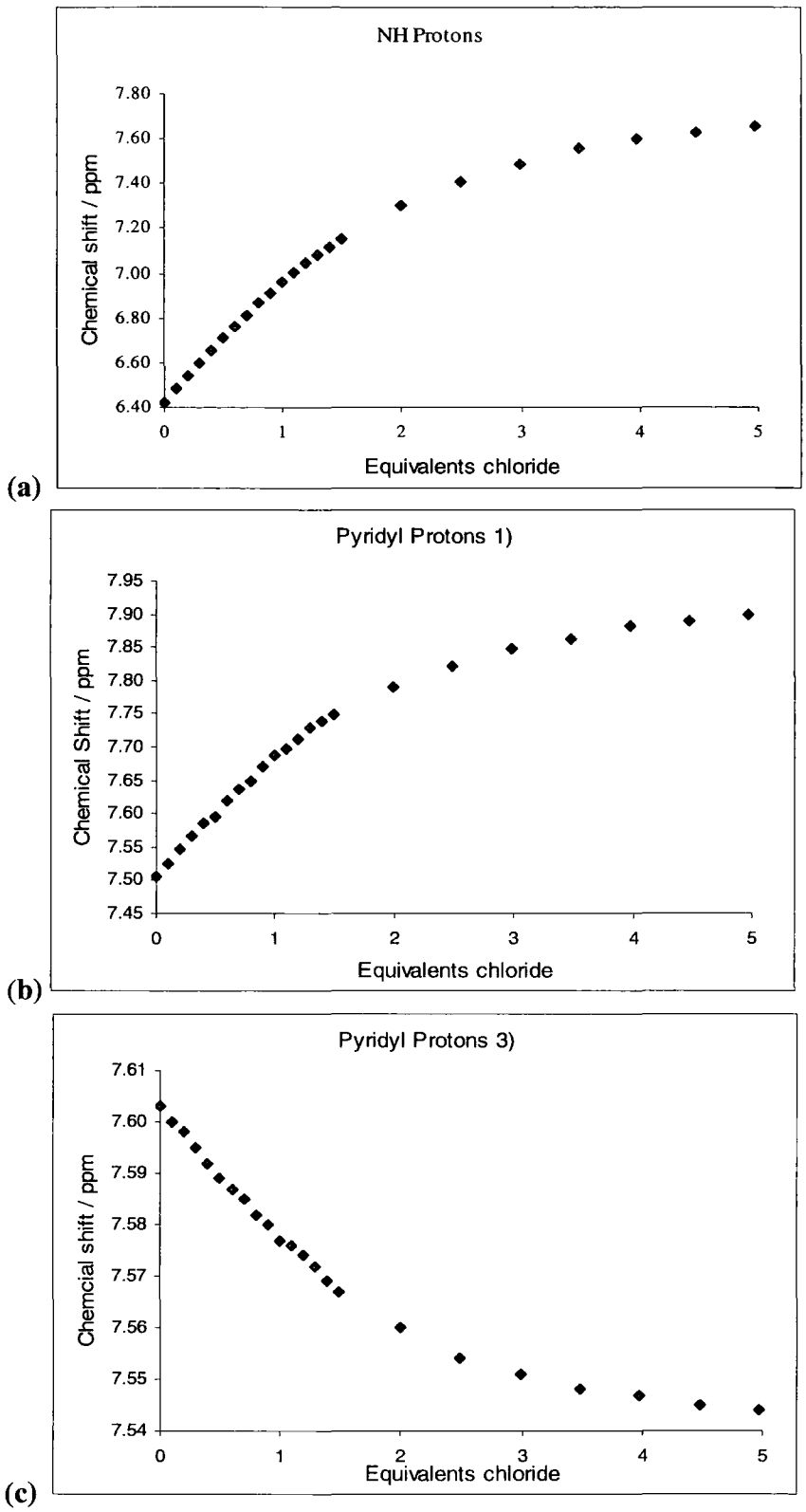

Figure 33 ^{1}H NMR titration plots for **2.20c**·4PF_6^- with tba chloride following the resonance of NH protons **a)** pyridyl protons 1) **b)** and pyridyl protons 3) **c)** in CD_3CN-d_3.

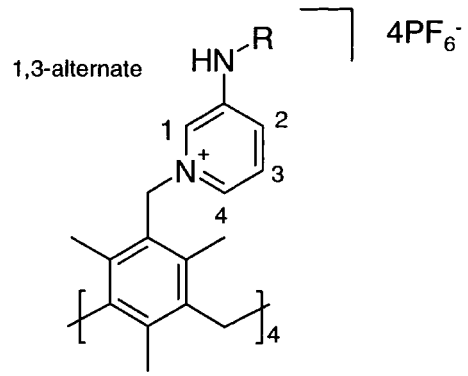

R=$CH_2C_6H_4(CH_2)_4CH_3$

2.20a·$4PF_6^-$

The resonances assigned to NH and pyridyl protons upon titrations with anions behave in a fashion similar to the ones of the cone calix[4]arene described in section 2.3.3. As portrayed in Figure 33 the NH and pyridyl protons hydrogen bond to anions splitting the pyridyl resonances into two types of behaviour: downfield and upfield shifts depending on the distance from incoming anion.

2.5 Conclusions

Magnitudes of the binding constants K_{11} and K_{12} of host **2.20a**·$4PF_6^-$ with Cl^- and Br^- suggest selectivity towards smaller chloride anion, although both values are relatively modest. There were only very small shifts in ^1H NMR resonances when titrations with the halides were carried out in DMSO. In order to obtain reasonable chemical shift changes, CD_3CN-d_3 solutions were prepared however very low concentrations were used due to solubility problems. At higher concentrations resonances were much clearer but the complexes precipitated very quickly particularly on addition of halides. At lower concentrations on the other hand, the resonances became very weak and much longer acquisitions times were needed. Slightly higher affinity for nitrate was observed possibly due to π-π overlap between the benzyl and N=O groups. The second binding constant is much lower in almost all the cases suggesting a potential charge quenching on the pyridinium cation upon binding of the first anion. Since receptor **2.20a**·$4PF_6^-$ is ditopic and there is a considerable degree of fluxionality between the pyridinium appendages, another plausible explanation is that a conformational change upon binding of the first anion could account for the second affinity constant being much lower due to negative allosteric effect.

The most noticeable difference between K_{11} and K_{12} was being observed for binding between the host and dicarboxylates. This behaviour is most likely due to the high basicity of the anions and also their size which could be inducing an allosteric effect. A situation where a ditopic receptor only binds one anion stoichiometricaly has been observed by Lhotak *et al.* who noticed that the tetrakis(phenylureido)calix[4]arene **2.21** with two possible binding sites exhibits a strong allosteric effect which leads to exclusive complexation of only one anion. Receptor **2.21** shows selectivity towards halides in the order $Cl^- > Br^- > I^-$ with corresponding constants K_{11}=4660, 1450 and 570 M^{-1} respectively in $CDCl_3$:CD_3CN-d_3 4:1 solvent mixture. The complexation of the first anion results in outstretching of the two ureido clefts engaged in the binding to adopt the ideal mutual distance needed for hydrogen bonding. As a consequence the two propoxy groups on the opposite site of the 1, 3 -alternate receptor **2.21** become closer to each other thus disturbing the geometry suitable for binding of a second anion. This behaviour is illustrated in Figure 34.[126]

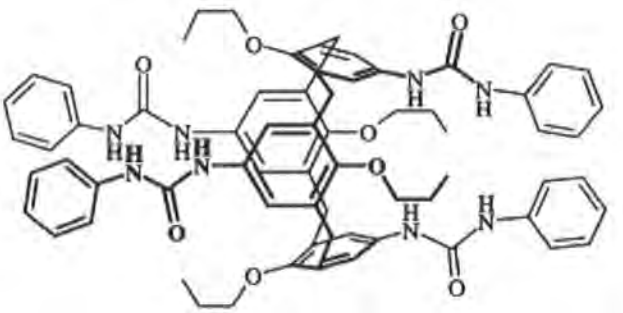

2.21

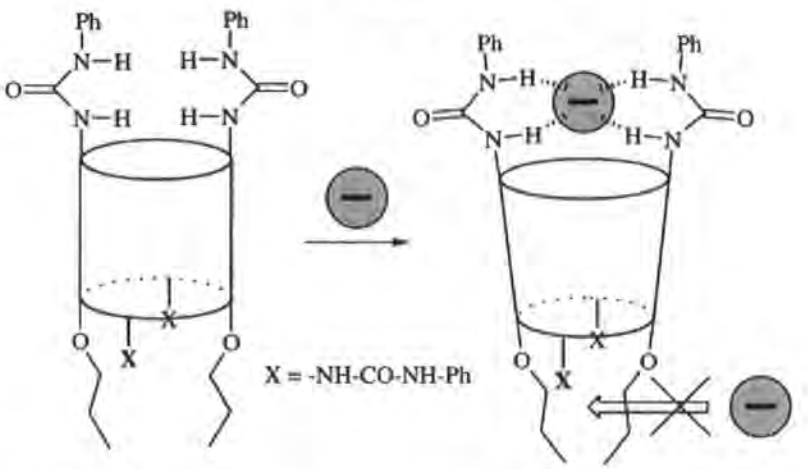

Figure 34 Exclusive formation of complex 1:1 in derivative **2.21** (reproduced from 127).

In case of the cone calix[4]arenes both hosts **2.17b**·$4PF_6^-$ and **2.17b**·$4PF_6^-$ bound Br^- and NO_3^- much stronger than the ditopic calix[4]arene. The differences between K_{11} and K_{12} are not as significant as in **2.20a**·PF_6^-, indicating strong affinity for further anions after addition of the first equivalent.

Since the aminopyridinium group has been utilised for the first time with the calix[4]arene scaffold, the comparison to association constants reported by others is not appropriate. The nature and number of functional binding groups, solvent and method of obtaining such constants have to be considered.

Beer *et al.* have utilised amide moiety in a combination with cobaltocenium both as a bridging unit in disubstitued cone calix[4]arene **2.22** and as two separate binding entities in **2.23**. The bridged calix[4]arene selectively binds carboxylates, particularly benzoate (K_a=4.2 x 10^4 M^{-1}) in DMSO-d_6, over other simple anions e.g. Cl^-, NO_3^-, $H_2PO_4^-$. The rigidity of **2.22** contributes towards the receptor's selectivity. The high binding constants arise from the electrostatic charge on the metal cation. Biscobaltocenium receptor **2.23** on the other hand binds much longer dicarboxylates, particularly adipate, in comparison to oxalate or malonate which was observed by the largest chemical shift in ^1H NMR spectra of the host (in acetone-d_6). [105]

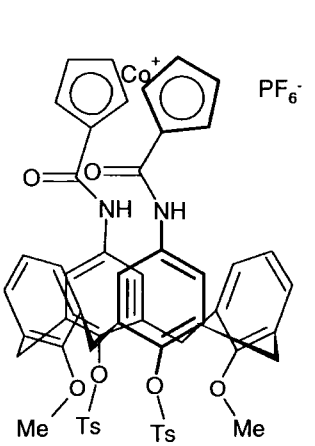

2.22

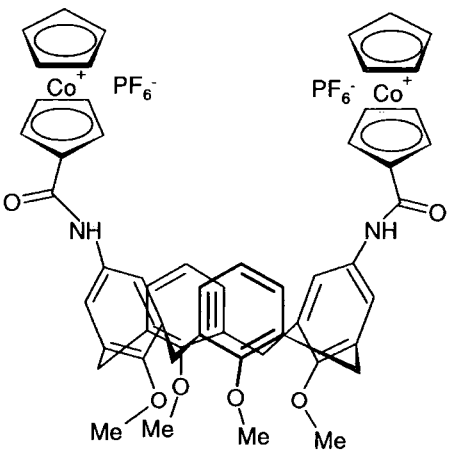

2.23

A similar amide binding motif has been used by Loeb *et al.* The directionality provided by the two amides in close proximity are in an appropriate orientation for carboxylate recognition. Receptor **2.24** has been found to bind tba benzoate (K_a=107 M^{-1}) selectively over a range of other simple anions. The highest downfield shift has been observed for the amide protons indicating an interaction shown in Figure 35. Substituting one H atom for Cl in **2.24**, results in much higher

binding constant with tba benzoate (K_a=5.2 x 10^3 M^{-1}) in $CDCl_3$, due to the increased electron withdrawing effect of group X.[127] The change in conformation upon binding benzoate to adopt pinched cone has been followed by ^1H NMR. Interestingly host **2.24** also binds oxalate anion in 1:1 stoichiometric ratio, this time the unsubstituted rings are parallel. However, larger dicarboxylate anions such as isophthalate, terephthalate and fumarate were found to bind the host in 1:2 ratio (guest to host), also determined by Job plot.

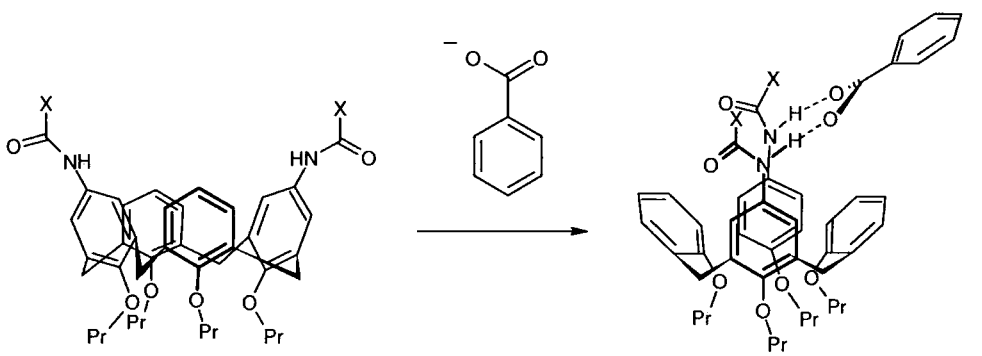

2.24 X=CH_2Cl
2.25 X=$CHCl_2$

Figure 35 Ditopic receptor developed by Loeb *et al.* The calixarene adopts a 'pinched cone' conformation with the calixarene rings attached to the two amide groups becoming parallel, so allowing the amide groups to align in a complementary manner to the carboxylate guest (reproduced from ref 127).

2.6 1,3-Alternate Calix[4]arene as a molecular sensor

The high selectivity for dicarboxylates exhibited by **2.20a** was an inspiration to synthesize an analogous host which could transduce the selective binding into an observable signal. It was expected that a relatively flexible receptor would offer the possibility of induced fit signal transduction in which analyte binding results in a conformation change that brings about signal generation. The aminopyridinium-based receptors can be developed further, by incorporating sensing moieties into the framework of the molecular host. [20] Pyrene and its many derivatives have very versatile photophysical and photochemical properties. The widespread use of pyrene in supramolecular systems has been discussed in section 2.1. Pyrene can be incorporated into a

calixarene scaffold via anion binding linkers in an analogous synthetic procedure to the preparation of **2.20a** to give host **2.20e**·$4PF_6^-$.

2.6.1. Synthesis of tetra[3- (Pyren-1-ylmethylamino)pyridinium-mesityl]calixarene

The reaction between **2.19** and **2.16e** was attempted several times manipulating both the duration and temperature. The monitoring of the reaction's progress was impeded due to precipitation of the products within 0.5 h, hence progress was difficult to follow by ^{1}H NMR means. The final disappearance of **2.19** from the reaction mixture was an indication of completion having taken place. Ultimate optimal conditions of the reaction were 48 h in dichloromethane at room temperature. Any higher temperatures resulted in **2.16e** breaking into free pyrene and 3-aminopyridine (seen in the final products by ^{1}H NMR spectroscopy). The probability of interaction of the bulky **2.16e** with **2.19** can only be achieved thus by the increased time and using an excess (5 equivalents) of **2.16e**. The excess amount of **2.16e** can then be rinsed off the precipitate with dichloromethane. The product as the bromide salt is only soluble in DMSO or acetonitrile/water 1: 1 mixture. The salt metathesis can be carried out in the latter solvent mixture by adding 10 equivalents of $NaPF_6$ upon which the pure hexafluorophosphate analogue precipitated out within 0.5 h. The difference in position of resonances assigned to NH and pyridyl protons between both salts is minimal. The comparison can only be carried out in DMSO-d_6 which is a very highly coordinating solvent.

2.6.2 ^{1}H NMR spectroscopic studies of host-guest association

The anion binding behaviour of the pyrene-incorporating calixarene **2.20e** in solution, as its hexafluorophosphate salt, has been studied through the use of ^{1}H NMR titration. The host is soluble in acetonitrile and acetone, however on addition of tba salts of chloride, bromide or malonate it readily precipitates and very low concentrations had to be used in order to avoid this difficulty. Both deuterated acetonitrile and acetone have been used as solvents in this experiment. Acetonitrile being more polar, however causes severe broadening of some resonances, particularly the NH one. As the resonance assigned to the NH proton chemical shift is the best indication of the strength of hydrogen bonding with the anion, several anion titrations

are depicted in Figure 36 following this resonance. The binding constants from acetonitrile solution titrations could not be determined and the data gave poor fit, whilst the titrations carried out in acetone could not be completed due to the adducts precipitating out. Hence the curvature was never obtained and came to a plateau. However the initial shape of the curve and its tangental gradient gives some indication of differences in magnitude of binding constants between selected anions. Additionally the chemical shift of the NH resonance is very dependent on the concentration of the sample and on the solvent used. The position of NH resonance of **2.20e**·$4PF_6^-$ in acetone occurs at around 7.45 ppm in acetonitrile at 6.4-6.7 ppm and in DMSO at 8.03 ppm. The solvent effects play a crucial role in the titration. The polarities of the solvents are comparable (0.881 for acetone versus 0.895 for acetonitrile obtained from Solvent Polarity/Polarizability Scale SPP[128]) therefore this property does not affect the chemical shift of NH resonance.[129] It is hence assumed that the sulfinyl group of DMSO and ketyl group of acetone hydrogen bonds to the active sites more strongly than the nitrile group of acetonitrile.

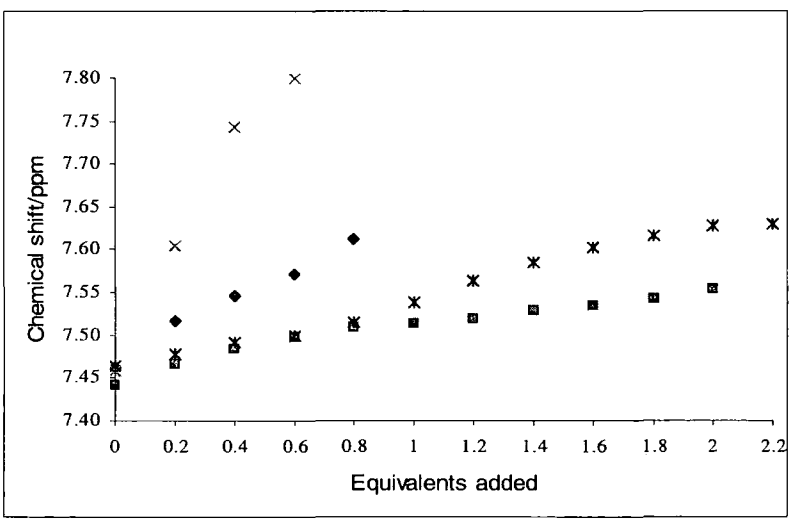

Figure 36 Plots comparing the titration of **2.20e**·$4PF_6^-$ with tba chloride (squares) , tba succinate (stars), tba acetate (diamonds) and tba malonate (crosses) in d_6-acetone, following the NH signal.

The large change in chemical shift upon binding tba malonate (Figure 36), seen previously in **2.20a**·$4PF_6^-$ is consistent with a good match between the anion and the ditopic host c.f.; Figure 30. Additionally the acidity and presence of two carboxylate groups accounts for the large change in chemical shift. Chloride and bromide bind very similarly in acetone, the bromide data

almost overlap the chloride data and hence are omitted for clarity. However, in acetonitrile chloride binds much more strongly. The displacement of solvent by chloride anion hence can be more easily achieved in comparison to bromide.

Figure 37 shows the difference in binding between **2.20e**·$4PF_6^-$ with chloride and bromide in acetonitrile. Due to small differences in concentrations of the hosts used, the chemical shift of the NH singal in pure sample differs slightly.

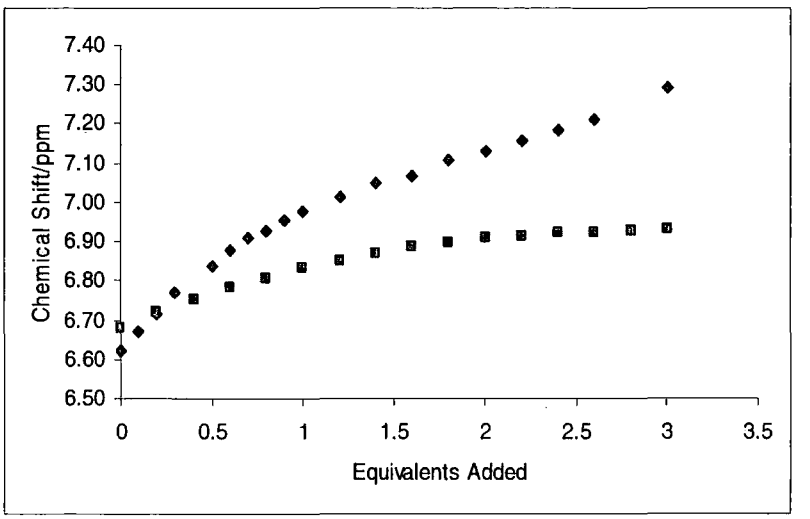

Figure 37 Plots comparing the titration of **2.20e**·$4PF_6^-$ with tba bromide (squares) and **2.20e**·$4PF_6^-$ with tba chloride (diamonds) in CD_3CN-d_3, following the NH signal.

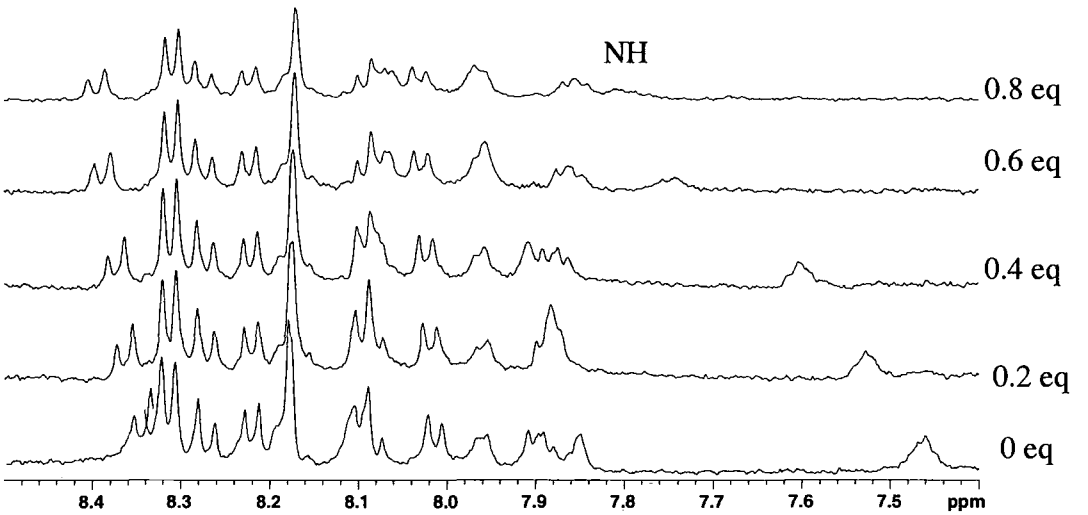

(a)

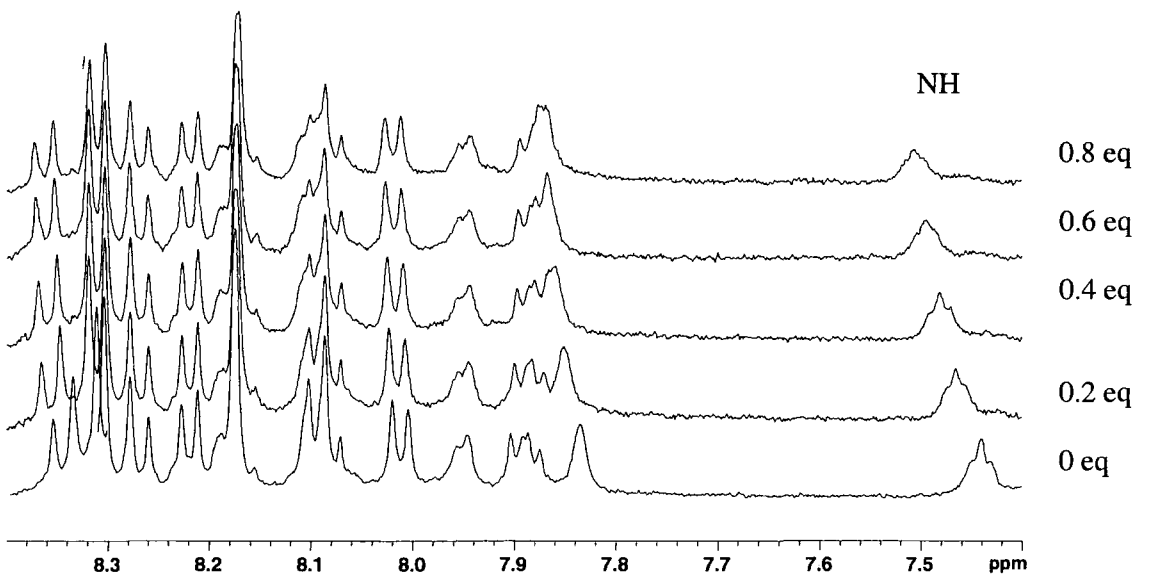

(b)

Figure 38 The ^{1}NMR spectra of **2.20e**·4PF_6^- upon addition of up to 0.8 equivalents of malonate (a) and chloride (b) in d_6-acetone.

2.6.3 DFT calculations

The structure of **2.20e** in the presence of two equivalents of chloride and malonate was modelled using DFT calculations (see experimental section). The calculations were carried out by Dr. Martin Paterson of Heriot Watt University. Figure 39 displays differences in geometry between the host bound to malonate and chloride anions. The host is clearly a very flexible species that is adaptable to suit a variety of guests. The directional hydrogen bonds between NH, pyridyl H and carboxylate oxygen atoms in a) appear to push the pyrene moieties away from each other and in different planes to adopt the most energetically preferred conformation. Contrarily to malonate binding mode, chloride anion of simpler spherical shape seems to induce closer interaction between the aminopyridyl clefts and ultimately results in partial overlap of the pyrene moieties due to the size and high symmetry of chloride anion. The partial interaction between the pyrene groups may contribute to an additional stabilisation energy of the complex.

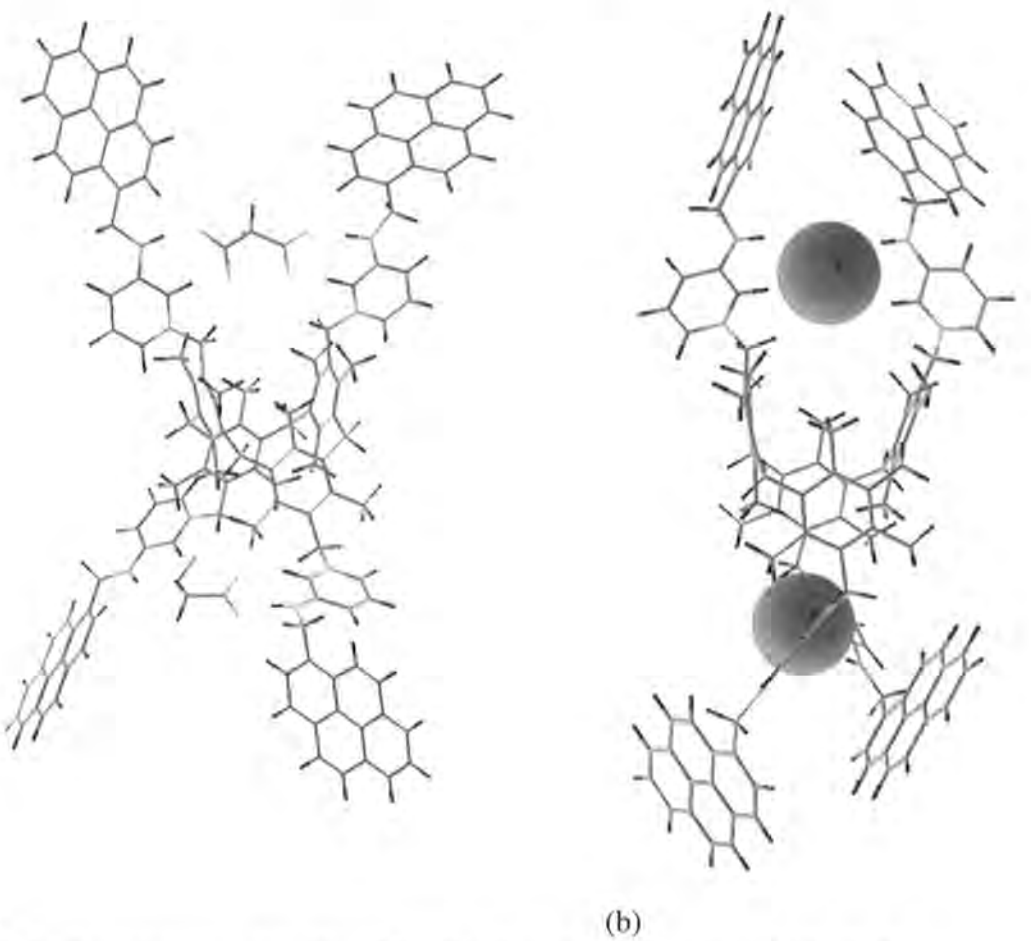

(a) (b)

Figure 39 DFT calculations models of host **2.20e**·4PF_6^- bound to malonate (a) and chloride (b).

2.6.4 Photophysical properties of 1,3-alternate calix[4]arene

The following results were obtained in collaboration with Prof. Luca Prodi of University of Bologna. All the photophysical experiments were performed in acetonitrile solutions. The absorption spectra of **2.20e**·$4PF_6^-$ and a control host **2.26**·$4PF_6^-$ (synthesised by Sara-Jane Dixon within the group) are superimposable, both showing two sets of bands in the 250-300 and in the 300-400 nm region.

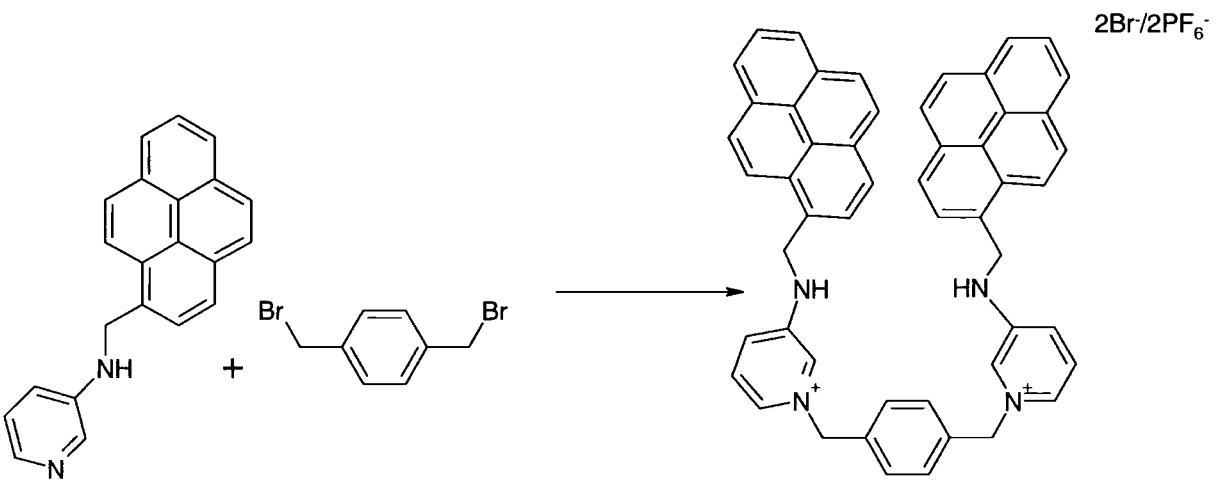

2.16e **2.26**

These absorption spectra are similar to the one of pyrene in the same experimental conditions.[114] The absorption band in the 300-400 nm region is broader and less intense, with a negligible tail above 380 nm which is not present in the parent chromophore. This behaviour is attributed to the small inter-chromophoric interactions also in the ground state and/or to the occurrence of an emissive charge transfer transition between the pyrene group and the pyridinium ions present in the structure of **2.20e**·$4PF_6^-$ and **2.26** ·$2PF_6^-$.

In contrast, the fluorescence spectra of **2.20e**·$4PF_6^-$ and **2.26**·$2PF_6^-$ are very different from those typically presented by pyrene derivatives. In particular, the band at ca 400 nm typical of the monomeric species of pyrene is, in this case, much less intense. The quantum yields for **2.20e**·$4PF_6^-$ and **2.26**·$4PF_6^-$ are $\Phi=5 \times 10^{-4}$ and 7×10^{-4} respectively, while that for pyrene itself in aerated solution is 0.07[130] and the band is structured. The spectrum of **2.20e**·$4PF_6^-$ consists of an additional band in the 500-620 nm region (Figure 40). The presence of this broad un-

structured band in the emission spectrum of free **2.20e**·$4PF_6^-$ is indicative of intramolecular interaction resulting in a static excimer. The maximum is red shifted by ca 80 nm compared to typical pyrene dimers.[130, 131]

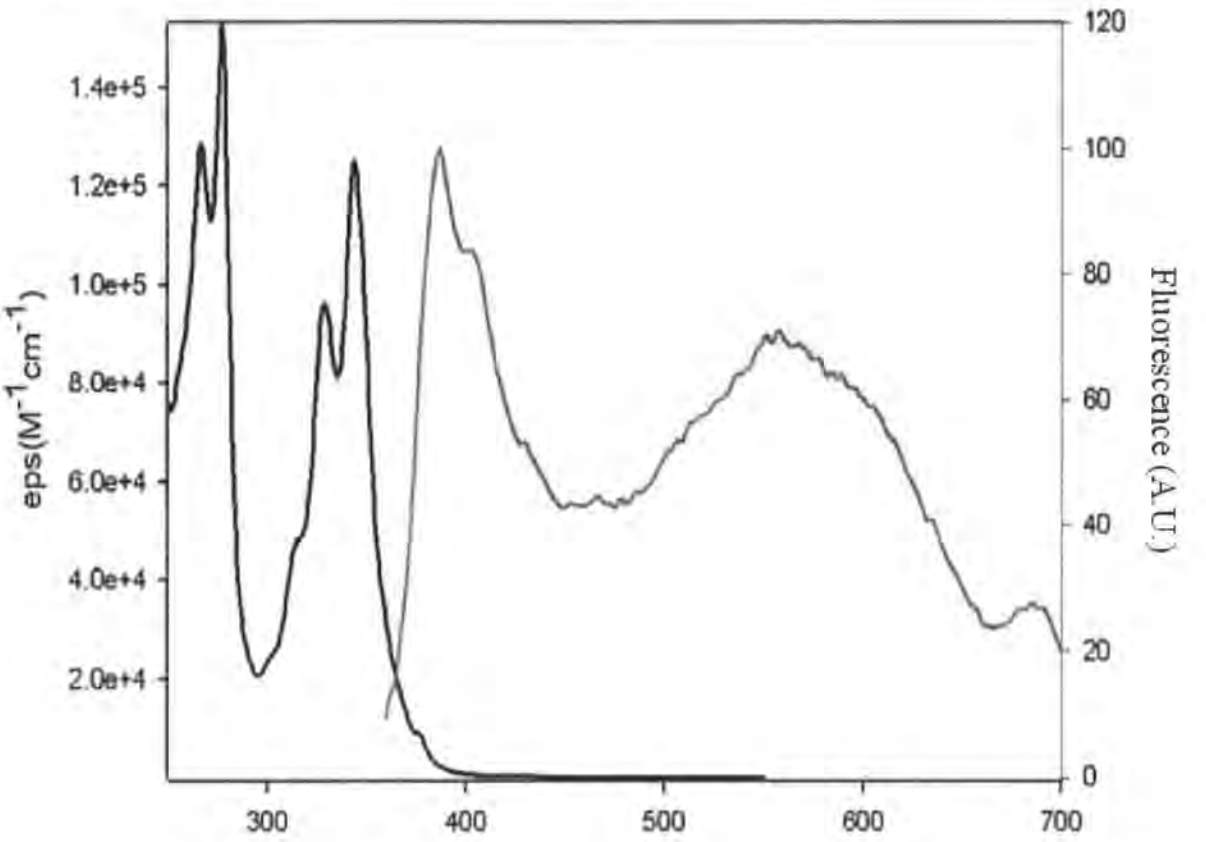

Figure 40 Absorption and fluorescence (λ_{exc} = 340 nm) spectra of **2.20e**·$4PF_6^-$ in acetonitrile solution.

The above spectrum illustrate a formation of static excimer. The excited state lifetime is also very short in **2.20e**·$4PF_6^-$ (does not allow an efficient dynamic excimer formation) (τ<0.3 ns for both compounds, compared to 18 ns, for pyrene in aerated solution).

The strong quenching of the fluorescence in **2.20e**·$4PF_6^-$ and **2.26**·$2PF_6^-$ is most likely due to a photoinduced electron transfer (PET) process from the pyrene moieties to the electron deficient pyridinium ions (Figure 12). The fluorescence band observed for **2.20e**·$4PF_6^-$ in the 500-620 nm region shows that some interaction, as observed in the absorption spectrum among the different chromophoric units is present.

2.6.5 Binding to anions

Binding of chloride, bromide, acetate, malonate and succinate by **2.20e**·$4PF_6^-$ and **2.26** ·$2PF_6^-$ was studied by means of UV-Vis and fluorescence titrations in acetonitrile alone or in the presence of tba PF_6 [$1x10^{-2}$ M]. The addition of chloride anions to **2.20e**·$4PF_6^-$ results in significant changes both in the absorption and in the emission spectra. Upon addition of chloride to **2.20e**·$4PF_6^-$ (Figure 41), the absorption bands typical of the pyrene chromophore, decrease, broaden and red shift together with an increase in the absorbance in the 350-550 nm region. There is absence of clear isosbestic points.

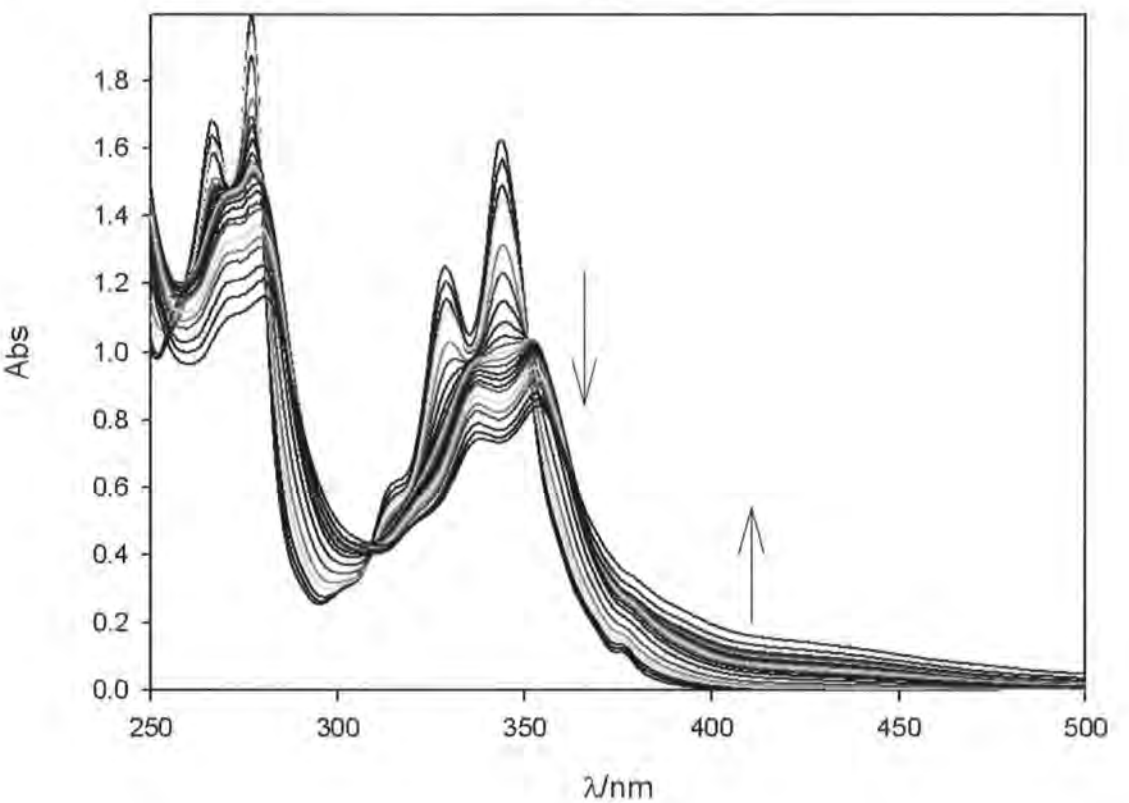

Figure 41 UV-Vis spectra of **2.20e**·$4PF_6^-$ [1.27 x 10^{-5} M] in CH_3CN and upon addition of increasing amount of tba Cl.

Similar changes have been attributed to the formation of dimeric species of the pyrene derivatives, also at the ground state, indicating that the complexation with this anion leads to a conformational change of the host structure, in which the pyrene moieties are interacting two by

two. The titration data can be fitted [132] assuming the presence of equilibria of 1 and 2, with stability constants log β_{11}=3.7 (5012 M^{-1}) and log β_{12}=8.1 (25 118 M^{-1}), respectively.

2.20e $4PF_6^-$ + Cl^- $\rightleftharpoons$ [**2.20e** Cl^-]$(PF_6^-)_3$ + PF_6^- Eq (1)

[**2.20e** Cl^-]$(PF_6^-)_3$ + Cl^- $\rightleftharpoons$ [**2.20e** $2Cl^-$]$(PF_6^-)_2$ + $2PF_6^-$ Eq (2)

The second equilibrium constant is evidently higher than the first one, indicating that the complexation of the first anion favours, through the induced conformational changes, the complexation of the second chloride. Only very small changes in the absorption band were observed in **2.26e**·$2PF_6^-$ upon addition of chloride.

In the case of addition of tba bromide anions, similar changes in the absorption spectra were observed. In addition, in the case of bromide, it was possible to obtain from the fitting of the titration data only the global constant log β_{12} = 6.1 (1.25 x10^5 M^{-1}) (for the formation of the 1: 2 (ligand: anion) complex, indicating that K_{11} is significantly lower than K_{12}. The absorption spectra of compound **2.26**·$2PF_6^-$ do not change upon addition of a large excess of bromide. This result could be consistent with two different explanations, i.e., a rather low association constant or the absence of any spectral change upon complexation.

When acetate anions are added, again significant changes in the absorption spectrum are observed in the case of **2.20e**·$4PF_6^-$, as in the case of bromide, an increase of the monomer band in the 380-400 nm region is observed. A global constant log β_{12} =7.7 (5.01 x 10^7 M^{-1}) for the formation of the 1: 2 (ligand: anion) complex can be calculated from the titration data. Very similar spectral changes have been observed also with the addition of dicarboxylate anions, succinate and malonate. In these cases, however, higher association constants (log β_{11} =5.5 (3.12 x10^5 M^{-1}) and log β_{12} =11.2 (5.01 x10^5 M^{-1})) for succinate and log β_{11}=5.2 (1.58 x10^5 M^{-1}), (with large error) and log β_{12} = 11.0 (6.30 x10^5 M^{-1}) for malonate were observed, indicating a clear selectivity of host **2.20e**·$4PF_6^-$ for dicarboxylate anions. With acetate, spectral changes were also observed in the case of **2.26**·$2PF_6^-$ with a decrease of the absorption in the 320-340 nm region accompanied by a small red shift. In this case, the appearance of an absorption tail at longer wavelength is almost negligible. Larger changes, with an up to 70% decrease of absorbance at 340 nm, were observed upon addition of malonate (β_{11} =5.4 (2.5 x10^5 M^{-1}) and succinate β_{11} =5.0 (1 x10^5 M^{-1})) (Table 3).

Anion	Host K/M^{-1}		
	2.20e·$4PF_6^-$		**2.26**·$2PF_6^-$
	K_{11}	K_{12}	K_{11}
Cl^-	5012	25118	Very small change no change in absorptic
Br^-	$K_{11}+K_{12}=1.25x10^5$		
AcO^-	$K_{11}+K_{12}=5.01x10^7$		
Malonate	$1.58x10^5$	$6.30x10^5$	$5.0x10^5$
Succinate	$3.12x10^5$	$5.01x10^5$	$2.5x10^5$

Table 3 Binding constants in MeCN for hosts **2.20e**·$4PF_6^-$ and **2.26**·$2PF_6^-$ with various anions obtained from fitting of the UV-vis absorption titration data at 343 nm.

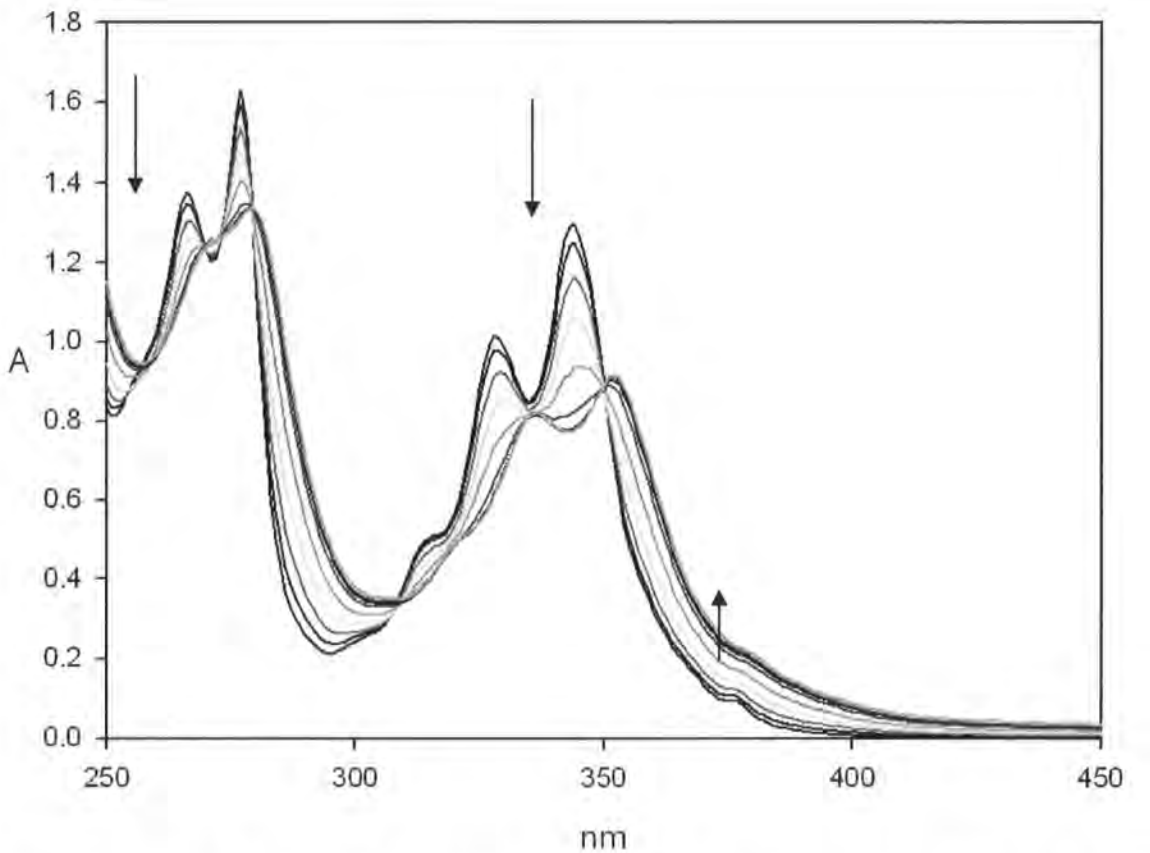

Figure 42 Absorption spectra of **2.20e** [1.035 x 10^{-5} M] in CH_3CN and upon addition of increasing amounts of tba malonate [1.21 x 10^{-3} M].

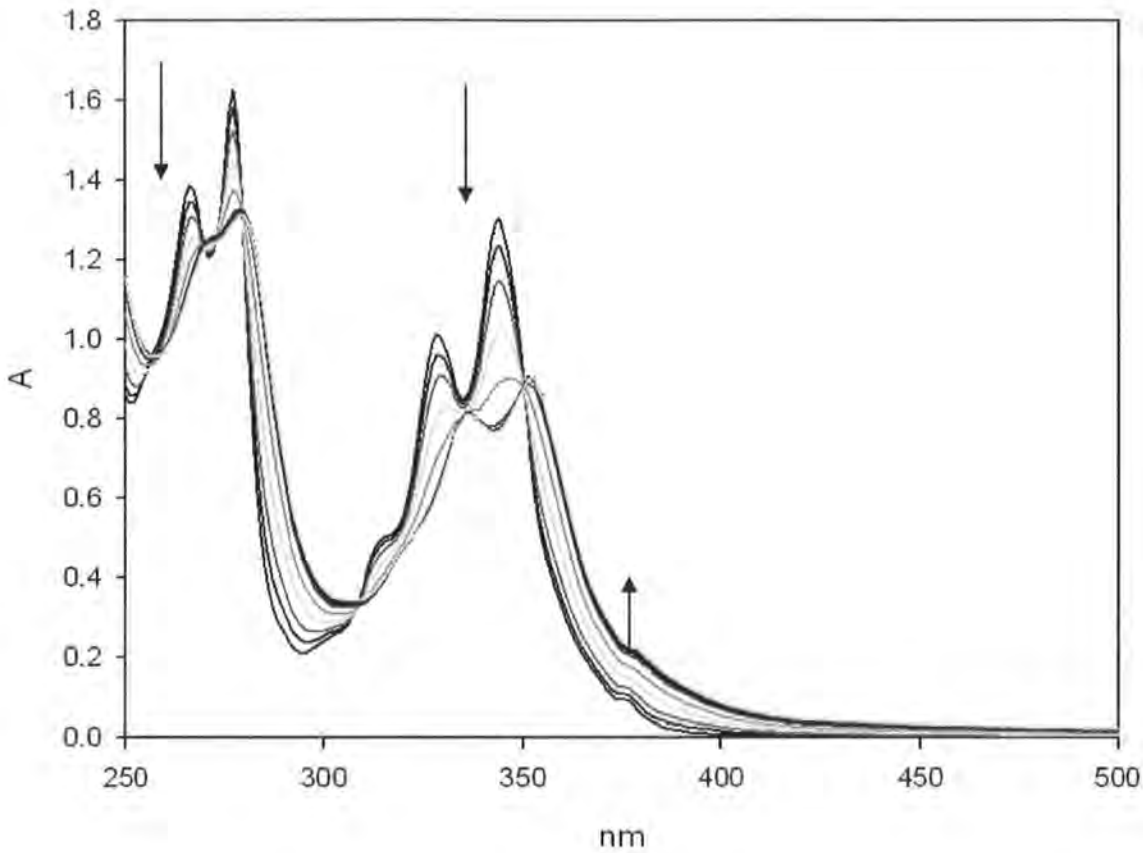

Figure 43 Absorption spectra of **2.20e**·$4PF_6^-$ [1.035×10^{-5} M] in CH_3CN and upon addition of increasing amounts of tba succinate [4.78×10^{-3} M].

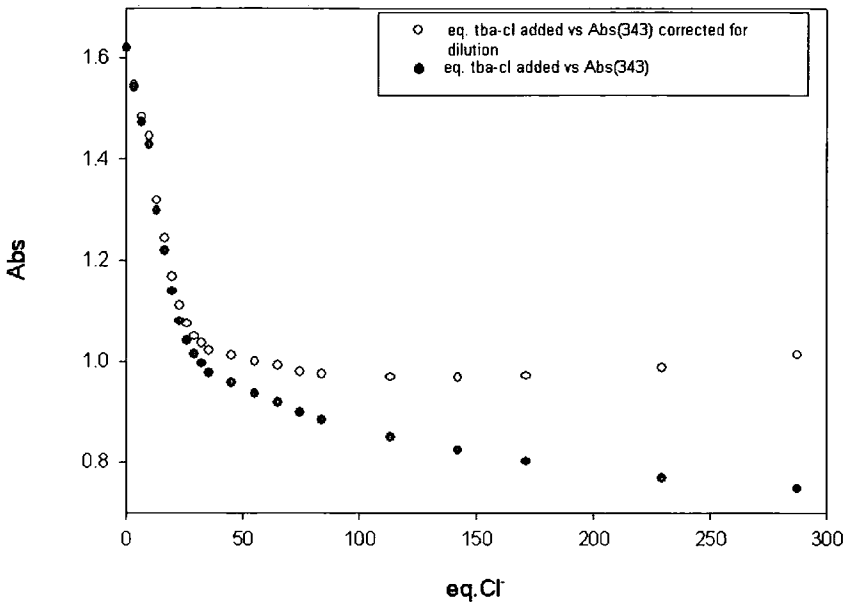

Figure 44 Absorbance at 343 nm of a [1.27 x 10^{-5} M] CH_3CN solution of **2.20e**·$4PF_6^-$ and upon addition of increasing amount of tba Cl (black circles). Absorbance corrected for dilution effects are shown with white circles.

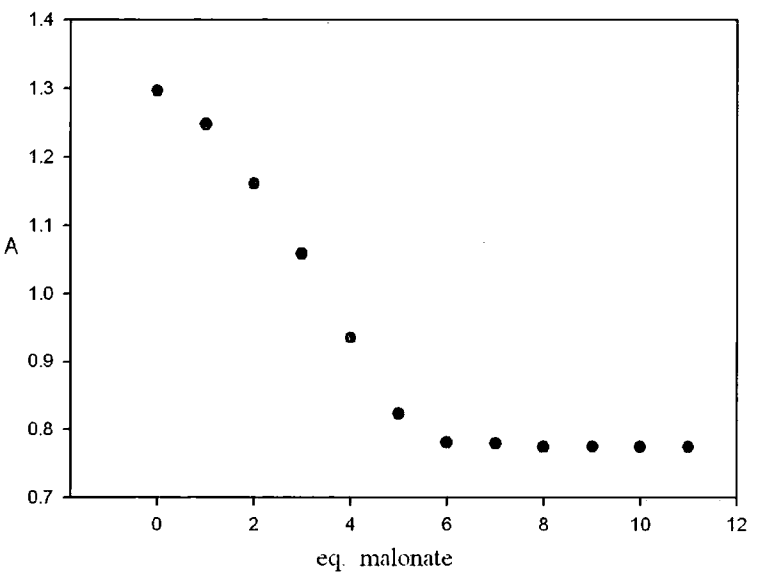

Figure 45 Absorbance at 343 nm of a [1.035 x 10^{-5} M] CH_3CN solution of **2.20e**·$4PF_6^-$ and upon addition of increasing amount of tba malonate [7.21 x 10^{-3} M]

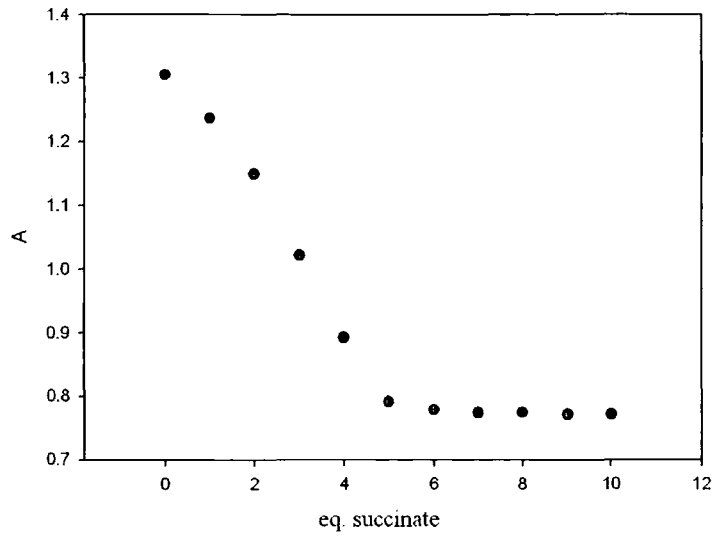

Figure 46 Absorbance at 343 nm of a [1.035 x 10^{-5} M] CH_3CN solution of **2.20e**·$4PF_6^-$ and upon addition of increasing amount of tba succinate [4.78 x 10^{-3} M].

Figures 45 and 46 display slightly different mode of binding of **2.20e**·$4PF_6^-$ with dicarboxylate to previously suggested for compound **2.20a**·$4PF_6^-$ (Figure 30). Indeed the sharp change in the slope's gradient to an immediate plateau at around 4 equivallents of guest anion added indicate binding of the host with the guest at the ratio of 1: 4 (discrepancies occur due to water content in the tba dicarboxylate). This can be rationalised by comparing with the crystal structure of **2.20a**·$4Br^-$ (Figure 29) in which all pyridinium arms interact independently with the bromide anions which presumably are too large to bind between the two binding arms. Similarly the bulkiness of the pyrene groups in **2.20e**·$4PF_6^-$ or indeed distant π stacking interaction between them hinders the fitting of the dicarboxylates in-between the two binding arms.

With regards to the fluorescence spectra of **2.20e**·$4PF_6^-$ an increase of the emission intensity across the spectrum is observed upon addition of chloride anions. On addition of less than 20 equivalents of the anion, the spectrum shows a relevant intensity increase and a large blue-shift of the non structured, low energy band (Figure 47). In these conditions, this band shows a shape that is the one typical of the excimeric form of pyrene. Upon addition of higher amounts of chloride, a more modest increase of the intensity of this band occurs, concomitant with a red shift and an increase of the fluorescence of the monomeric form of pyrene. The complexation of the second equivalent of anion has also an influence on the host's structure. The increase of the overall fluorescence intensity may be ascribed to the diminishing acceptor properties of the

pyridinium ion during interaction with the anion, hence reducing efficiency of the electron transfer process. PET can occur both from monomeric and dimeric pyrene, and the PET efficiency depends on the binding of the anions, so that both the fluorescence of the monomeric and dimeric form can partially come up.

In the emission spectra upon addition of Br^- and acetate (Figure 48) only a general increase of the monomeric band in the 380-400 nm region was observed. Similarly malonate and succinate cause only negligible changes in the spectra, i.e. the fluorescence remains quenched. There was no change in fluorescence spectra upon addition of F^-, HPO_4^{2-} or triflic acid.

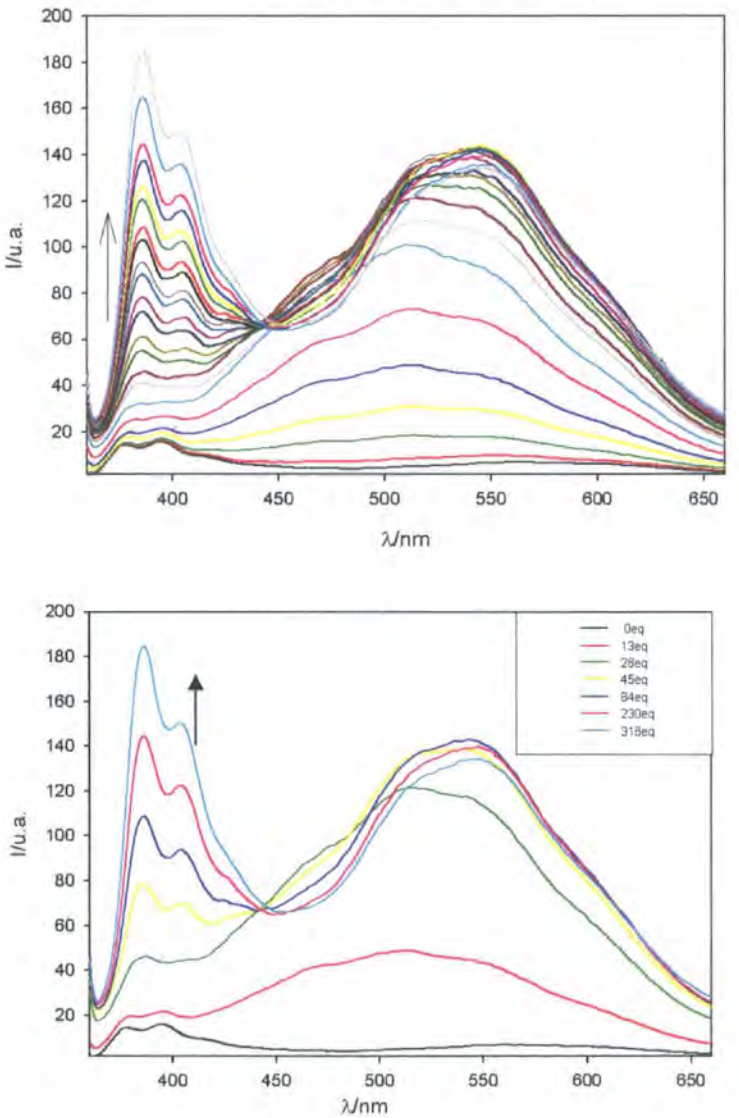

Figure 47 Fluorescence spectra (λ_{exc} = 343 nm) of **2.20e**·$4PF_6^-$ [1.27 x 10^{-5} M] in CH_3CN upon addition of increasing amount of tba Cl (lower graph: selected spectra).

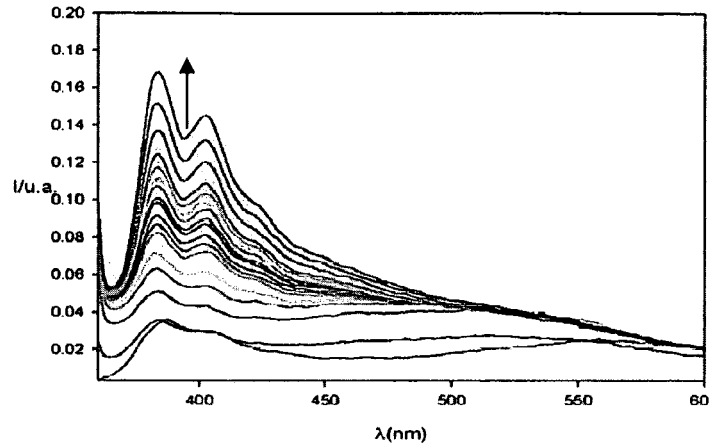

Figure 48 Fluorescence (λ_{exc} = 340 nm) spectra of **2.20e**·4PF_6^- and upon increasing amount of tba acetate anions in acetonitrile solution.

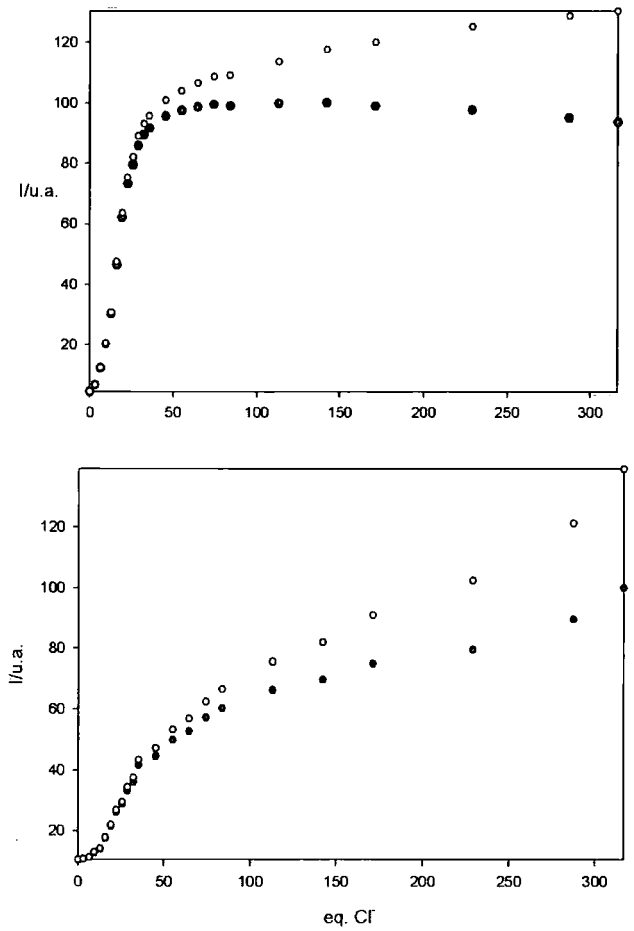

Figure 49 Fluorescence intensity (λ_{exc} = 343 nm; upper plot: λ_{em} = 395 nm, lower plot λ_{em} = 550 nm) of a [1.27 x 10^{-5} M] CH_3CN solution of **2.20e**·4PF_6^- and upon addition of increasing amount of tetrabutylammonium Cl (black circles). Emission corrected for dilution effects are shown with white circles.

2.7 Conclusions

The absorption spectra of **2.20e**·$4PF_6^-$ clearly demonstrate selectivity for dicarboxylate anions with binding constants being the highest. This is in agreement with the ^1H NMR titrations results in which an addition of the dicarboxylates results in the largest chemical shift of the NH protons. The DFT calculation model confirms the good match between the malonate anion and the aminopyridinium binding sites. However this geometrical fit does not result in the pyrene chromophores' overlap which is consistent with the lack of enhanced excimer emission. The only anion that caused a dramatic change in fluorescence spectra amongst all tested anions was chloride, despite the binding constants being lower than for the dicarboxylates. The receptor's response to a particular anion in this case exemplifies its sensing ability. It appears from the DFT calculation model that the spherical, close match diameter of chloride anion is of the best fit for the rearrangement of pyrene groups to occur. [115]

The lack of enhanced fluorescence in the control host **2.26**·$2PF_6^-$ upon addition of chloride anions also reaffirms that PET is not the main contributor to the increased fluorescence in **2.20e**·$4PF_6^-$ (both compounds contain the same fluorescent and anion binding units). PET is thought to occur in both compounds as an additional process, however the spatial arrangement of the fluorescent units in **2.20e**·$4PF_6^-$ only, allows them to interact and generate an excimer emission.

2.8 Preparation of the dicarboxylate salts

The tba malonate and succinate for the ^1H NMR and UV-vis/fluorescence titrations experiments were prepared as shown in Scheme 9.

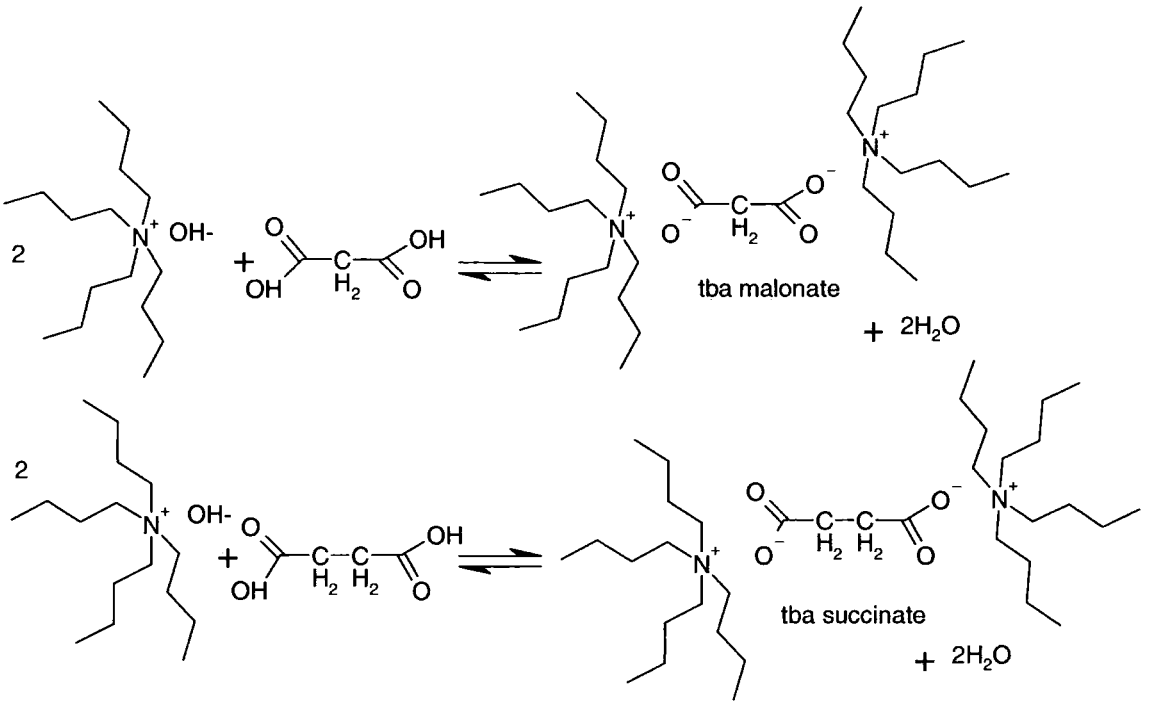

Scheme 9 Synthesis of tetrabutylammonium dicarboxylates.

A methanolic 1M solution of tba hydroxide was combined with a half molar equivalent of organic acid (succinic and malonic acids) and stirred for 2 h in the presence of molecular sieves ($MgSO_4$ use was avoided due to possibility of ion exchange as $MgSO_4$ partially dissolves in methanol). Removal of water by molecular sieves aids in the shift of equilibria to the right. After separation of molecular sieves the removal of solvent was accomplished firstly on the vacuum line followed by a transfer to a glove box in order to avoid any moisture affecting the weight.

Due to the highly hygroscopic nature of the organic salts, all of the weighings for the purpose of ^1H NMR titration experiments were carried out in the glove box under nitrogen. However even with very careful handling which included filling of an air-tight capsule in the glove box for microanalysis, the elemental analysis still showed presence of 2.5 molecules of water per molecule of tba succinate and 2.5 molecules of water per molecule of tba malonate. Presence of water in the salts not only affects the accuracy of equivalents calculations for the purpose of the titrations but also severely broadens the NH signal in the ^1H NMR spectra reducing the titration span. The amounts of water increased to 6 and 5 respectively when the microanalyses were repeated with handling in air.

Chapter 3

Hosts based on metal and nanoparticle scaffolds

3.1 Coordination Complex Hosts

The organic scaffold such as a calixarene which bears hydrogen bonding ligands can be replaced by a relatively inert metal such as Pt(II) or Ru(II) forming a 'semi-labile' coordination complex. Work by Loeb and Gale has produced several urea containing Pt(II) species able to bind NO_3^-, ReO_4^- and SO_4^{2-} in a highly concerted fashion.[24, 55, 56, 133] A neutral ion receptor must contain *a priori* (known ahead) binding sites for both anion and cation either as a contact or separated ion pair.[133, 134] In these complexes the metal ion plays the role of both counter ion to the bound anion and core organizing module. The host geometry depends on the metal ion's preferred coordination geometry. Thus, according to our modular approach the triethylbenzene module is readily exchanged for a metal ion core. Reaction of the Ru(II) species [[Ru(η^6-*p*-cymene)Cl_2]$_2$] with 3-aminopyridine or its ferrocenylmethylene (**3.1**) or anthracenylmethylene (**3.2**) derivatives gives both 1:1 and 2:1 complexes, **3.3a, 3.3b** and **3.4a**, Scheme 10.[135] The ruthenium(II) complex **3.4a** proved to be an effective chloride binder exhibiting comparable affinity to the analogous dipodal benzene-derived dication **3.5**, however the lability of the complex is such that nucleophilic anions like Cl^- displace the pyridyl ligands over a period of hours, re-generating monoadduct **3.3a**. With less nucleophilic anions the system proved to be stable and exhibits a particularly high affinity for NO_3^-, K_{11} = 1412, K_{12} = 52. Two binding constants are observed because the lower formal positive charge on the ruthenium complex allowed the formation of a 2:1 host: guest complex as well as the target 1:1 species. This speciation was not observed for the organic analogue. The ruthenium complex also exhibited interesting dynamic NMR behaviour with two forms apparent at low temperature, Scheme 11.[135] In CH_2Cl_2 solvent shifts in the Fc/Fc^+ redox couple of up to 82 mV were observed upon chloride addition. Analogous Pt(II) species [$PtCl_2$(**3.1**)$_2$] **3.6** and [$Pt(PPh_2CH_2CH_2PPh_2)$(**3.1**)$_2$]$^{2+}$ **3.7** may also be prepared. In contrast to the success of the ruthenium species, the platinum complexes proved to be poor anion hosts. In the case of the dichloride **3.6** an X-ray crystal structure revealed a *trans* geometry,

unsuitable for anion chelation while the anion binding by the dppe derivative **3.7** is apparently inhibited by the bulk of the dppe spectator ligand.

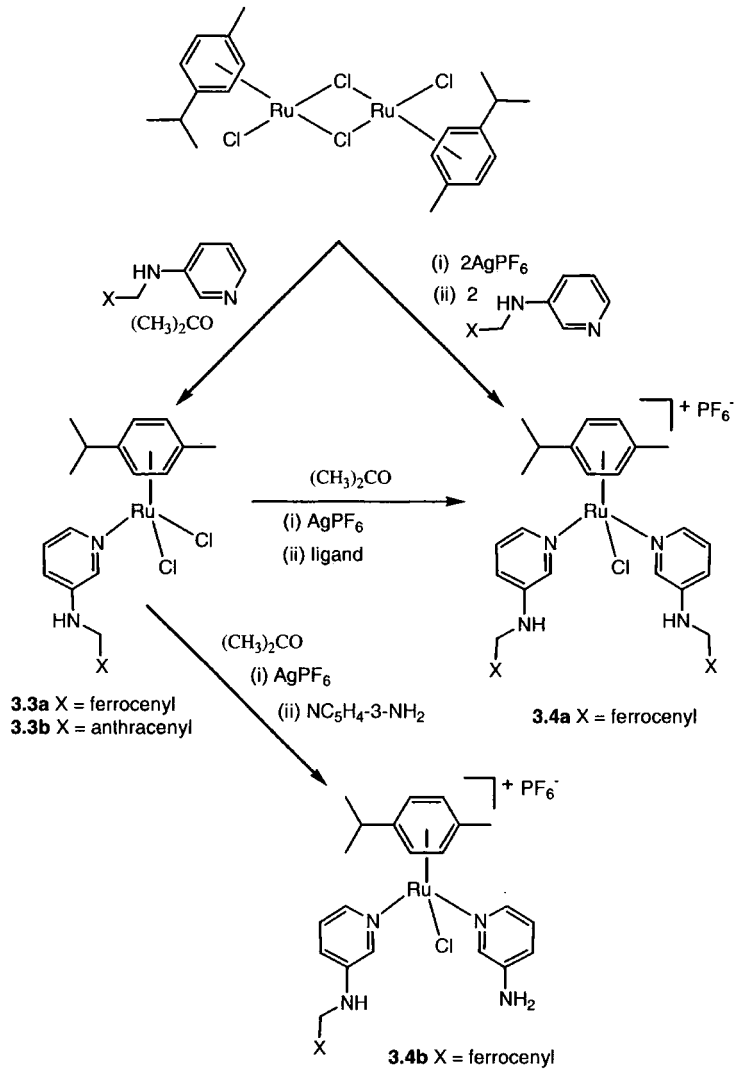

Scheme 10 Synthesis of Ru(II) receptors.

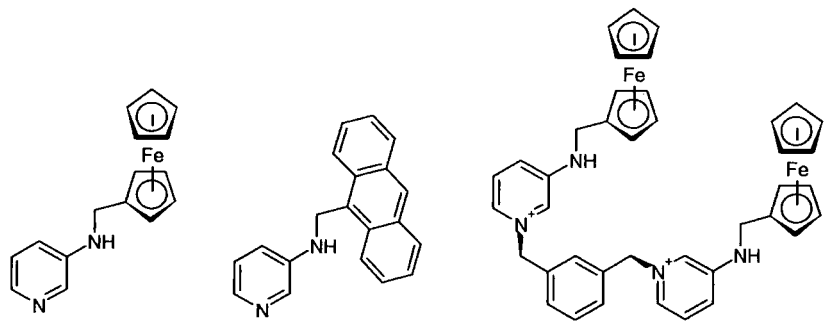

3.1 **3.2** **3.5**

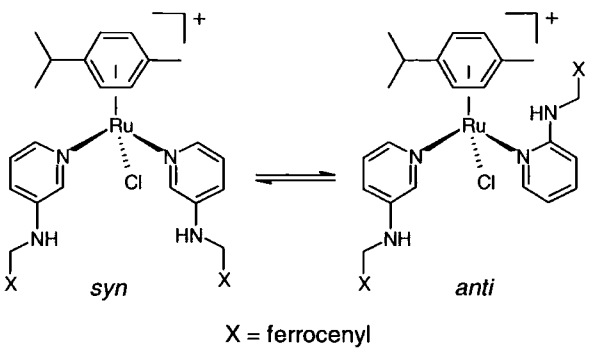

Scheme 11 Conformational exchange in **3.4a**.

The very versatile urea ligand **TUP** used by Steed *et al.* in host **1.15a** has also been extensively investigated within the context of coordination complex hosts.[136] While the Ru(II) and Pt(II) complexes **3.4a** and **3.7** are relatively kinetically inert, the chemistry of **TUP** was investigated with much more labile metal centres, particularly Ag(I) and first row transition metal dications. The coordination chemistry is relatively unexceptional, resulting in linear 2- or 3-coordinate complexes for Ag(I) and tetrahedral or octahedral 2:1 and 4:1 complexes for transition metal ions, depending on counter anion. The complexes prepared are summarized in Scheme 12.

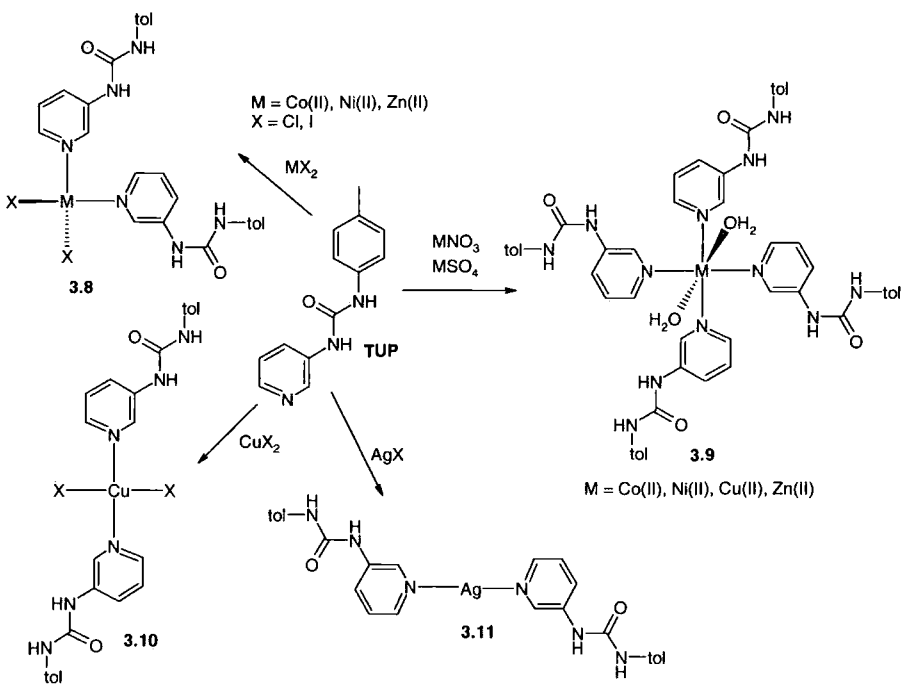

Scheme 12 Metal complexes of the ligand TUP.

Reaction of **TUP** with labile Ag(I) as the nitrate, triflate and sulfate salts in methanol-water (~50:50) resulted in formation of a series of complexes of 1:2 stoichiometry, namely $[Ag(\mathbf{TUP})_2](NO_3)\cdot S$ (**3.11a**, S = MeOH or NO_2Me), $[Ag(\mathbf{TUP})_2](CF_3SO_3)\cdot 0.5\ H_2O$ (**3.11b**) and $[Ag(\mathbf{TUP})_2](SO_4)$ (**3.11c**), all of which were characterised crystallographically. Nitrate complex **3.11a** displays an interesting 1:1 assembly in which the nitrate anion is asymmetrically chelated by two ligands attached to the same metal centre (Figure 51a)[137], forming a highly complementary cavity. The whole structure is almost planar and stacking effects result in either 3.5 or 2.5 crystallographicaly independent molecules depending on the identity of the solvent molecule 'S'. In the case of complexes **3.11b** and **3.11c** NH interactions with oxygen in anions result in infinite hydrogen bonded assemblies in the solid state in which each anion is surrounded by an array of two (**3.11b**) or four (**3.11c**) urea groups. The high complementarity of **3.11a** with nitrate is confirmed by ^{1}H NMR titrations studies in actone-d_6 which show that the complex persists in solution, K_{11}= 30 200 M^{-1}. Once again, CH···anion interactions also prove to be important. Titration of **3.11a** with acetate produced a notably different response to that of nitrate. There was no change in chemical shift values until after the addition of one equivalent of tba acetate. The addition of further aliquots of guest resulted in significant binding (K_{11} = 4.97x10^5 M^{-1}). This process is due to the ligation of the Ag(I) centre by the first equivalent of acetate, unlike nitrate, which does not ligate until an excess of nitrate is present (Figure 50).

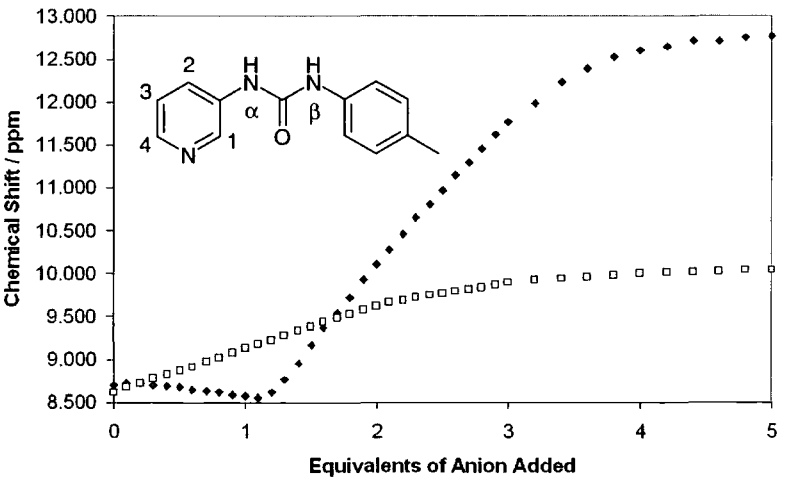

Figure 50 ^{1}H NMR binding isotherms for the NH(α) proton of TUP in **3.11a** on addition of NO_3^- (squares) and AcO_2^- (diamonds) (reproduced from ref 137).

A remarkable similar nitrate-binding motif is observed in the Cu(II) complex $[Cu(\mathbf{TUP})_4(H_2O)_2](NO_3)_2$ **3.9a**. The X-ray crystal structure shows a symmetric double chelation of the two nitrate anions between pairs of **TUP** ligands, (Figure 51b).[138] The cobalt and nickel analogues have also been characterized by X-ray crystallography. They are mutually isomorphous but differ from the Cu(II) complex in that the symmetric nitrate binding mode is disrupted. Apparently the elongation of the axial M-OH_2 bonds due to the Jahn-Teller distortion in the Cu(II) complex is sufficient to favour nitrate chelation. Conversely, the coordinated water molecules are more involved in interactions to the anions in the Co(II) and Ni(II) complexes.

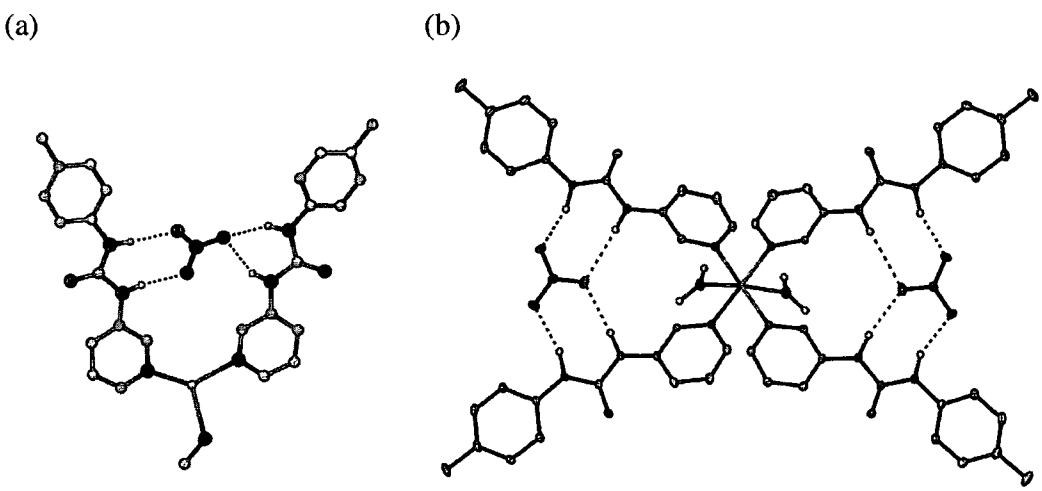

Figure 51 (a) The discrete $[Ag(TUP)_2](NO_3)\cdot MeOH$ in **3.11a** showing the slight tilt of the nitrate anion; (b) double nitrate chelation in the Cu(II) complex **3.9a**.

3.2 Aims of this project

The high versatility of modular approach ranging from triethylbenzene, calixarene-based compounds through to self-assembled metal complexes with labile metal centres can be translated into much larger scaffolds of nano size dimensions such as nanoparticles. The structure of **3.11a** in Figure 51a in which nitrate anion is bound by two ligands **TUP** chelated to silver atom provides an inspiration to a design in which the ligands can bind metal atom (or metal nanoparticles) and anion via a variety of interactions. The chosen ligand would be covalently bound to the gold nanoparticle stabilising it simultaneously and would bear anion binding moiety. Since gold nanoparticles are very sensitive to changes in surrounding

environment i.e. dielectric constant, it is anticipated that any binding of anions would produce change in their surface plasmon resonance absorbance. The initial concept was to attach covalently to the surface of gold either calix[4]arenes or dipods of type **2.26** 'upside down' *via* sulphur atom which can be synthetically added to the arms' structure. The compounds would additionally be cationic for stronger interactions, however a counter anion would also have to be present to balance the charge. Attachment of such host to gold nanoparticle would also impede the host's flexibility.

3.3 Gold nanoparticles

3.3.1 Surface plasmon band

Gold nanoparticles (GNPs) capable of optically sensing molecules have been of increasing interest.[139-142] As GNPs have very high molar absorptivity in the visible region [143], they offer considerable potential for optical detection of ions and molecules.[144, 145] Their size- dependent optical properties are due to surface plasmon band (SPB), a phenomenon observed in transmission, due to the presence of nanoparticles (NPs), bigger than 2nm in solution or in the solid phase. Surface plasmons, also known as surface plasmon polaritons, are surface electromagnetic waves that propagate parallel along a metal/dielectric interface. This condition is met in the IR-visible wavelength region for air/metal and water/metal interfaces (where the real dielectric constant of a metal is negative and that of air or water is positive). For surface plasmons to exist, the complex dielectric constants of the two media must be of opposite sign. For nanoparticles, localized surface plasmon oscillations can give rise to the intense colours of solutions of plasmon resonance nanoparticles and/or very intense scattering. Nanoparticles of noble metals exhibit strong UV-visible absorption bands that are not present in the bulk metal. This absorption is also referred to as Mie resonance from one of the most prominent contributors to the SPB theory; Gustav Mie.[146] Mie theory assumes that the particle and the surrounding medium are homogeneous and can be described by bulk dielectric function. Solving Maxwell's equations leads to a relationship for the extinction cross-section σ_{ext} (σ_{ext}= σ_{abs}+σ_{sca}=absorption cross-section+scattering cross-section) for metallic nanoparticles as a summation over all electric and magnetic oscillations. For nanoparticles which are significantly smaller than the wavelength of the exciting light (λ>>2R where R is the nanoparticle radius) the Mie theory is reduced to

$$\sigma_{ext}(\omega) = 9\frac{\omega}{c}\varepsilon_{3/2}Vo\frac{\varepsilon_2(\omega)}{[\varepsilon_1(\omega)+2\varepsilon_m]^2+\varepsilon_2(\omega)^2}$$

Where V_0 =$(4\pi/3)R^3$, ω is the angular frequency of the exciting radiation, ε_m is the dielectric function of the medium surrounding the nanoparticle and $\varepsilon_1$and ε_2 are the real and imaginary parts of the dielectric function of the metallic nanoparticles respectively.[147] Mie theory is only applicable to non-interacting nanoparticles that are well separated in the solid state or are present

at low concentration in dispersions. For interacting particles, the plasmon resonance red-shifts with a simultaneous appearance of a lower energy absorption band. There are two types of interactions: near-field coupling and far-field dipolar interations. Dipolar interactions are electrodynamic in nature, the dipole fields, resulting from a plasmon oscillation of a single particle, induce surface plasmon oscillation in the adjacent particle.

The position, the shape and the intensity of the SPB strongly depends on various factors: the dielectric constant of the surrounding medium, the electronic interaction between the stabilising ligands and the nanoparticle (which alter the electron density inside the nanoparticle) and the size, shape and monodispersity of the NPs. Nanoparticles can be seen as an immobile and periodic cationic network in which a cloud of conducting electrons move. The latter are usually considered as free electrons. NPs dimensions are very small compared to the wavelength of the UV-visible light for which the phenomenon is observed and also comparable to the mean free path of electrons. [148] In order to understand SPB the conditions for which the electron cloud would resonate have to be determined. The displacement of the electron cloud under the effect of the electromagnetic field leads to the creation of surface charges, positive where the cloud is lacking, negative where it is concentrated (Figure 52).[146, 148] This dipolar charge repartition imposes a new force on the electron cloud. The electrons undergo a restoring force which opposes the external electric field. This model can be compared to classical forced, damped harmonic oscillator.

Another approach[146] considers electric field seen by the nanoparticle as the external one altered by the effect of the polarisability of the medium. The electron cloud oscillates under the effect of incident light. The restoring force is provided by the surface charges formed at the edge.

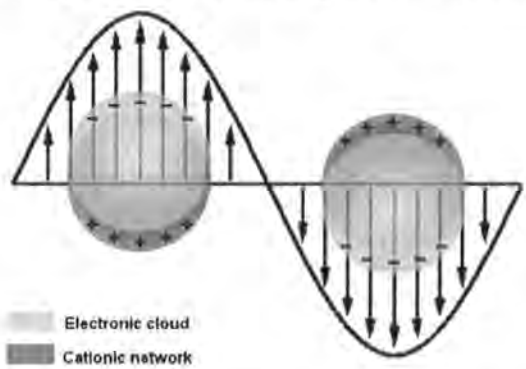

Figure 52 Schematic description of electronic cloud displacements in nanoparticles under the effect of an electromagnetic wave (reproduced from ref 146).

3.3.2 Properties of nanoparticles

The behaviour of NP SPB is very much dependent on several factors such as the dielectric medium, the composition, the charge, the size and the shape of the particles. Changing the medium surrounding the NPs for another medium having a markedly different refractive index strongly alters the plasmon behaviour of the NPs. Mulvaney *et al.* have shown that gold NPs surrounded with thin silica shells of increasing thickness first feature a red shift (with thickness from 0 to 20nm), due to an increase of the local refractive index around the particle. It is only with thicker shells scattering becomes significant, resulting in a strong increase in the absorbance at shorter wavelengths (Figure 53).[149, 150]

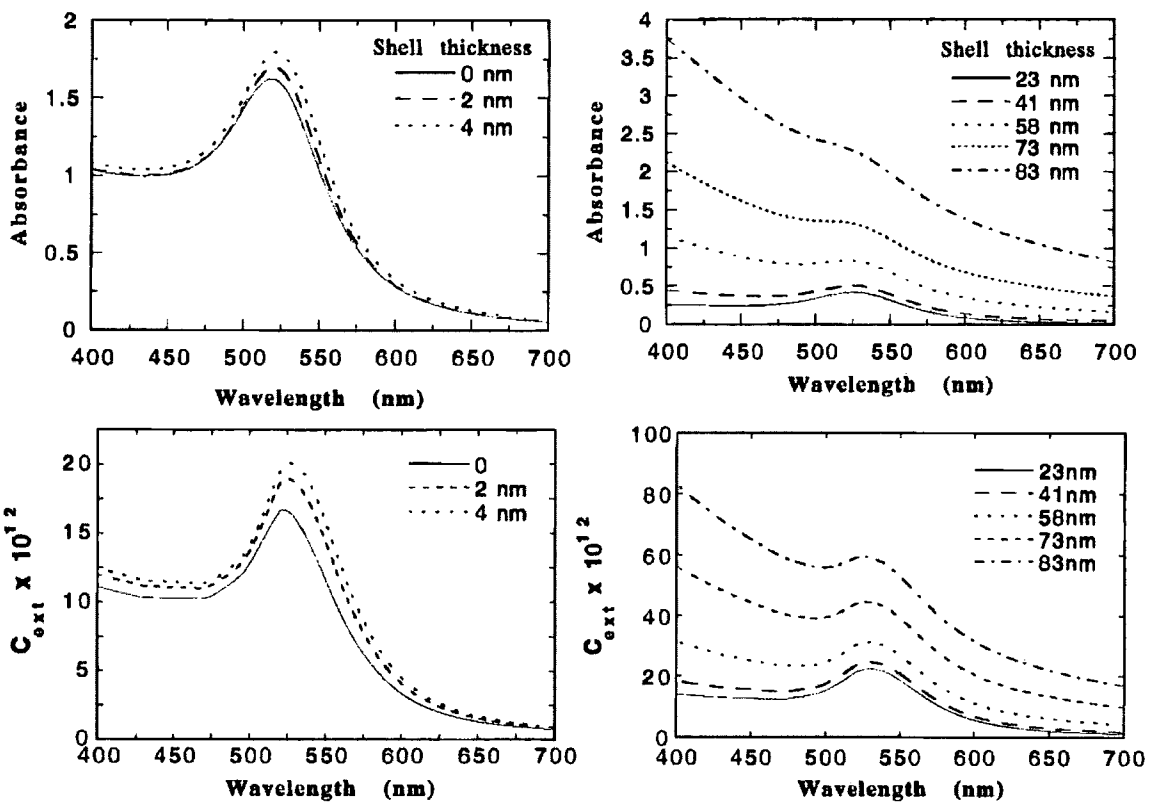

Figure 53 Influence of thin silica shells on the UV-visible spectra of aqueous (left) ethanolic (right) gold colloids: (top) experimental; (bottom) calculated (reproduced from ref 149).

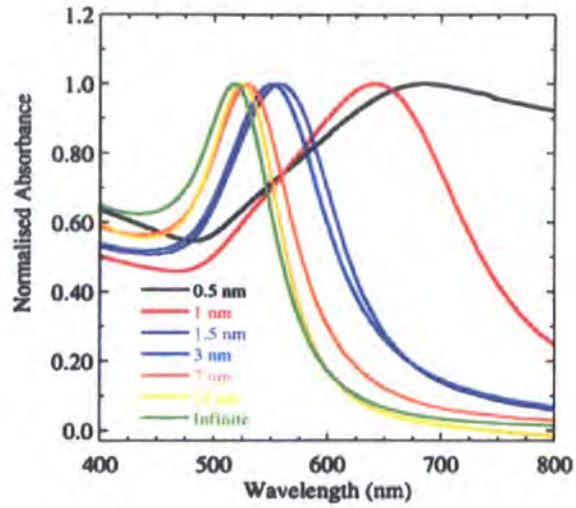

Figure 54 Influence of the interparticle distance on the SPB position (reproduced from ref 150).

Ung *et al.* has shown that it is possible to fine tune the interparticle distances of silica coated NP as composite layers.[150] The colours of those layers vary strongly i.e. blue-shift with increasing interparticle separation and red-shifts with increasing film thickness or layer band (Figure 54).

The surface of GNPs is usually protected with stabilising molecules, such as amines, thiols, phosphine, *etc.*, which prevent the agglomeration and the further growth of the NPs. By analogy with coordination chemistry these molecules are usually called ligands. A ligand shell strongly impacts the plasmon behaviour of the NPs mainly because it modifies the dielectric constant of the surrounding medium. So any chemical changes to the ligands including noncovalent interactions will also affect highly sensitive plasmonic absorption due to changes in the local refractive index. There is also electronic interaction with the gold atoms, as the ligands partially reduce or oxidise the NPs.

3.3.3 Gold nanoparticles as sensors

The sensitivity of surface plasmon band to its immediate environment offers the possibility of detecting attached molecules and environmental changes (assays based on changes of the localized surface plasmon resonance absorbance). Several types of assays have been conducted, in dispersions, on metallic nanoparticles immobilized on substrates,[151] on metallic nanoislands.[152] Sensing, detection and quantification of molecules when they attach is monitored

by shift of the nanoparticles' SPR upon interacting with their ligand. The shift of the surface plasmon absorption band was found to be proportional to the concentration of the ligand and related to the kinetics of the interaction.[153] Most assays have been carried out, however, on surface immobilized sensing elements. Confinement of the metallic nanoislands onto substrates has several advantages. First, their interparticle distances and position can be controlled, since they are immobilized on the surface. Second, stabilizers and surfactants can be omitted and can therefore be functionalized in their pristine state. Third, adsorbed substances can be desorbed and bound molecules can be released with the concomitant recovery or the original localized surface plasmon absorption band.[152] The reversible aggregation of plasmon resonant particles through specific linkers privides an excellent means for colorimetric assays (assays based on the aggregation of metallic nanoparticles). An interesting approach for constructing sensor is the immobilization of the gold nanoparticles in molecularly imprinted polymers. The polymer swells upon selective binding of the analyte, the distance between immobilized gold nanoparticles increases and hence their localised SPR spectrum changes.[147]

3.3.4 Alkanethiolate protected gold nanoparticles

An important step in synthesis of very stable monodisperse nanoparticles was achieved by Brust *et al.*[154] Briefly, hydrogen terachloroaurate (aqueous) was extracted into toluene and metathesized to the tetraoctylammonium salt with a toluene solution of tetraoctylammonium bromide (TOAB). To this solution was added an equivalent amount of alkanethiol followed by an aqueous solution of sodium borohydride. This creates inverse micelles in the organic layer, with a central hydrophilic region. These act as small reaction vessels and the particles grow to the size of the inverse micelle. However the particle size also depends on the amount of stabilising agent added. Increasing the number of ligands relative to the number of TOAB molecules, produces smaller clusters as the thiols inhibit growth by attaching to the surface.[155] A 1:1 ratio produced nanoparticles with a maximum in the particle size distribution at 2.0-2.5nm. An alternative method was reported by Schiffrin[156] in which the gold tetraoctylammonium salt is reduced first followed by an addition of a thiol. Thiol concentration is not relevant in this case since the nanoparticles have already been formed (inside the inverse micelles) and protected by the weak binding tetraoctylammonium group. This method produces slightly larger nanoparticles

(4-5nm in diameter). In both cases the nanoparticles can be precipitated with polar solvent such as ethanol and any excess ligand washed also with ethanol. Several centrifugation cycles eliminates either smaller particles (present in the supernatant) or larger agglomerates– at the bottom of the centrifuging tube. Varying the ratio of two solvents of different polarities (chloroform and ethanol) also aids selective precipitation. The model of protected layer on the nanoparticle is depicted in Figure 55.

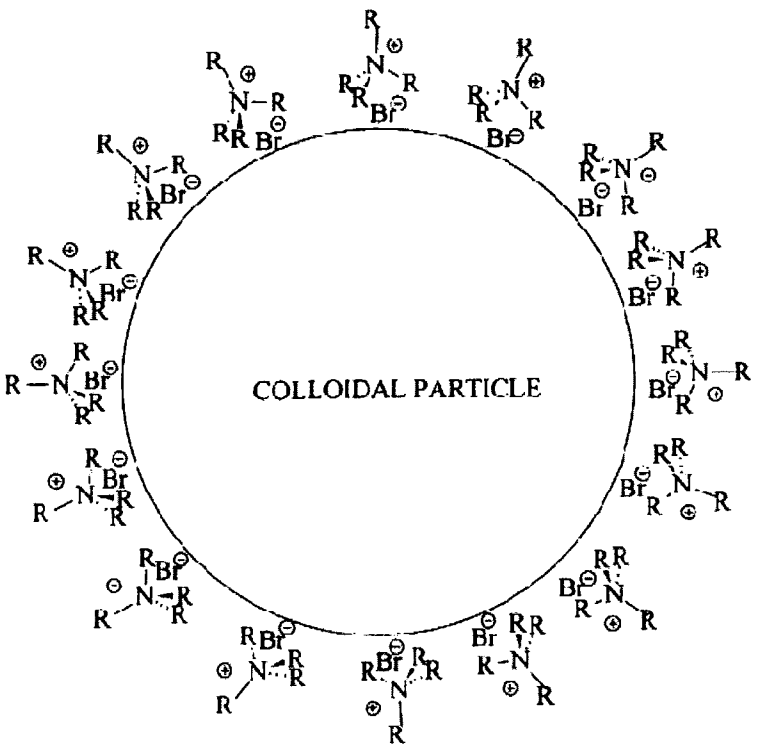

Figure 55 The proposed model of tetraalkylammonium bromide stabilized gold nanoparticle (reproduced from ref 155).

It is proposed that the stabilization of the gold particles, both in solution and in the colloidal particles observed, is due to the attachment of $R_4N^+Br^-$ ion pairs to the Au surface. In these structures, not only does anion adsorption give an anchoring point to the quaternary ammonium ions but also the hydrocarbon chains provide further stabilization by dispersion forces. Brust has also reported one phase synthesis where the $HAuCl_4$ is mixed with p-mercaptophenol in methanol followed by reduction of the gold with freshly prepared aqueous $NaBH_4$, the methanol-soluble nanoparticles obtained are 4nm in diameter.[157] The Brust/Schiffrin method has been widely used and a whole plethora of functionalised nanoparticles for various applications have

appeared. The molecules on the surface can exchange with others depending on the relative concentration and adsorption energies.

3.3.5 Sensing of anions by nanoparticles

An event of binding at the surface can be utilised in sensing. Simple amide-functionalised gold nanoparticles for sensing anions have been reported.[139] The nanoparticles 3.12 were synthesised by ligand exchange of alkanethiolate protected nanoparticles without structural changes in the gold core.[154] The exchange reactions of hexanethiolate-protected gold nanoparticles with n-BuNHCO($C_{10}H_{20}$)SH in CH_2Cl_2 for 24 h are carried out for a 1:1 molar ratio of n-BuNHCO($C_{10}H_{20}$)SH to C_6H_{13}S-Au. Purification can be achieved via sequential precipitation. The mean diameter of gold core determined by powder X-ray diffraction was 4.0 ±0.5nm. From the elemental analysis results it was estimated that there are more than 3:1 amides to thiol ligands present on each nanoparticle.

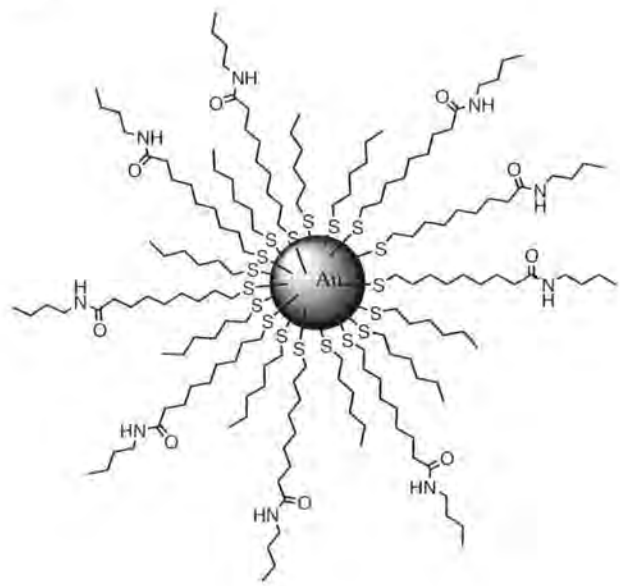

Figure 56 A schematic representation of amide-functionalised gold nanoparticles **3.12**.

CH_2Cl_2 solutions of **3.12** were found to absorb at 520nm. When the nanoparticles solutions were probed with various anions $H_2PO_4^-$, HSO_4^-, AcO^-, NO_3^-, Cl^-, Br^-, and I^-, (as their tba salts), dramatic changes in intensity with a slight red shift in wavelength occurred. The decrease in extinction was by as much as 45-55% on addition of $H_2PO_4^-$, HSO_4^- (0.5 equiv. of anion/BuNHCO($C_{10}H_{20}$)S-Au). Lazarides and Schatz [158] have previously reported such decrease

in extinction upon DNA addition which induced aggregation. It was suggested that the decrease in extinction can be attributed to the screening of nanoparticles embedded deeply within the aggregate interior. It has been reported previously using a coupled dipole approximation that a dramatic red shift occurs in the plasmon band when the interparticle distance in the aggregates decreases to less than the average particle radius.[158] The hydrogen-bond formation between the anions and the interparticle amide ligands in **3.12** was the suggested explanation for the decrease in extinction. However the nanoparticles within the anion-induced aggregates might have not been close enough to cause the colour change. It was also noted that further addition of anions to solution of **3.12** caused an increase in absorbance reflecting the disaggregation of the supernanoparticles composed of **3.12** and anions. An excess addition of $H_2PO_4^-$, HSO_4^-, AcO^-, results in regaining the original UV-vis spectrum. However the initial extinction was not recovered even after addition of a large excess of Cl^-, Br^-or I^-. In order to elucidate the fundamental features of binding selectivity, optical sensing studies between **3.12** and anions were further performed in CH_2Cl_2 containing DMSO as a competitive solvent. The decrease in extinction was approximately halved which emphasized the hydrogen-bonding existence in non-competitive solvent and its reduced strength of it when DMSO was added.

A very elegant example of an anion binding GNP was reported by Beer *et al.* Nanoparticles were modified with amide-disulfide functionalised zinc metalloporphyrin. The nanoparticles were synthesized via Brust method,[154] using dodecanethiol as the protecting thiol. **3.13** were subsequently obtained by ligand substitution. Several UV-Visible titrations of both the NPs **3.12** and the zinc metalloporhyrin were conducted with a variety of anions in dichloromethane solution.

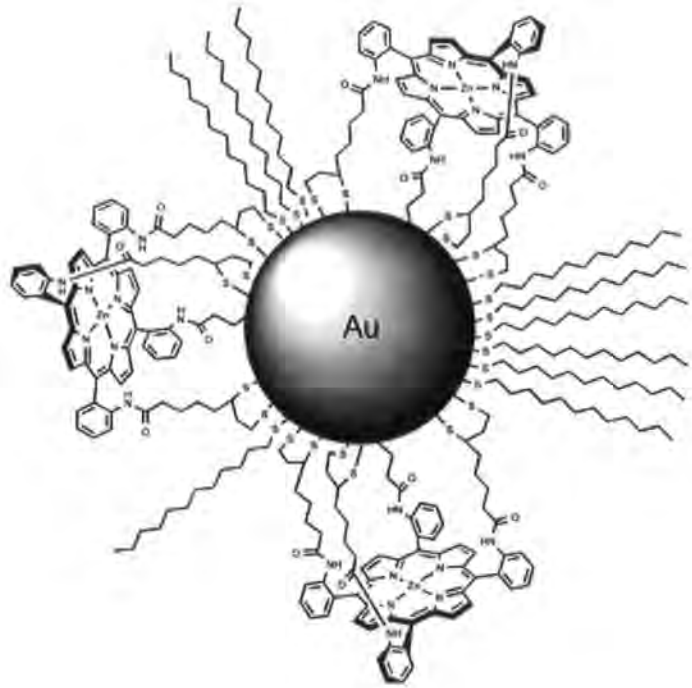

Figure 57 A schematic representation of gold nanoparticles **3.12** (reproduced from ref 26).

It was noted that the the zinc metalloporphyrin-functionalised nanoparticle **3.13** exhibits significantly larger magnitudes of association constant, in comparison to the free ligand, for Br^-, I^- and NO_3^-. Even in a competitive solvent such as DMSO the binding constant of **3.13** for chloride was still more 10^2 M^{-1}. Overall the binding affinities reflected a trend expected on the basis of relative anion basicities ie $H_2PO_4^->Cl^->Br^->I^->NO_3^-$. The enhanced binding of the receptor when confined to a surface was explained by the control over enthalpy and entropy. The pre-organisation and reduction of the receptors' conformational flexibility however increases the energetic cost of association therefore entropic contributions are more likely to be favourable.

The number of the porphyrin receptor moieties per nanoparticle was estimated using TEM-derived nanoparticle diameters, an estimate of the receptor 'footprint' and elemental analysis, to be 30-80 (depending on the particle size 3-4).

The place-exchange reactions, in which the original protecting molecules on the Au surface are partially replaced by new ligands is not a very stoichiometrically reliable method .[159] The inherent problem of mixed monolayer nanoparticles prepared by the above technique is the dispersity of metal core size and variable composition of the organic shell. As both the size and the composition of the nanoparticles affect physical and chemical properties several techniques of monodispersity improvement have been developed such as annealing.[160, 161] Figure 58 depicts

hypothesized core-shell reactivities of the alkanethiolate-capped gold nanoparticles under thermal activation. Larger core sizes result from an evolution of the smaller-sized starting particles *via* sequential shell desorption, core coalescence and shell re-encapsulation.

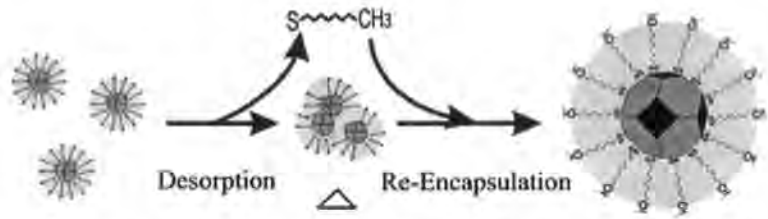

Figure 58 Schematic illustration of the core shell reactivities in the thermally-activated size and shape evolution process of thiolate-capped nanoparticles (reproduced from ref 160).

This process has indeed produced GNP of much higher monodispersity in comparison to their precursor. An alternative way of improving monodispersity is size separation, for example, by fractional crystallization[162] or gel permeation chromatography and HPLC[163]of both thiol-protected particles and mixed monolayers of hexanethiolate and mercaptoundecanoic acid. The dispersity in size of the nanoparticles can be easily studied using the chromatographic peak width and also TEM. Dispersity in the composition of the organic shell in mixed monolayer-protected nanoparticles is more difficult to characterize. By labeling the nanoparticles with stable free radicals such as TEMPO Chechik *et al.* has managed to follow the extent of alkanethiol ligand displacement by an oncoming ligand. However the exchange reaction of ligands **3.14-3.16** with thiol-protected gold nanoparticles is very poor (i.e. little exchange), and only small number of spin-labelled ligands (<10) can be adsorbed on a nanoparticle. Instead Chechik used much weaker binding ligand such as triphenyl phosphine which are much more likely to exchange.[142, 164] The drawback of this method is that nanoparticles produced only reach the size of 1.5-2nm. Since the strong UV absorption occurs only for nanoparticles of 2 nm diameter and above, those nanoparticles have only limited use with regards to their optical properties. It has been reported that the line shape of electron paramagnetic resonance (EPR) spectra of spin-labeled Au nanoparticles is strongly affected by the spin-spin interactions between the spin labeled adsorbed on the same particle.[140, 165] As spin-spin interactions are distance-dependent, the spectral line shape is very sensitive to the average distance between the spin labels and consequently depends on the average number of spin labels per particle. The coverage of spin labeled nanoparticles can

be thus monitored in the place-exchange reactions using EPR. By controlling the stoichiometry for the exchange reaction it has been possible to synthesize a series of Au nanoparticles with different coverage of nitroxides. At low spin label to nanoparticle ratios (<10), most spin labels are exchanged onto the Au surface. However when higher ratios are applied, the exchange reaction does not go to completion. The maximum of spin label bound to one particle does not exceed 20. The EPR spectra of nanoparticles with different coverage (GPC fractions) show peaks of various width and intensity and can be quantitatively integrated to estimate the number of radicals per particle.

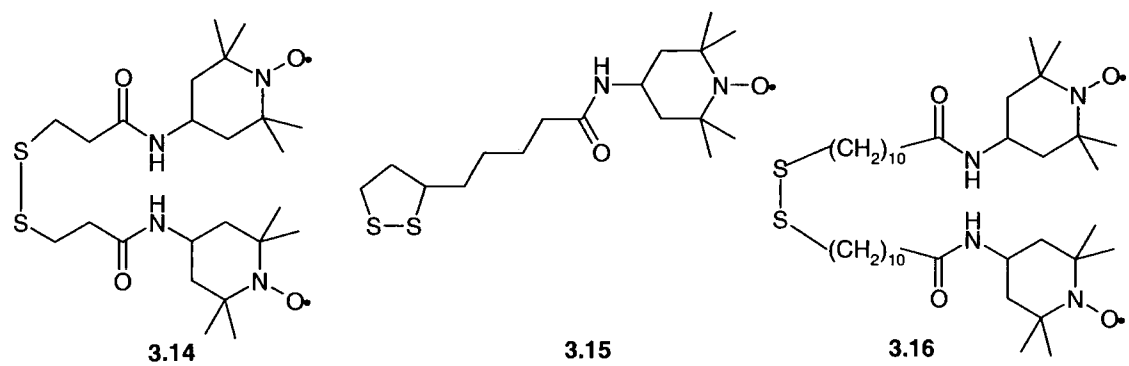

Figure 59 Disulfide-modified nitroxide spin labels

Chechik *at al.* have also previously shown that in diradical ligands **3.14** the S-S bond is broken during adsorption, and only one branch of the disulfide molecule is adsorbed on the Au surface[165]. This event can be observed as disappearance of the second and fourth lines and decreasing peak height of the fifth (high-field) line in the EPR spectra. The spectrum at the end of the reaction contains just three lines which correspond to a monoradical.

As demonstrated by Mirkin *et al.*, the use of multithiolated species improves the stability of gold nanoparticle colloids. The increase of stability is intuitively attributed to the presence of at least two thiol groups per molecule which all interact with surface gold atoms.[166, 167] Garcia *et al.* have proved the attachment of both sulfur atoms to gold in dihydrolipoic acid (DHLA) (a reduced form of thioctic acid) by using X -ray absorption near edge structure (XANES) spectroscopy at the sulfur K-edge. This is a powerful tool to assess the electronic structure, coordination geometry and oxidation state of the absorbing atom and has ben used extensively for characterizing sulfur oxidation states in biological samples.[168, 169] By following the peaks attributed to molecular orbitals of the S-S bond (S 1s→ S-S transitions), (2472 eV) and the

second peak to S 1s→S-C and 1s→S-H transitions (2473.6 eV) of thioctic acid and (2472.8 eV) of DHLA, which are at similar energy positions, it was possible to determine that most sulfur atoms were consequently placed in the same surroundings: in the solid state, almost each DHLA molecule is anchored on the gold particles by both sulfur atoms with concomitant appearance of energy peak position at 2473.6 eV. As a control an increasing known amounts of free DHLA ligand were added in order to observe a separate peak for the Au-unbound sulfur atoms (Figure 60).[141]

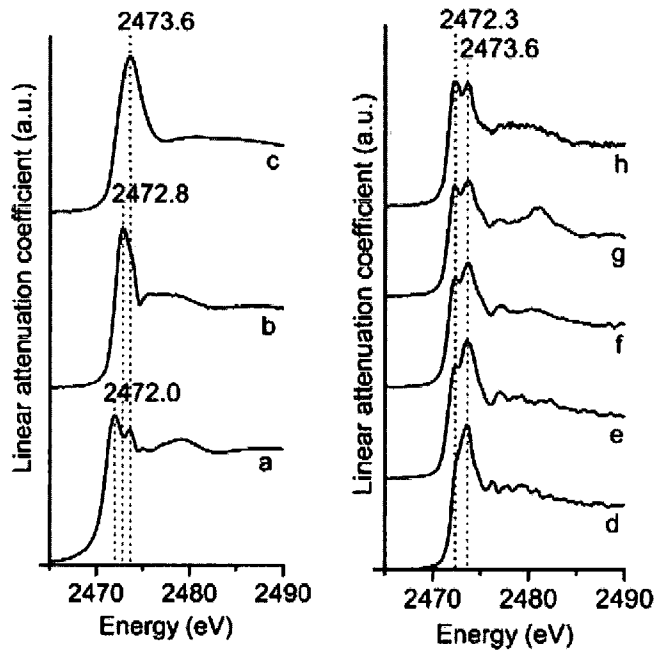

Figure 60 Sulfur K-edge XANES spectra of (a) thioctic acid, (b) dihydrolipoic acid, (c) Au@DHLA (solid state), (d) Au@DHLA (liquid state) in the presence of (e) r= 5%, (f) 13%, (g) 33% and (h) 50% of free DHLA (with r=$[DHLA]_{free}/([DHLA]_{free}+[DHLA]_{grafted})$) (reproduced from ref 141).

Functionalisation of gold nanoparticles in organic solvents that does not involve two phase synthesis was recently reported by Jansen *et a.l* [170] The method omits the use of surfactants and weak stabilizing agents so no exchange reaction with unknown composition occurs. Jansen also managed to tailor the size of resultant nanoparticles from approx 4 to 9 nm by varying the ratio of reducing agent added (sodium naphthalenide). The solvent in this case (diethylene glycol dimethyl ether or diglyme) also acts as a weak stabilizing agent in which the nanoparticles are stable for short periods (up to 1 h). Subsequent functionalisation takes place in situ and the ligand-capped nanoparticles are isolated and purified by standard precipitation and redispersion

cycles. Despite the claimed dispersities of 15-20% the UV spectra appear very broad and the peak's wavelength is difficult to assign.

3.4 Synthesis of ligand 3.18

A simple ligand was designed which would bind strongly to gold surface and have anion binding moiety. The ligand **3.18** was obtained by coupling of thioctic acid **3.17** and 3-aminopyridine with DCCI (3-dimethylamino-propyl)-ethyl-carbodiimide and HOBt (hydroxybenzatriazole hydrate) (Scheme 13) in dichloromethane. The use of DCCI and HOBt benefits from the solubility of combined reagents and final product **3.18** in organic solvent and of all the unwanted side products being soluble in water which can be washed out. A slight excess of thioctic acid is used (as there is always some percentage of disulfide polymer present even in the commercial compound). Thioctic acid also tends to polymerise in solution.[171] Any excess of **3.17** can then be removed as it is also water soluble and can be also washed out from final crude product. The coupling takes 24 h. After solvent removal the product **3.18,** which is an oil, can be thoroughly washed with water. The ligand **3.18** consists of disulfide providing two potential points of attachment to gold and anion binding NH group. The association constants for anions with neutral amide ligands are generally not so high (K_a < 100 M^{-1}) even in low dielectric solvents.[172] However it was anticipated that attachment of the ligand to the nanoparticle surface and cooperative association of pairs of ligands with cation-anion pairs would result in enhanced binding of anions. Beer *et al* have reported a simple amide **3.19** that binds Br^-, Cl^- and NO_3^-

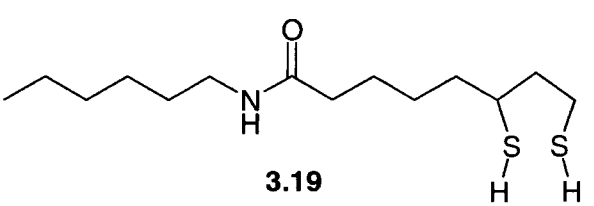

3.19

with association constants (log *K*) of 5.0, 4.5 and 5.8, respectively. Also zinc porphyrin receptor on gold nanoparticle binds Cl^- and $H_2PO_4^-$ around 100 times more strongly than as a free receptor.

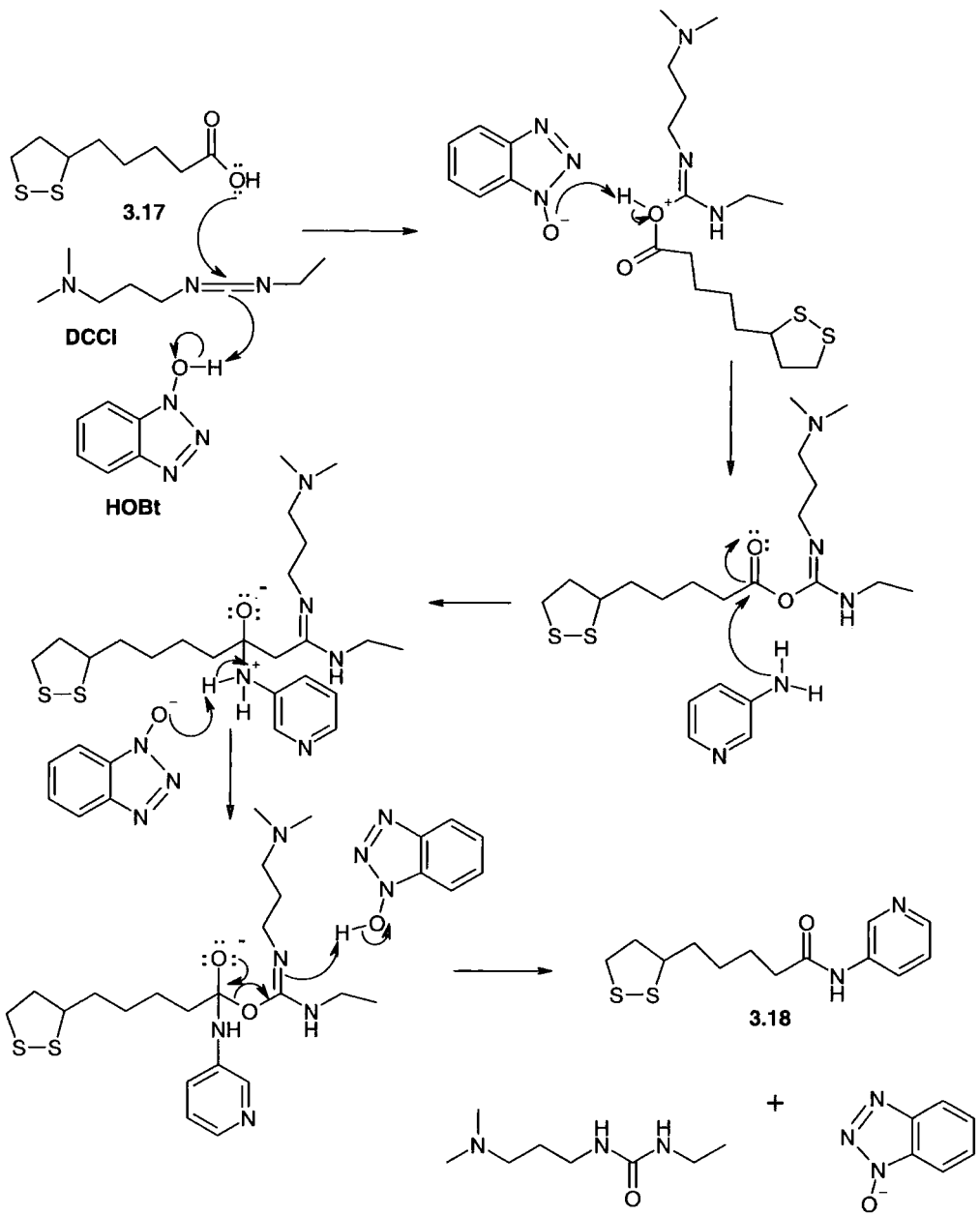

Scheme 13 Proposed mechanism for the HOBt/DCCI facilitated thioctic acid /3-aminopyridine coupling reaction.

3.4.1 Synthesis of pure ligand functionalised gold nanoparticles

The choice of functionalised nanoparticles synthesis was driven by simplicity of preparation. The first method was inspired by Jansen's paper [170] in which the functionalisation involved the surfactant-free single-phase reaction in diglyme. Advantages of this method are the absence of

other stabilising agents which decrease purity but also a good control of size. Disadvantages are strict anaerobic conditions which entails Schlenk-techniques during synthesis of the reducing agent sodium naphthalenide and consequently the reduction of gold. The $HAuCl_4$ was weighed out into a Schlenk tube and dissolved in dry diglyme. Freshly prepared sodium naphthalenide was then added dropwise under vigorous stirring until the solution first turned brown and then dark purple (Scheme 14).

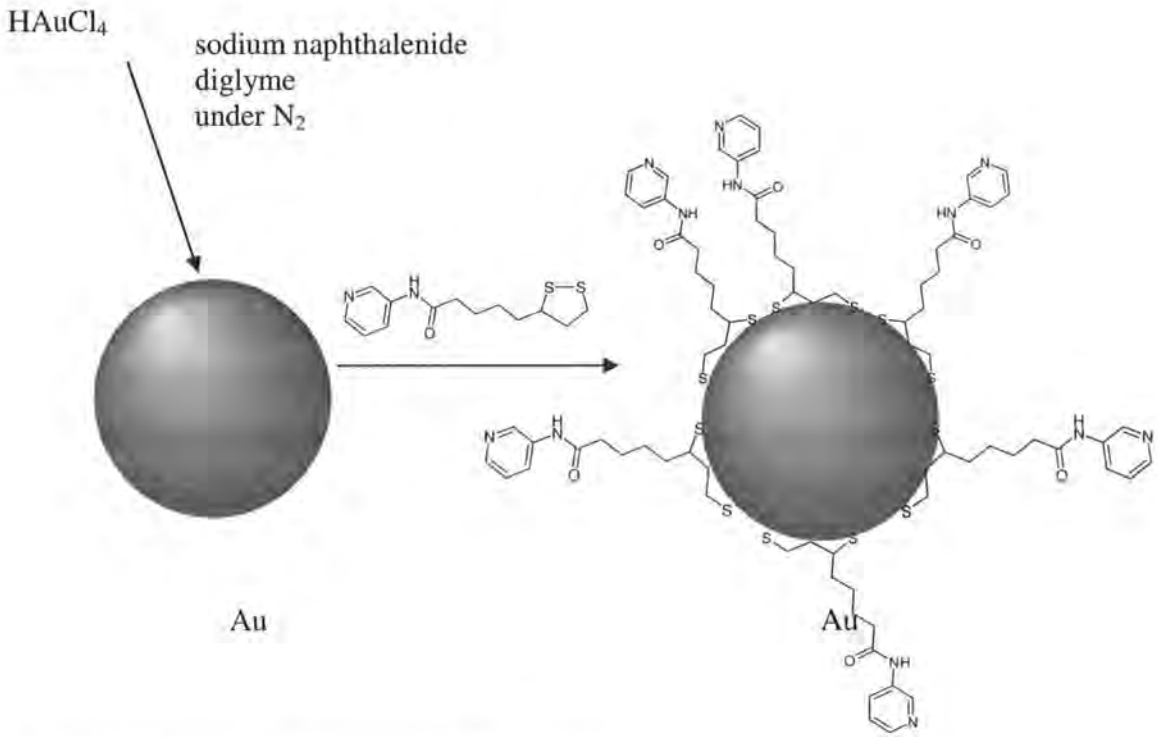

Scheme 14 Cartoon of gold nanoparticles **3.20** synthesis.

According to the literature the size of the nanoparticles depends on the amount of the reducing solution added and reaches a maximum of 5 nm. Diglyme is only a temporary stabilising agent and the nanoparticles precipitate/agglomerate slowly after 1h. As the nature of this reducing agent is rather harsh, the reduced gold after being stirred for ten minutes was exposed to air to quench any remaining reducing agent which could degrade the ligand. The ligand was then added (2 equivalents based on $HAuCl_4$) and stirred for a further hour. The functionalised nanoparticles **3.20** precipitate readily in diglyme solution and were purified by ultracentrifugation and several washings with diethyl ether to remove any unreacted ligand,

naphthalene and diglyme. The nanoparticles were then re-dissolved in methanol. TEM images confirm the presence of nanoparticles with sizes varying between ca. 4-9 nm agglomerating on the carbon grid (Figure 63). A UV-visible spectrum was recorded with a broad peak at 531 nm. The nanoparticles remained stable and didn't agglomerate in the solution at room temperature for a period of 6 months. The solvent can be removed and the nanoparticles can be redispersed for instance in deuterated solvents for ^{1}H NMR analysis which confirm presence of broad peaks[173] assigned to the nanoparticle attached ligands.

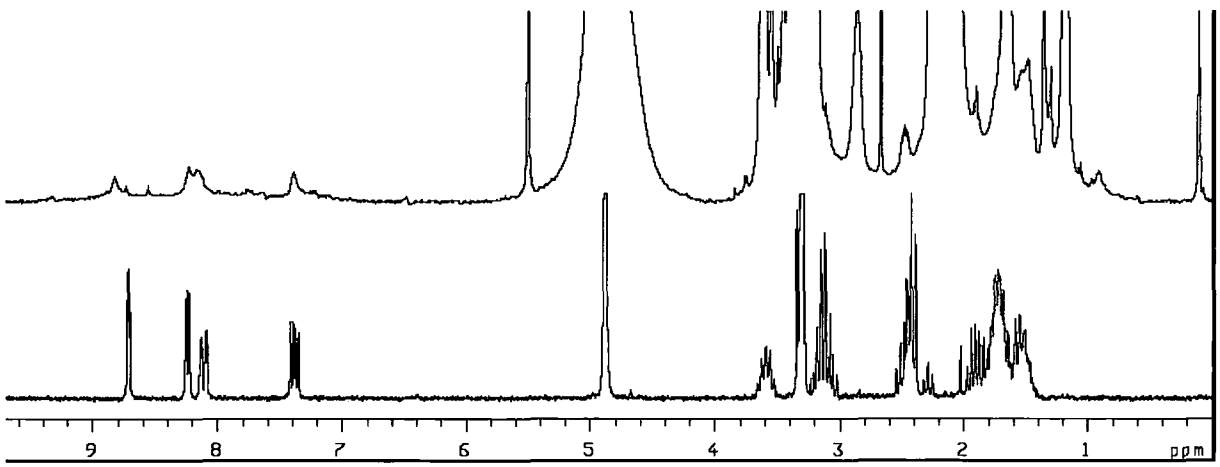

Figure 61 ^{1}H NMR spectra of functionalised gold nanoparticles **3.20** (top) and free ligand (bottom) in MeOD-d_4.

^{1}H NMR spectroscopy is particularly informative about the structure and content of the synthesized nanoparticles. ^{1}H NMR resonances are characteristically broadened relative to those of free ligand; the factors include spin-spin relaxational (T_2) broadening, differences in Au-SR binding sites, and a gradient in monolayer packing density from near-core to ligand terminus with associated dipolar broadening. A particularly noticeable broadening is observed for methylene protons on the ligand chain closest to the gold surface. Broadening was also observed for the pyridyl protons. The IR spectra were taken as KBr disks of the free ligand, reduced ligand (to observe disappearance of S-S stretch for comparison with the functionalised gold nanoparticles) and of ligand functionalised gold nanoparticles (Figure 62).

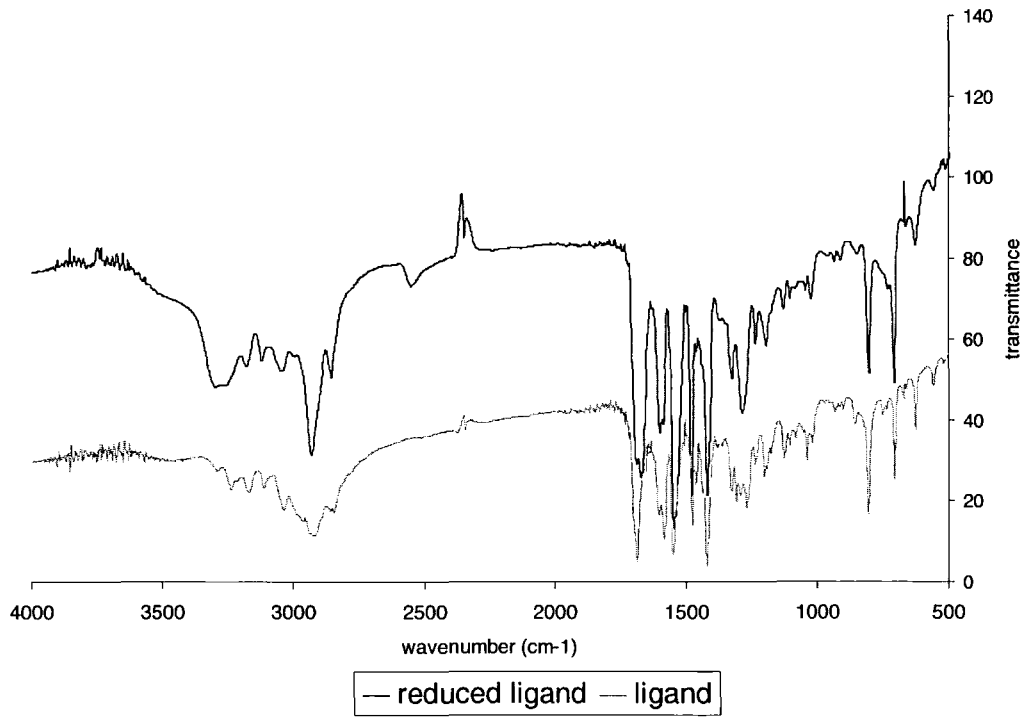

a)

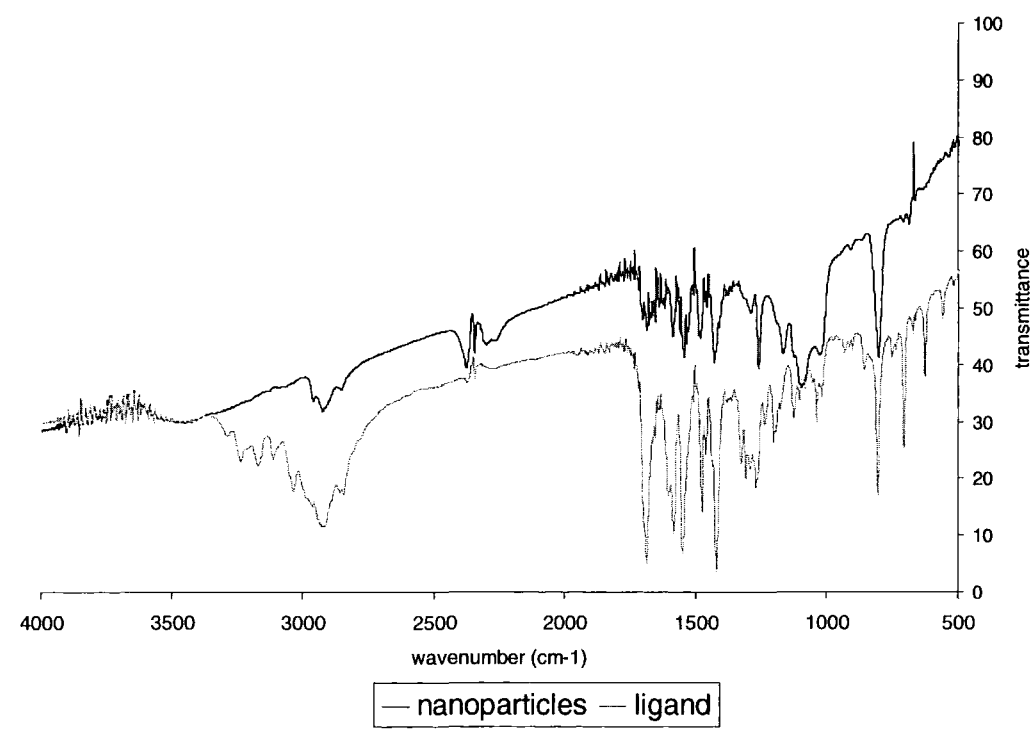

b)

Figure 62 IR spectra of a) reduced ligand **3.21** versus ligand **3.18** and b)nanoparticles **3.20** versus ligand **3.18**.

The peaks at 634 cm^{-1} and 706 cm^{-1} are the S-S stretch and C-S stretch respectively which both disappear upon adsorption onto the gold surface. The IR spectrum for the reduced ligand **3.21** also shows disappearance of the S-S stretch but not the C-S stretch and concomitant appearance of S-H stretch at around 2536 cm^{-1}.

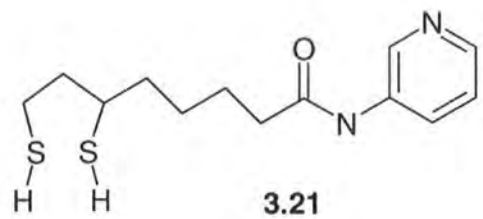

3.21

It was thought that ligand **3.21** could be a more versatile reagent in the subsequent reactions and undesired processes such as polysulfide polymerisation as seen in solution of **3.17** would be avoided. In terms of reactivity with gold nanoparticles, **3.18** proved to be a better stabilising agent. It is possible that preorganised disulfides chemisorb better onto the surface of gold and only one S-S bond is broken.

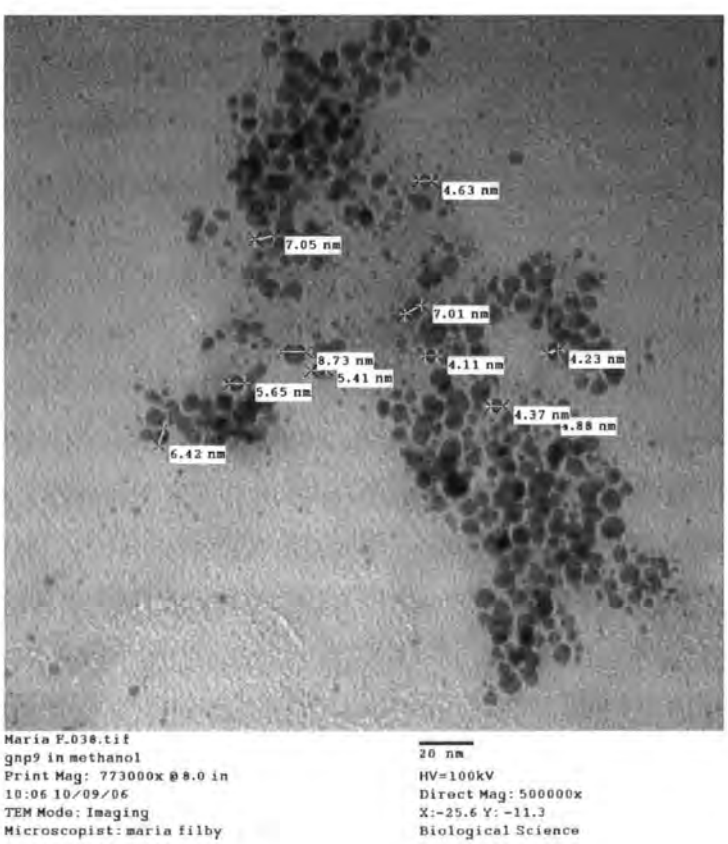

Figure 63 TEM image of **3.20** gold nanoparticles.

3.4.2 UV-vis spectroscopic titrations of **3.20** gold nanoparticles methanolic solution

UV-visible spectrum of the pure ligand functionalised gold nanoparticle solution in methanol was recorded at 532 nm and repeated one week later without any sign of aggregation or ageing (red-shift).[140] Several titrations were acquired at one minute intervals on a Perkin Elmer Lambda UV/Visible spectrophotometer at 293 K. Background correction was made with neat solvent (2 mL) in the reference cell and a blank sample cell. In a typical experiment, 10 μL aliquots of guest (0.216 M) were added to a 2.0 mL solution of gold nanoparticles. Each series represents an addition of 10 μL with an exception of series 1 to which no anion was added. In some cases spectra were recorded without any addition of the anion solution in order to observe any time dependence of the spectrum.

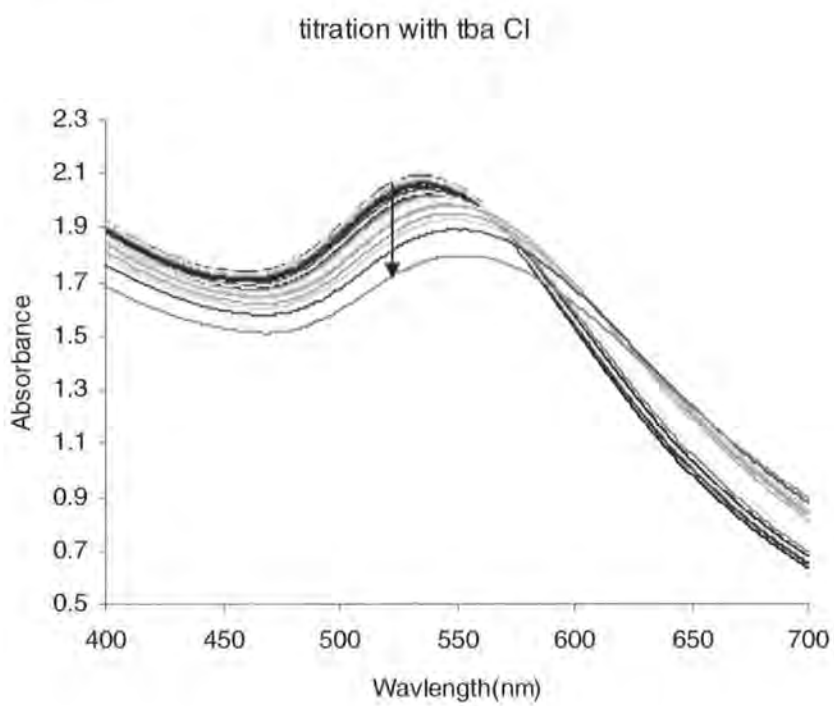

Figure 64 Titration of a gold nanoparticle **3.20** solution with tba Cl in methanol.

Figure 64 reveals a slow red shift which occurs with an addition of up to 6 aliquots of tba Cl solution and the UV shifts from 532 to 535 nm. Then on each further addition a much larger change is observable and the peak shifts up to 553 nm after an addition of 0.1mL in total of the stock solution. The change is ascribed to an anion binding event to the hydrogen bonding moiety

of the ligand and consequently altering of the local index of refraction. This experiment was further supported by titration of the nanoparticle solution **3.20** with tba Br in methanol. No significant changes other than dilution effects occurred (Figure 65) indicating much weaker binding of the bromide anion. When the nanoparticles were titrated against tba NO_3 there was a similar change to the chloride titration however the binding appeared weaker as the shift had reached 550 nm only after an addition of 0.2 mL in total (Figure 66). In all the cases there was a decrease in absorbance due to the dilution effects. When the nanoparticle solution was however titrated against tba AcO^- firstly an increase in absorbance and a red shift was observed after an addition of 3 aliquots followed by a drop in absorbance and a further red shift which reaches 556 nm after an addition of only 8 aliquots (Figure 67). The increase in absorbance can be attributed to a self-assembled layer of acetate anions binding to the ligands and simultaneously changing the refractive index of the surrounding medium. When the amount of acetate added exceeds the availability of binding sites on the nanoparticles the acetate may form aggregates with the nanoparticles deeply embeded within them hence cause the decrease in absorption. The red shift can be explained by nanoparticles being pulled closer together by these aggregates.

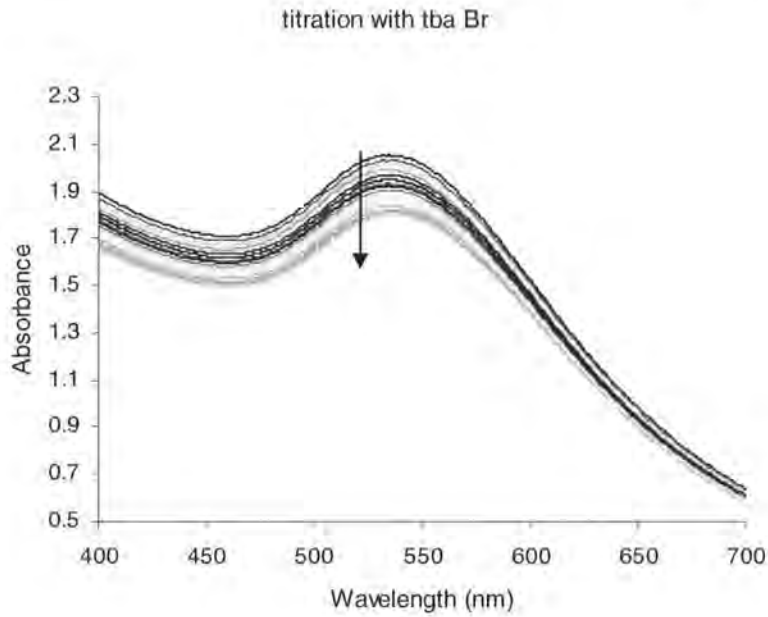

Figure 65 Titration of a gold nanoparticle **3.20** solution with tba Br in methanol.

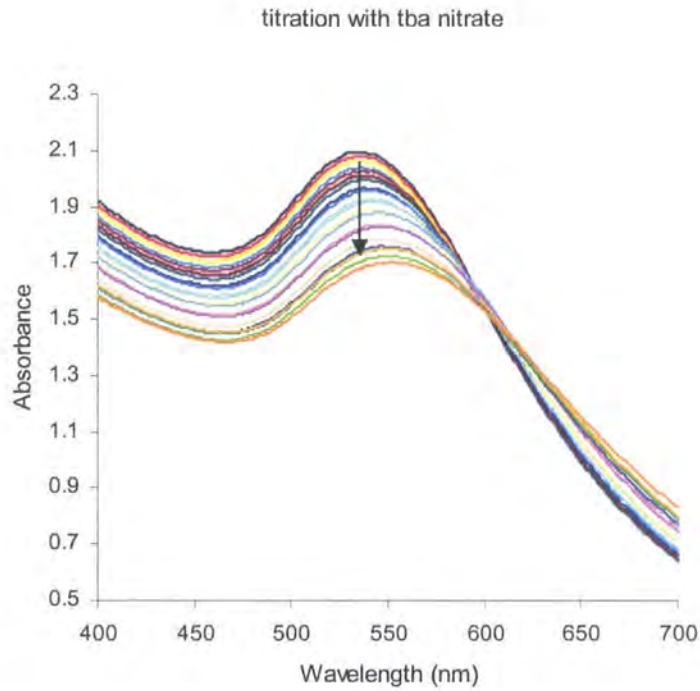

Figure 66 Titration of a gold nanoparticle **3.20** solution with tba NO_3 in methanol.

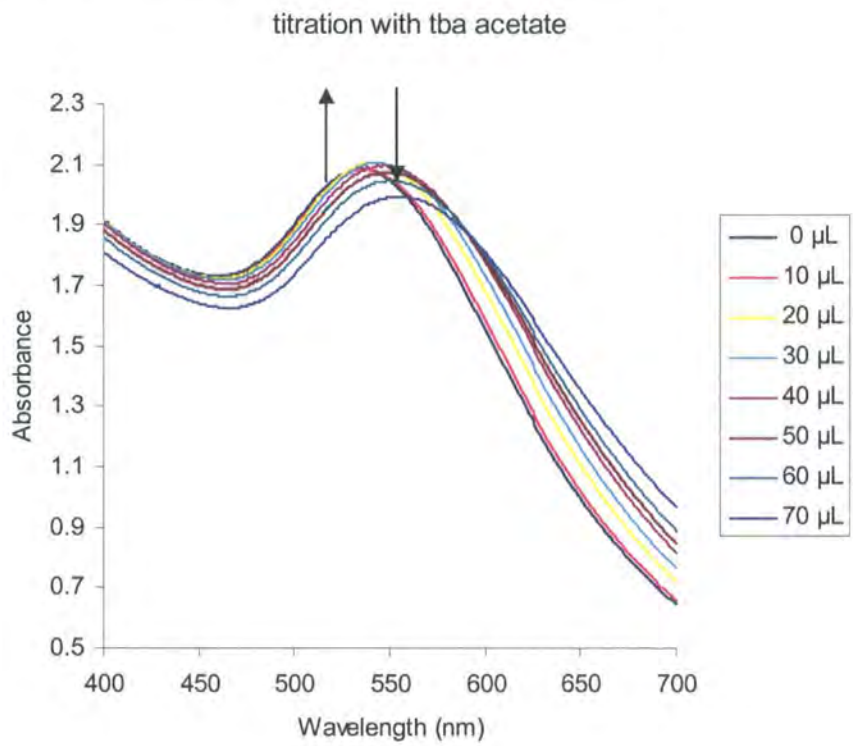

Figure 67 Titration of a gold nanoparticle **3.20** solution with tba AcO^- in methanol.

A very interesting result was obtained when the nanoparticle solution was titrated against Ag BF_4. As seen previously by Mulvaney[149] the absorbance goes up when silica shells on nanoparticles increase which is explained by an increase in significance of scattering. The large increase in absorbance of nanoparticles on addition of silver tetrafluoroborate is thought to be due to the formation of an additional silver metal layer being coordinated to the gold nanoparticle surface monolayer. When the layer deposition is saturated, an excess silver tetrafluoroborate causes the gold nanoparticles to aggregate and eventually precipitate out of solution (red shift on total addition of 50 µL of stock solution) simultaneously with a drop in absorbance (Figure 68).

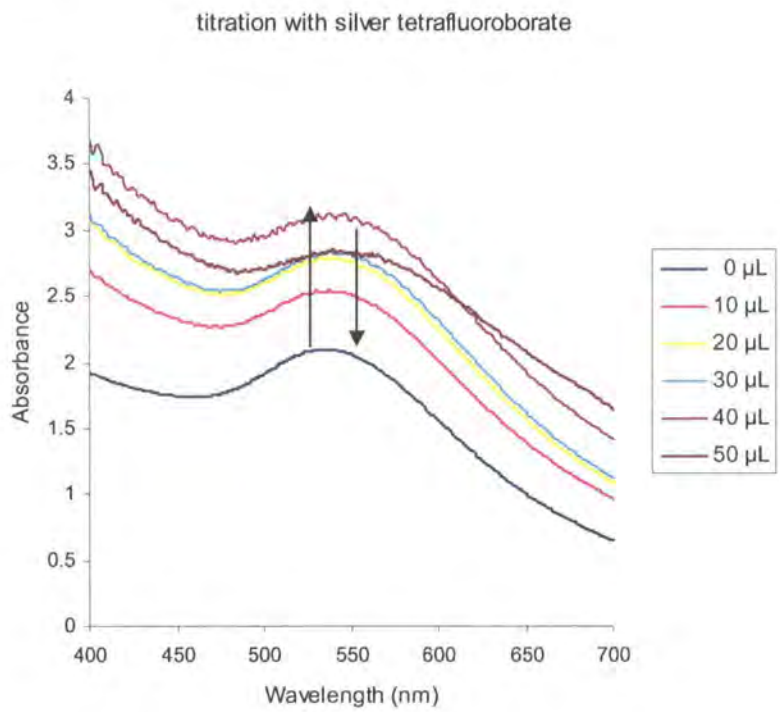

Figure 68 Titration of gold nanoparticles **3.20** solution with $AgBF_4$.

3.4.3 Synthesis of dodecanethiol protected nanoparticles control solution **3.22**.

As a control dodecanethiol protected nanoparticles were synthesized using the Schiffrin [154] method. The nanoparticles were then subjected to several anion UV titrations in chloroform. The concentration of dodecanethiol protected nanoparticle solution was the same as of the thioctic

ligand nanoparticles used in UV titrations. Several solutions of tetrabutylmmonium anions were prepared. The concentrations used were the same as in the ligand nanoparticles titration. Chloroform had to be used as dodecanethiol functionalised nanoparticles precipitate out from methanol. There was no spectral change in any of the titrations including $AgBF_4$ (Figure 69) other than a decrease in absorbance due to dilution effects.

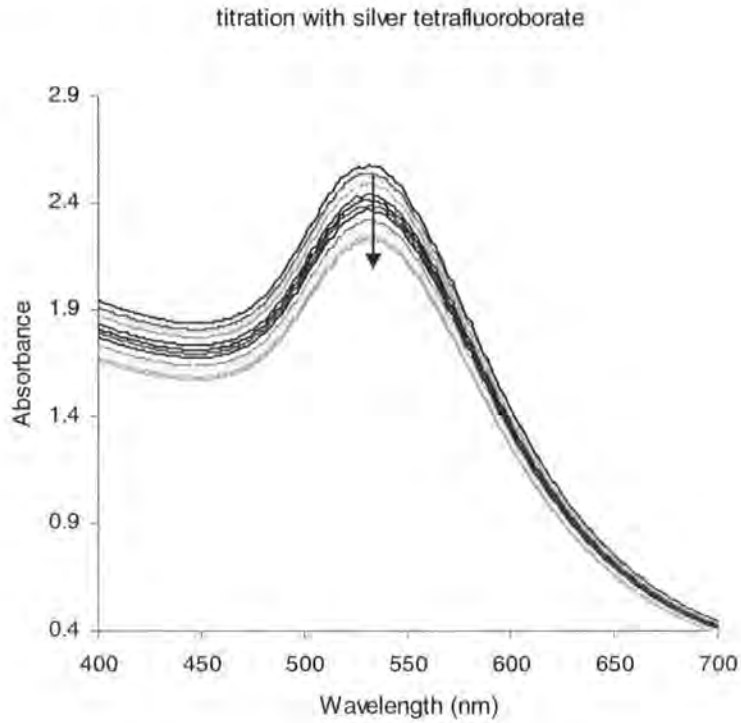

Figure 69 Titration of dodecanethiol protected nanoparticles **3.22** with $AgBF_4$ in chloroform. The decrease in the absorbance is only due to the solvent dilution effect.

An attempt was also made at synthesizing ligand **3.18** protected nanoparticles using the Schiffrin method. However the nanoparticles precipitated within a course of several hours probably due to the formation of larger aggregates which hydrogen bond the ligand to an excess of bromide, an event which is more likely to occur in low polarity solvent such as chloroform.

3.4.4 Synthesis of mixed (dodecanethiol/ligand) layer stabilized nanoparticles **3.23** solutions

Another approach was a method which involved ligand exchange. A method previously described [26, 139]was adopted and 1 molar equivalent of ligand: $HAuCl_4$ was added to the dodecanethiol protected nanoparticle solution **3.22** followed by stirring for 24 h. The nanoparticles were then precipitated with methanol, centrifuged and washed several times with methanol and then ether. Nanoparticles were redissoved in chloroform and obtained nanoparticles were characterized by ^1H NMR, IR and TEM. The ^1H NMR spectrum reveals the ratio of dodecanethiol to ligand as 1.7: 1 by integration of several methylene protons on the dodecanethiol and on the ligand. Broadening of the peaks is also noted, however not to such an extent as was seen in the pure ligand nanoparticle. This could be attributed to more regular size of the nanoparticles and slightly smaller diameter. It was seen previously that the broadness of ^1H NMR resonances varies with the size of the nanoparticles. The larger the diameter, the broader the peaks. The smallest clusters have fewer different types of binding sites (predominantly vertices), thus diminishing effects due to chemical shift distributions.[155] The mixed monolayer protected nanoparticle were also probed with UV titration. There was only an observable change in SPR shift on addition of chloride anion. The titration was also conducted in chloroform. Interestingly first addition produced larger red shift than in pure ligand nanoparticle solution. This is most likely due to the solvent used of lower polarity promoting stronger hydrogen bonding. Subsequent additions produced further red shift until the SPR peak reached 535 nm after which point the nanoparticles' SPR started to return to almost their original peak at 530 nm (Figure 70). This behavior could be attributed to mobility of the ligand around on the surface of nanoparticle or insufficient presence of the ligand on the nanoparticle and therefore lacking the cooperative binding. The movement of ligands around the nanoparticle might be the 'preferred' way of retaining the nanoparticles' stability and dodecanethiol ligands tend to repel them from each other (Figure 71).

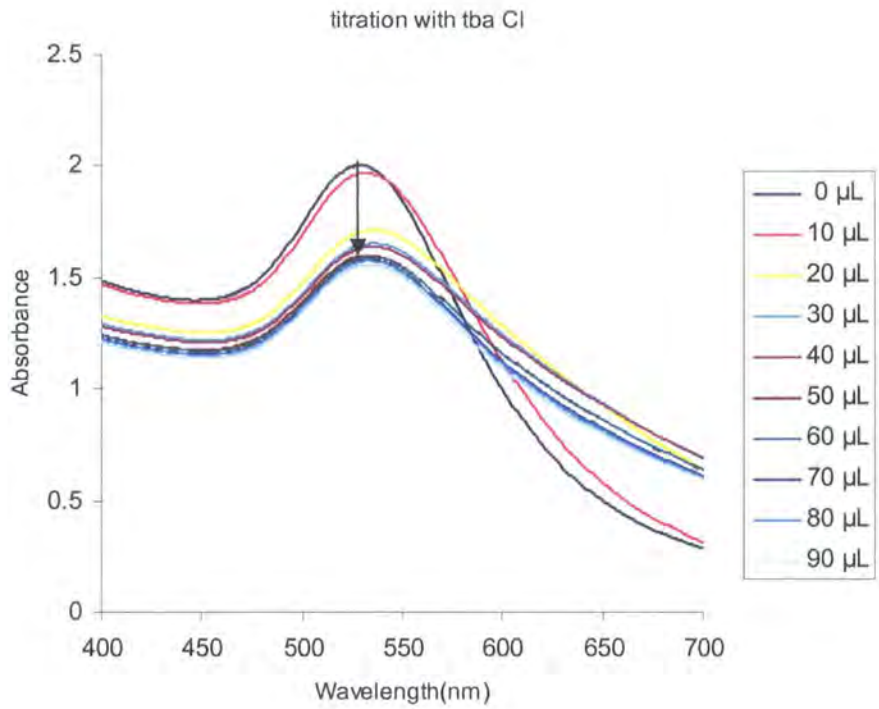

Figure 70 Titration of gold nanoparticles **3.23** solution with tba Cl.

Figure 71 A schematic representation of ligands' movement around the surface of **3.23** nanoparticle.

The TEM images reveal much higher monodispersity with nanoparticles with the highest distribution of diameters around 5nm. The nanoparticles appear to be more agglomerated in comparison to dodecanethiol protected NPs.

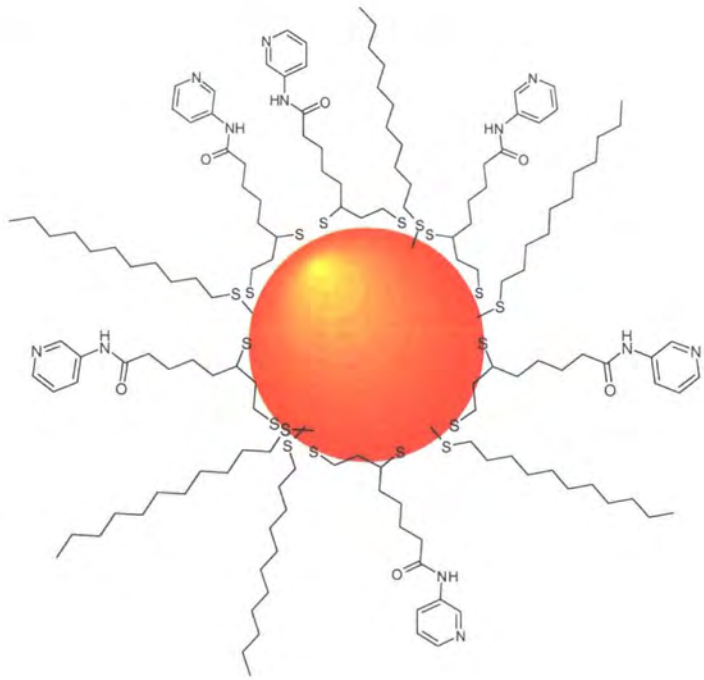

Figure 72 Schematic representation of mixed layer gold nanoparticle **3.23**.

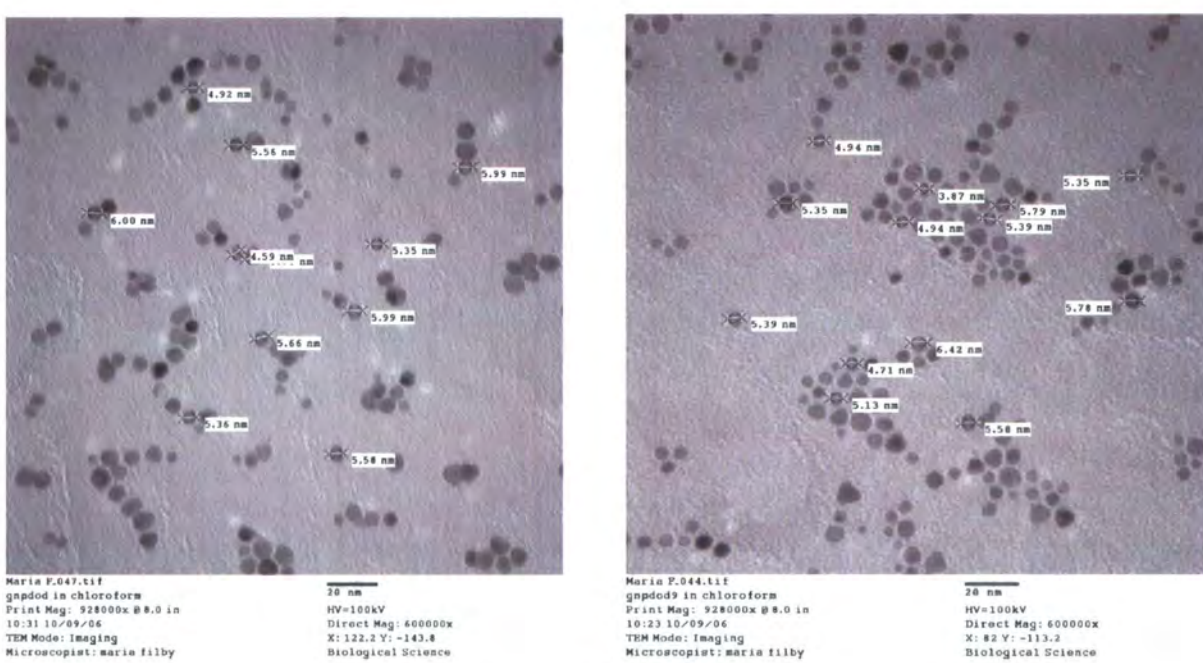

Figure 73 TEM images of dodecanethiol layer functionalised nanoparticles **3.22** (left) and mixed (dodecanethiol/ligand) protected nanoparticles **3.23** (right). The nanoparticles with ligand present appear to agglomerate more readily whereas the dodecanethiol protected only form strands upon solvent evaporation.

3.4.5 An attempted exchange of citrate stabilized gold nanoparticle with ligand **3.18**

Several attempts have been made at exchanging citrate stabilized commercial solution of gold nanoparticles of an average diameter of 8-12 nm with ligand **3.18**. The absorption wavelength of the citrate stabilized nanoparticles occurs at 524 nm, upon addition of small aliquots of methanolic solution of **3.18** (various concentrations). Each addition resulted in profound red shift of the absorption wavelength (depending on concentration) and finally the nanoparticles precipitated out irreversibly. This behaviour could be due to the ligand adsorbing onto the surface of gold and then binding the citrate anions still present in solution, which could subsequently lead to formation of larger aggregates *via* hydrogen interactions. Another plausible reason behind the precipitation is the insolubility of ligand **3.18** in water. A mixture of water/methanol 1: 1 as a solvent medium for the ligand exchange was also used. However, an addition of methanol itself caused the nanoparticles to lose stability.

3.4.6 An attempted synthesis of calix[4]arene appended with ligand **3.18.**

Synthesis of caix[4]arene with sulphur gold binding functionality was attempted. The reaction was carried out in $CDCl_3$ monitored by ^1H NMR spectroscopy. A 24 h reaction (stirring at room temperature) resulted in crude product which had the characteristic resonance at δ=5.58 ppm asigned to CH_2 protons adjacent to the pyridinium nitrogen atom. Upon solvent removal or an attempt to carry out salt metathesis by adding KPF_6, however, the S-S bond polymerized to form an insoluble product. The same reaction was attempted with a reduced ligand **3.21**. However similar polymerization impeded the progress. It may be possible to obtain pure calix[4]arene **3.24** for future applications by preparative HPLC.

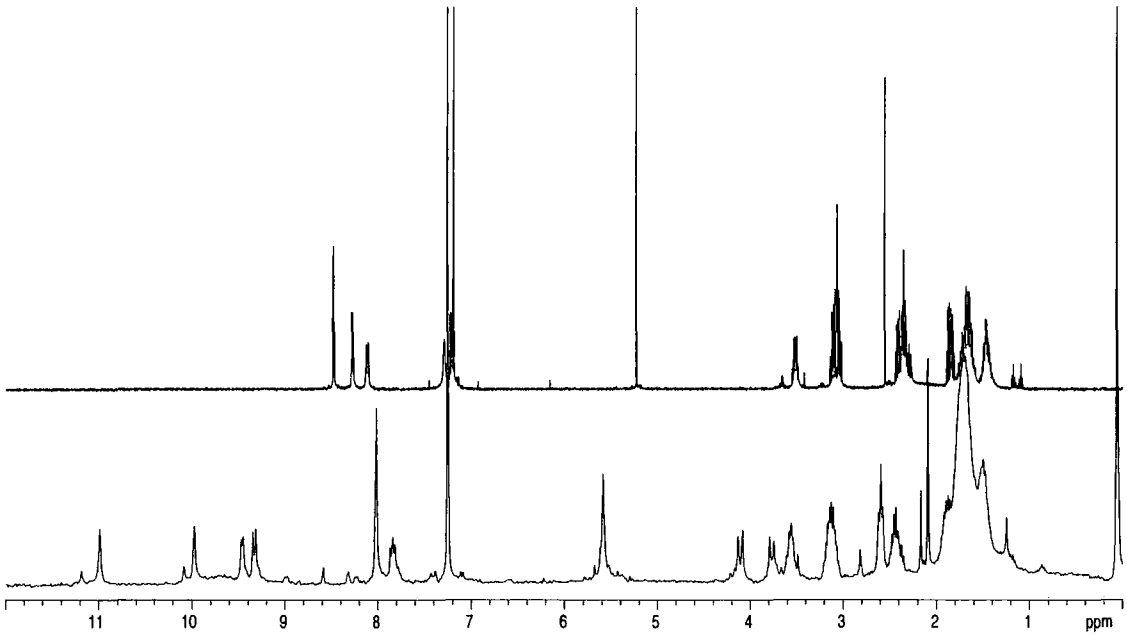

Figure 74 ^{1}H NMR of ligand **3.18** (top) and an attempted synthesis of calixarene (bottom).

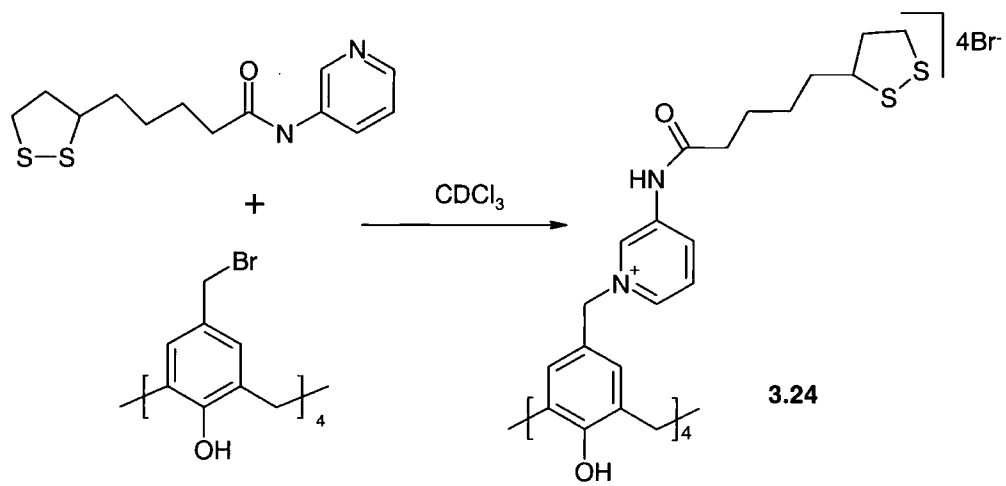

Scheme 15 Synthetic route to calix[4]arene **3.24.**

3.5 Conclusions

The UV titrations demonstrate contrasting differences between dodecanethiol protected and the ligand functionalised gold nanoparticles. The red shift in plasmon resonance band upon addition of anions occurs much more readily in the particles which are either fully or partially fuctionalised with anion binding ligand. The extent in red shift is proportional to the degree of functionalisation for a particular anion addition. The magnitude of the bathochromic shift generally correlates with the polarity and basicity of the added anions, the highest shifts being observed for the tba salts of Cl^->NO_3^->Br^-. The change in dielectric constant in the immediate surrounding environment of nanoparticles is hence the most plausible explanation. Red shifts were generally accompanied by a reduction in absorbance with an exception for the tba acetate and silver tetrafluoroborate. The initilal increase in absorption is probably due to self assembly of an additional organic layer (in case of the acetate anion) and silver atoms layer coordinating to the pyridinyl nitrogen atoms resulting in both cases in increased scattering.

Chapter 4

Experimental

4.1 Density functional Theory (DFT) calculations

The DFT calculations were carried out by Dr. Martin Paterson of Herriot-Watt University.
The B3LYP functional in conjuction with the following basis set: 4-31G on all atoms except the Hydrogens involved in bonding to the ligand, which were augmented with extra polarisation and diffuse basis funcitons as taken from the 6-31++G** basis. For the chloride system, a 6-31+G* basis was used on the chloride, while for the malonate the 4-31G basis was used for C and H, while for the 6-31+G* basis was used on the oxygens. Geometry optimisations for both the chloride and malonate systems were started using the same pyrene calix[4]arene conformation, which was obtained from prior molecular mechanics optimisation.

4.2 X-Ray Crystallography

Suitable single crystals were mounted using silicon grease on a thin glass fibre. Crystallographic measurements were carried out using Bruker SMART 1K (Durham University). The instrument was equipped with graphite monochromatic Mo-Kα radiation (λ = 0.71073 Å). The stardard data collection temperature was 120 K, maintained using an open flow N_2 Oxford Cryostream device. Integration was carried out using SAINT software. Data sets were corrected for Lorentz and polarization effects and for the effects of absorption. Structures were solved using direct methods in SHELXS-97[174] and developed using conventional alternating cycles of least-squares refinement with SHELX-97 and difference Fourier synthesis with the aid of the graphical interface program XSeed. In all cases non-hydrogen atoms were fixed in idealised positions and allowed to ride on the atom to which they were attached. Hydrogen atom thermal parameters were tied to those of the atom to which they were attached. Where possible O-H hydrogen atoms were located experimentally and their positionand displacement parameters refined. Molecular graphics were produced using the program POV-Ray.

4.2.1 Crystal data for methoxy ethyl calix[4]arene

$C_{36}H_{40}O_8$, M = 600.68, 0.18 × 0.13 × 0.15 mm^3, triclinic, space group P-1 (No. 2), a = 9.7386(7), b = 10.7213(7), c = 15.3770(11) Å, α = 89.1120(10), β = 75.9290(10), γ = 74.7240(10)°, V = 1500.30(18) Å^3, Z = 2, D_c = 1.330 g/cm^3, F_{000} = 640, MoKα radiation, λ = 0.71073 Å, T = 120(2)K, $2\theta_{max}$ = 58.0°, 18879 reflections collected, 7915 unique (R_{int} = 0.0336). Final *GooF* = 1.032, *R1* = 0.0470, *wR2* = 0.1310, *R* indices based on 5822 reflections with I >2sigma(I) (refinement on F^2), 433 parameters, 0 restraints. Lp and absorption corrections applied, μ = 0.093 mm^{-1}.

4.2.2 Crystal data for the bromomethylated calix[4]arene (**2.15**)

$C_{33}H_{34}Br_4Cl_2O_4$, M = 885.14, 0.20 × 0.10 × 0.10 mm^3, monoclinic, space group $P2_1/c$ (No. 14), a = 17.541(4), b = 21.250(4), c = 17.502(4) Å, β = 90.099(5)°, V = 6524(2) Å^3, Z = 8, D_c = 1.802 g/cm^3, F_{000} = 3504, SMART 1k, MoKα radiation, λ = 0.71073 Å, T = 120(2)K, $2\theta_{max}$ = 56.8°, 69561 reflections collected, 15231 unique (R_{int} = 0.2667). Final *GooF* = 1.103, *R1* = 0.1243, *wR2* = 0.1754, *R* indices based on 7607 reflections with I >2sigma(I) (refinement on F^2), 675 parameters, 0 restraints. Lp and absorption corrections applied, μ = 5.136 mm^{-1}.

4.3 Materials and Synthesis

All purchased starting materials were of commercial quality and were used without further purification. Solvents were used as obtained unless mentioned otherwise. Dichloromethane and dichloroethane were dried using calcium hydride still. Diglyme (diethylene glycol dimethyl ether) was dried over sodium under vacuum. Reactions were carried out under air unless specifically mentioned.

4.4 Analysis

^{1}H NMR spectra were run at room temperature using Bruker AV-400, Varian Inova-500, Varian Unity-300, Varian Mercury-200 NMR spectrometers at Durham University. Chemical shifts are reported in parts per million (δ) relative to tetramethylsilane as an internal reference. Coupling

constants (J) are reported in Hertz (Hz). Multiplicities are reported as singlet (s), doublet (d), doublet of dublets (dd), doublets of doublets of doublets (ddd), multiplets (m) or broad singnals (b). Mass spectra were run using a Micromass Autospec operating in EI or ES mode at Durham University. Micro-analysis for C, H, N were recorded at Durham University. IR spectra were collected using Perkin Elmer Spectrum 100 (spectral resolution $4cm^{-1}$) as KBr discs. Peaks are reported in wavenumbers (cm^{-1}) and are described as weak (w), medium (m) and strong (s). UV spectra were recorded on Perkin Elmer Lambda 900 UV/VIS/NIR spectrometer.

4.5 ^{1}H NMR Titration Experiments

^{1}H NMR titration experiments were carried out at room temperature using Varian Inova-500 spectrometer operating at 500 MHz (Durham University). All chemical shifts are reported in ppm relative to TMS as an internal reference. A solution of the host species of known concentration typically 0.5-1.5mM, was made up in an NMR tube using the appropriate deuterated solvent (0.5 mL). Solutions of the anions, as tba salts, were made up in volumetric flasks (2.0 mL) with a concentration five times greater than that of the host. The guest solution was typically added in 10 μl aliquots, representing 0.1 equivalents of the guest with respect to the host. Larger aliquots were used in some cases where no inflection of the trace was evident. Spectra were recorded after each addition and the trace was followed simultaneously. Results were analysed using the curve-fitting progrom HypNMR.[120]

4.6 Variable Temperature (VT) ^{1}H NMR Experiments

^{1}H VT-NMR experiments were conducted using a Varian Inova-500 spectrometer operating at 500 MHz (Durham University). Spectra were run in acetone-d_6 with TMS as an internal reference. An initial spectrum was run at room temperature before reducing the temperature in 20°C steps to -20°C and then in 10°C steps to -70°C. The temperature was allowed to equilibrate at each temperature before collection of the spectra. Experiments were conducted using the free receptor species (i.e. the PF_6 salt) and with one equivalent of added anion guest as tba salt.

4.7 Synthesis of New Compounds

(4-Pentyl-benzyl)-pyridin-3-yl-amine (**2.16b**).

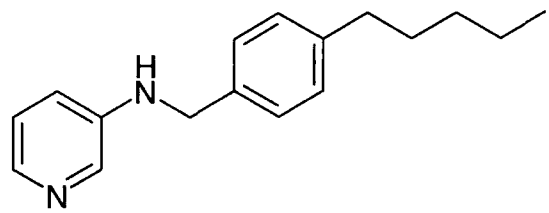

Pentylbenzyldehyde (1.99g, 11.3 mmol) and 3-aminopyridine (1.06g, 11.3 mmol) were refluxed in $CHCl_3$ (20 mL) for 18 h, under N_2. The solvent was removed under reduced pressure to produce viscous oil. The imine was then redissolved in CH_3OH (75 mL) to which 3 molar equivalents of $NaBH_4$ was added slowly and stirred for 2 h. The solution was then made acidic to pH 3 with 2M HCl, then basic to pH 10 with NaOH. An extraction with CH_2Cl_2 and water was then conducted. The solvent was removed under reduced pressure and the crude product was re-crystallised form CH_2Cl_2 and n-hexane and triturated in an acetone dry ice bath to produce the desired product as a white solid, which was filtered and washed with ether. Yield =2.1 g, 8.3 mmol, 74%.

^{1}H NMR: ($CDCl_3$, J/Hz, δ/ppm): δ 0.82 (t, 3H, *J*=7.2, CH_3), 1.26 (m, 4H, CH_2), 1.53 (m, 2H, CH_2), 2.52 (t, 2H, *J*=7.6, CH_2), 3.97 (br, s,1H, NH,), 4.23 (d, *J*=5.6, 2H, CH_2,), 6.81 (ddd, 1H, *J*=1.2, 2.8, 8.4 PyH), 6.99 (dd, *J*=4.8, 8.4, 1H, PyH), 7.09, 7.19 (AA'BB', 4H, *J*=7.6, ArH), 7.90 (dd, *J*=1.2, 4.8, 1H, PyH), 8.03 (d, 1H, *J*=2.4, PyH).

ES+ MS: m/z=255$[M+H]^+$

IR (v/cm^{-1}): 3426 m (NH)

Anal: Calcd. for $C_{17}H_{22}N_2$: C, 80.27, H, 8.72, N, 11.01%. Found: C, 80.10, H, 8.70, N, 10.95%.

Pentalidene-pyridin-3-yl amine (**2.16c**).

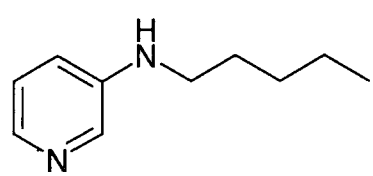

n-Pentaldehyde (2.3g, 27.0 mmol) and 3-aminopyridine (2.0g, 21.0 mmol) were stirred in dry CH_2Cl_2 (100 mL) with $MgSO_4$ under N_2 at r.t. for 2 h. The solvent was removed under reduced pressure. The imine was then redissolved in CH_3OH (75 mL) to which 3 molar equivalents of

$NaBH_4$ was added slowly and stirred for 2 h. The solution was then made acidic to pH 3 with 2M HCl, then basic to pH 10 with NaOH. An extraction with CH_2Cl_2 and water was then conducted. The dichloromethane extracts were then dried with $MgSO_4$ and reduced under pressure to 20 mL. The pure product slowly crystalised in the fridge and was separated on the Büchner funnel. Yield =3.0g, 18.3 mmol, 87%.

^{1}H NMR: ($CDCl_3$, J/Hz, δ/ppm): δ 0.82 (t, 3H, *J*=7.2, CH_3), 1.29 (m, 2H, CH_2), 1.44 (m, 2H, CH_2), 2.96 (q, 2H, *J*=5.2, CH_2). 4.23 (br, s, 1H, N**H**), 6.72 (ddd, 1H, *J*=1.2, 3.0, 8.4, Py**H**), 6.19 (dd, 1H, *J*=4.8, 8.2, Py**H**), 7.78 (dd, 1H, *J*=1.2, 4.6, Py**H**), 7.90 (d, 1H, *J*=2.8, Py**H**).

ES+ MS: m/z=165$[M+H]^+$

Anal: Calcd. for $C_{10}H_{16}N_2$: C, 73.12, H, 9.81, N, 17.05%. Found: C, 71.07, H, 9.97, N, 15.09%. The microanalysis for C and N is low due to presence of some starting material n-pentaldehyde. The purification was not necessary for the next reaction step.

IR (v/cm^{-1}): 2425w (NH)

Butyralidene-pyridin-3-yl amine (**2.16d**)

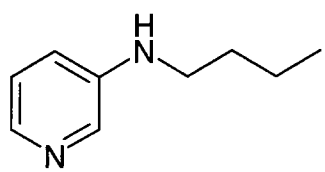

n-Butyraldehyde (3.8g, 53.1 mmol excess) and 3-aminopyridine (4.6g, 49.1 mmol) were stirred in dry CH_2Cl_2 (100mL) with $MgSO_4$ under N_2 for 2 h. The solvent was removed under reduced pressure producing oil. The imine was then redissolved in CH_3OH (100 mL) to which 3 molar equivalents of $NaBH_4$ was added slowly and stirred for 2 h. The solution was then made acidic to pH 3 with 2M HCl, then basic to pH 10 with NaOH. An extraction with CH_2Cl_2 and water was then conducted. The dichloromethane extracts were then dried with $MgSO_4$ and reduced under pressure to 20 mL. The pure product slowly crystalised in the fridge and was separated on the Büchner funnel. Yield =4.8 g, 31 mmol, 63 %.

^{1}H NMR: ($CDCl_3$, J/Hz, δ/ppm): δ 0.82 (t, 3H, *J*=7.2, CH_3), 1.29 (sp, 2H, *J*=7.6, CH_2), 1.45 (qu, 2H, *J*=6.8, CH_2), 2.96 (q, 2H, *J*=6.0, CH_2). 4.19 (br, s, 1H, N**H**),
6.73 (ddd, 1H, *J*=1.2, 3.0, 8.4, Py**H**), 6.24 (dd, 1H, *J*=4.8, 8.2, Py**H**), 7.78 (dd, 1H, *J*=1.2, 4.6, Py**H**), 7.90 (d, 1H, *J*=2.8, Py**H**).

ES+ MS: m/z=151[M+H]$^+$

Anal: Calcd. for $C_9H_{14}N_2$: C, 71.96, H, 9.39, N, 18.64%. Found: C, 69.15, H, 9.09, N, 17.51%. The microanalysis for C and N is low due to presence of some starting material n-butyraldehyde. The purification was not necessary for the next reaction step.

IR (ν/cm^{-1}): 3413w (NH)

Pyren-1-ylmethyl-pyridin-3-yl-imine

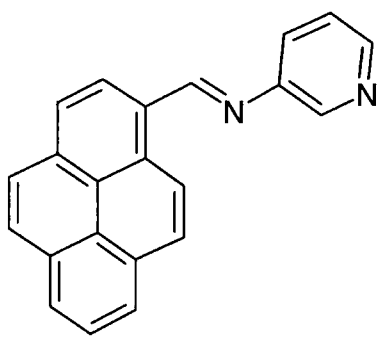

Pyrene-1-carboxyldehyde (2.0g, 86.9 mmol) was weighed out (in a glove box) and then dissolved in a degassed dichloroethane (100 mL), 3-aminopyridine (0.81g, 86.85 mmol) and $MgSO_4$ were added. The reaction was stirred under reflux for 25 h under N_2. The solvent was removed under reduced pressure and the crude reaction mixture redissolved in diethyl ether. Undissolved material was filtered off. The crude imine was then purified by precipitating out the solid from reaction mixture by placing the flask in acetone and dry ice bath. Yield =2.2g, 71.89 mmol, 82%.

^{1}H NMR: ($CDCl_3$, J/Hz, δ/ppm): δ 7.43 (dd, 1H, *J*=4.8, 8.4, Py**H**), 7.72 (ddd, 1H, *J*=1.6, 2.8, 8.4, Py**H**), 8.10 (t, 1H, *J*=7.6, Ar**H**), 8.15 (d, 1H, *J*=8.8, Ar**H**), 8.22 (d, 1H, *J*=8.8, Ar**H**), 8.28-8.31 (m, 4H, Ar**H**), 7.57 (dd, 1H, *J*=1.2, 4.8, Py**H**), 8.69 (d, 1H, *J*=2.4, Py**H**), 8.78 (d, 1H, *J*=8.0, Ar**H**), 9.85(d, 1H, *J*=9.6, Ar**H**), 9.51 (s, 1H, C**H**).

ES+ MS: m/z=307[M+H]$^+$

IR (ν/cm^{-1}): 1612 *s* (CH=N)

Anal: Calcd. for $C_{22}H_{14}N_2$: C, 86.25, H, 4.60, N, 9.14%. Found: C, 86.04, H, 4.49, N, 8.60%.

Pyren-1-ylmethyl-pyridin-3-yl-amine (**2.16e**).

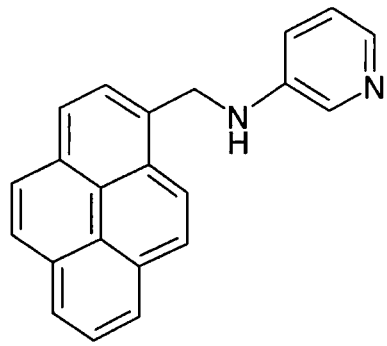

Pyren-1-ylmethyl-pyridin-3-yl-imine (2.0 g, 6.5 mmol) was dissolved in MeOH (700 mL) and 3 molar equivalents of $NaBH_4$ were added slowly. The reaction mixture was stirred for 2h. 2M HCl was added until the pH was 3 followed by a 2M NaOH until the pH was 9. The solvent was then removed under reduced pressure and during the process orange crystals of pure amine appeared which were separated. Further removal of MeOH followed by extraction into CH_2Cl_2 and washing with water resulted in crude amine which was washed with diethyl ether to remove any remaining unreacted aldehyde. Yield =1.32 g, 4.3 mmol, 66%.

^{1}H NMR: ($CDCl_3$, J/Hz, δ/ppm): δ 4.05 (s,br, 1H, N**H**), 4.89 (2H, *J*=4.8, C**H$_2$**), 6.88(ddd, 1H, *J*=1.6, 2.8, 8.4, Py**H**), 7.01 (dd, 1H, *J*=4.8, 8.4, Py**H**), 7.92 (dd, 1H, *J*=1.6, 4.8, Py**H**), 7.90-7.94 (m, 2H, Ar**H**), 7.96 (d, 2H, *J*=1.4, Ar**H**), 8.04 (d, 1H, *J*=8.4, Py**H**), 8.06 (d, 2H, *J*=3.2, Ar**H**), 8.09(d, 1H, *J*=1.6, Py**H**), 8.11 (t, 1H, *J*=1.2, Ar**H**), 8.17 (d, 2H, *J*=9.2, Ar**H**)

ES+ MS: m/z=309$[M+H]^+$

IR (v/cm^{-1}): 3419m (NH)

Anal: Calcd. for $C_{22}H_{16}N_2$: C, 85.68, H, 5.22, N, 9.08%.

Anal: Calcd. for $C_{22}H_{16}N_2$ 0.75 H_2O: C, 82.08, H, 5.47, N, 8.70%. Found: C, 81.90, H, 4.99, N, 8.49%.

4-(Pentyloxy-benzylidene)-pyridin-3-yl-amine (**2.16f**)

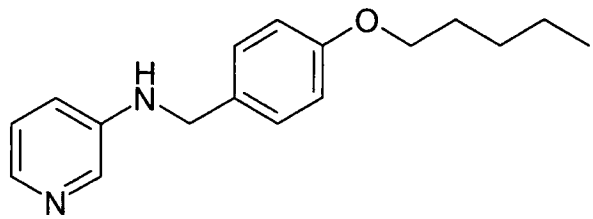

Pentyloxybenzyldehyde (2.5g, 13.00 mmol) and 3-aminopyridine (1.22g, 13.00 mmol) were refluxed in CH_2Cl_2 (50 mL) for 18 h, under N_2. The solvent was removed under reduced pressure to produce a viscous oil. 4-(Pentyloxy-benzylidene)-pyridin-3-yl-imine was redissolved in 50mL of MeOH to which 3 equivalents of $NaBH_4$ were added slowly. The reaction was stirred for 2 h then excess $NaBH_4$ was destroyed by addition of 2M HCl up to pH 3 then 2M NaOH was added until the pH was 9. The mixture was then extracted to CH_2Cl_2 which was dried with $MgSO_4$ followed by recrystallization from CH_2Cl_2 and n-hexane. Yield =2.2g, 8.14mmol, 78%.

^{1}H NMR: ($CDCl_3$, J/Hz, δ/ppm): δ 0.86 (t, 3H, *J*=7.2, CH_3), 1.33 (m, 4H, CH_2), 1.53 (qt, 2H, *J*=7.6, CH_2), 3.87 (t, 2H, *J*=6.8, CH_2), 3.94 (br, s,1H, NH,), 4.87 (d, *J*=5.2, 2H, CH_2,), 6.80 (dd, 1H, *J*=1.2, 8.2 PyH), 6.99 (dd, *J*=0.8, 8.4, 1H, PyH), 6.80, 7.19 (AA'BB', 4H, *J*=8.4, ArH), 7.89 (dd, *J*=1.2, 4.8, 1H, PyH), 7.99 (dd, 1H, *J*=0.8, 3.0, PyH).

ES+ MS: m/z=271$[M+H]^+$

IR (ν/cm^{-1}): 2226 m (NH)

Anal: Calcd. for $C_{12}H_{12}N_2O$: C, 75.52, H, 8.20, N, 10.36%. Found: C, 75.29, H, 8.18, N, 10.10%.

4.8 Synthesis of Host Molecules

Tetrakis-p-tert-butyl tetrahydroxycalix[4]arene (**2.1**).[118]

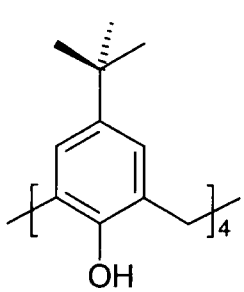

(10 g, 66 mmol) of p-tert-butylphenol was mixed with 3M NaOH (10 mL) and 9.7 g of 37% formaldehyde solution. The mixture was heated at 50-55°C for 45 h and then at 110-120 °C for 2 h to give a yellow solid. This was ground to a powder and stirred with 1M HCl (100 mL) for 1 h to neutralize the base and the solid was removed by filtration, washed with water and dried in an oven at 100-120 °C for 30 min. This greenish material was mixed with 70 g of diphenyl ether and heated to 210-220 °C for 2 h in an atmosphere of nitrogen. The reaction mixture was cooled, treated with 150 mL of ethyl acetate and filtered to yield 5.32g of white solid (8.2 mmol, 49%).

^{1}H NMR: ($CDCl_3$, J/Hz, δ/ppm): 1.12 (s, 36H, CH_3), 3.45 (br, d, 4H, CH_2), 4.23 (br, d, 4H, CH_2), 6.93 (s, 8H, Ar**H**), 10.21 (s, 4H, Ar**OH**).

Tetrahydroxycalix[4]arene (**2.2**). [118]

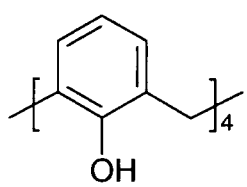

(5 g, 7.7 mmol) of tetrakis-*p*-tert-butyl tetrahydroxycalix[4]arene (**2.1**), dry toluene (50 mL) and phenol (0.87 g) stirred under nitroged for 10 min at a temperature of 55°C. To this colourless mixture was added aluminium trichloride (5 g, 36 mmol). The mixture turned slowly orange. Within 30 min deep red sticky phase separates on the walls of the flask. The reaction mixture was stirred for 2.5 h then was poured into 250 mL beaker containing 100g or crushed ice. The reaction mixture was washed with 50 mL of dichloromethane mixed with 50 g of crushed ice. Everything was transferred into a separating funnel and 200 mL of dichloromethane was added. The organic phase was washed three times with 50 mL HCl and then twice with water (50 mL). Organic solvents were then distilled under reduced pressure using rotary evaporator. 25 mL of diethyl ether was added to aid precipitation of product. The solids were collected by suction filtration and washed with diethyl ether. The resulting white powder was recrystallised from methanol and chloroform. Yield =2.9 g, 6.8 mmol, 88%.

^{1}H NMR: ($CDCl_3$, J/Hz, δ/ppm): 1.45 (s, 36H, CH_3), 3.45 (br, 4H, CH_2), 4.18 (br, 4H, CH_2), 6.65 (t, *J*=7.6, 4H, Ar**H**), 6.98 (d, *J*=7.6, 4H, Ar**H**), 10.12 (s, 4H, Ar**OH**).

Tetrakis-p-bromomethylated tetrahydroxycalix[4]arene (**2.15**).

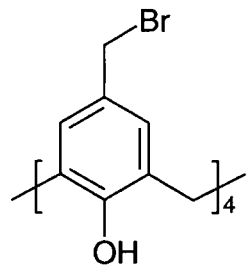

The coumpound was prepared by modification of the procedure described for the bromination of aromatic rings. Zinc (0.8g, 12.2 mmol) was placed in 200 mL of glacial acetic and 20 mL of HBr in acetic acid added then reaction mixture was heated and stirred at 70 °C until all the Zink had dissolved. Tetrahydroxycalix[4]arene (4.2g, 10 mmol) was added to the mixture followed by paraformaldehyde (15g, 0.52 mol) and HBr in acetic acid (100 mL) was added to this slowly. All the material dissolved followed by a formation of a pale pink precipitate few minutes later and the reaction mixture was sirred for a further 1 h at 70 °C then the precipitate was separated, washed thoroughly with water followed by diethyl ether. Yield =9.22g, 11.6 mmol, 95%.

^{1}H NMR: ($CDCl_3$, J/Hz, δ/ppm): δ3.46 (br, 4H, ArC**H**$_2$Ar), 4.13 (br, 4H, ArC**H**$_2$Ar), 4.26(s, 8H, C**H**$_2$Br), 7.18(s, 8H, Ar**H**), 10.02(s, 4H, O**H**).

Anal: Calcd. for $C_{32}H_{28}Br_4O_4$: C, 48.27, H, 3.54%.

Anal: Calcd. for $C_{32}H_{28}Br_4O_4$+1H_2O: C, 47.20, H, 3.71. Found: C, 47.45, H, 3.75%.

Tetra[(3-aminopyridium-methyl) tetrahydroxyl]calixarene bromide salt (**2.17a**·4Br^-)

Tetrakis-p-bromomethylated tetrahydroxycalix[4]arene (0.28 g, 0.35 mmol) and 3-aminopyridine (0.13 g, 1.4 mmol) were stirred for 24 h at room temperature in dichloromethane (50 mL). The precipitate formed immediately upon addition of the 3-aminopyridine. The solid was then separated on a Büchner funnel and washed several times with diethyl ether.

Anal. Calc for $C_{52}H_{52}N_8O_4Br_4$: C, 53.26, H, 4.46, N, 9.55.

Anal. Calc for $C_{52}H_{52}N_8O_4Br_4Cl$ 2H_2O: C, 50.20, H, 4.53, N, 9.00. Found C, 50.67, H, 4.44, N, 8.84.

Tetra[(3-aminopyridium-methyl)tetrahydroxyl]calixarene hexafluorophosphate salt (**2.17a**·$4PF_6^-$) Bromide salt (**2.17a**·$4Br^-$) was dissolved in a minimum amount of acetonitrile : water (1 : 1) mixture to which 10 molar equivalents of $NaPF_6$ were added and the reaction was stirred for 2 h. The collected precipitate was washed several times with diethyl ether.

ES^+-MS: m/z=332$[M-3PF_6]^{3+}$
Anal: Calcd. for $C_{52}H_{52}N_8O_4P_4F_{24}$: C, 43.58, H, 3.65, N, 7.82.

Anal: Calcd. for $C_{52}H_{52}N_8O_4P_4F_{24}$+ H_2O: C, 43.04, H, 3.75, N, 7.72. Found: C, 42.99, H, 3.72, N, 6.42.

Tetra[3- (Pentylbenzylmethylamino)pyridium-tetrahydroxy]calixarene bromide salt (**2.17b**·$4Br^-$).

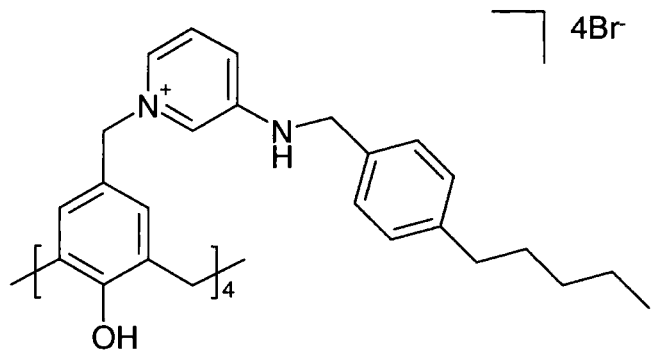

Tetrakis-p-bromomethylated tetrahydroxycalix[4]arene (0.32 g, 0.40 mmol) and pentylbenzylidene-pyridin-3-yl amine (0.41g, 1.61 mmol) were dissolved in dichloromethane (75 mL). The reaction was heated under reflux for 24 h. The reaction mixture was precipitated with diethyl ether and separated on Büchner funnel followed by washing several times with diethyl ether. Yield =0.68 g, 0.38 mmol, 95%.

^{1}H NMR ($CDCl_3$, J /Hz, δ/ppm): 0.67 (t *J*=6.8, 12H, CH_3), 1.30 (m, 16H, CH_2) 1.65 (qu, *J*=6.8, 8H, CH_2), 2.45 (t, *J*=6.8, 8H, CH_2), 3.69 (d, *J*=13.6, 4H, ArCH_2Ar), 4.03 (d, *J*=13.6, 4H, ArCH_2Ar), 4.27 (d, *J*=3.6, 8H, CH_2), 5.29 (s, 8H, CH_2), 6.73, 7.17 (AA' BB', 16H, Ar**H**), 6.98 (dd, *J*=5.2, 1.6, 4H, Py**H**), 7.39 (s, br, 4H, N**H**), 8.03 (s, 8H, Ar**H**), 8.95 (m, 4H, Py**H**), 9.64 (s, 4H, Py**H**), 9.67 (m, br, 4H, Py**H**).

Tetra[3- (Pentylbenzylmethylamino)pyridium-tetrahydroxyl]calixarene hexafluorophosphate salt (**2.17b**·$4PF_6^-$).

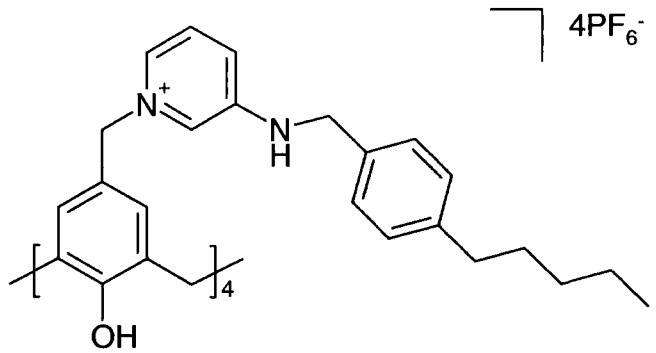

2.17b·$4Br^-$ (0.35 g, 0.19 mmol) was dissolved in methanol (75 mL). 10 molar equivalents of $NaPF_6$ were added and the reaction was stirred for 2 h. Precipitate formed within 0.5 h of addition of $NaPF_6$. The precipitate was separated on Büchner funnel then washed several times with water and dried with diethyl ether. Yield =0.37 g, 0.18 mmol, 93%.

^{1}H NMR (CD_3CN, J /Hz, δ/ppm): 0.86 (t, *J*=6.8, 12H, CH_3), 1.28 (m, 16H, CH_2) 1.55 (m, , 8H, CH_2), 2.55 (t, *J*=6.8, 8H, CH_2), 3.45 (br, 4H, ArCH_2Ar), 4.40 (br, 4H, ArCH_2Ar), 4.32 (d, *J*=3.6, 8H, CH_2), 5.15 (s, 8H, CH_2), 6.17 (t, *J*=5.2, 4H, N**H**) 7.03 (s, 4H, Ar**H**), 7.13, 7.18 (AA' BB', 16H, Ar**H**), 7.54-7.55 (m, 8H, Py**H**), 7.73 (m, 8H Py**H**,), 7.77 (m, 4H, Py**H**).

ES$^+$-MS: m/z=1930 $[M\text{-}PF_6]^+$, 892 $[M\text{-}2PF_6]^{2+}$, 546 $[M\text{-}3PF_6]^{3+}$.

Anal: Calcd. for $C_{100}H_{116}N_8O_4P_4F_{24}$: C, 57.91, H, 5.63, N, 5.40. Found C, 58.48, H, 5.66, N, 4.92.

IR (v/cm^{-1}): 3418m (NH)

Tetra[3- (Pentylmethylamino)pyridium-tetrahydroxy]calixarene bromide salt (**2.17c**·$4Br^-$).

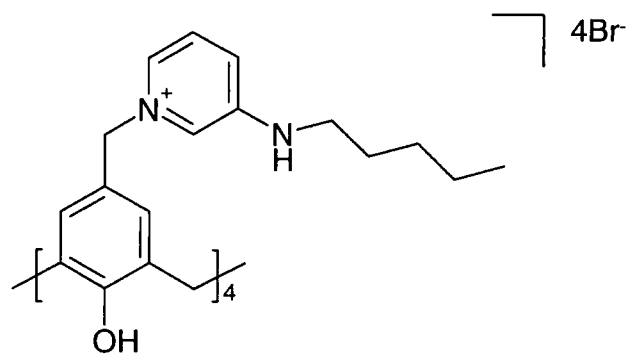

Tetrakis-p-bromomethylated tetrahydroxycalix[4]arene (0.27 g 0.34 mmol) and pentalidene-pyridin-3-yl amine (0.222g 1.35 mmol) were dissolved in dichloromethane (75 mL). The reaction was heated under reflux for 24 h. The reaction mixture was precipitated with diethyl ether and separated on Büchner funnel followed by washing several times with diethyl ether. Yield =0.45 g, 0.32 mmol, 95%.

^{1}H NMR ($CDCl_3$, J /Hz, δ/ppm): 0.67 (t *J*=6.8, 12H, CH_3), 1.30 (m, 16H, CH_2) 1.62 (m, 8H, CH_2), 3.06 (t, *J*=6.8, 8H, CH_2), 3.70, 4.02 (dd, *J*=130, 14, 8H, ArCH_2Ar), 5.36 (s, 8H, CH_2), 6.90 (br, 4H, N**H**), 7.50-7.54 (m, 8H, Py**H**), 7.48 (dd, *J*=6, 8.8, 8H, Py**H**), 7.75 (d, *J*=3.6, 4H, Py**H**), 8.02 (s, 8H, Ar**H**), 8.24 (d, *J*=2.8, 4H, Py**H**).

ES$^+$-MS: 404 $[M\text{-}4PF_6]^{3+}$, 283 $[M\text{-}4PF_6]^{4+}$
Anal: Calcd. $C_{72}H_{92}N_8O_4Br_4$: C, 59.50, H, 6.38, N, 7.71.

Anal: Calcd. $C_{72}H_{92}N_8O_4Br_4+2H_2O$: C, 58.07, H, 6.49, N, 7.52. Found: C, 57.94, H, 6.49, N, 8.31.

Tetra[3-(Pentylmethylamino)pyridium-tetrahydroxyl]calixarene hexafluorophosphate salt (**2.17c**·$4PF_6^-$).

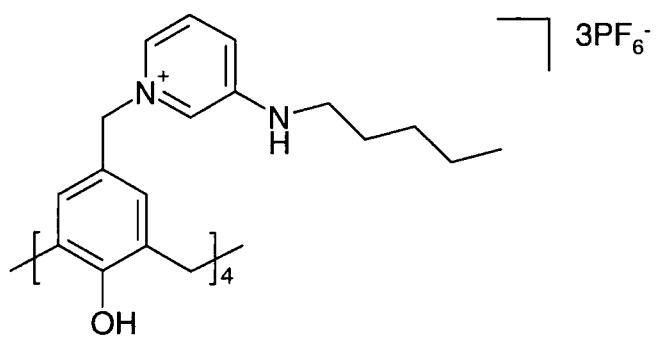

Tetra[3- (Pentylmethylamino)pyridium-tetrahydroxy]calixarene bromide salt (0.35 g, 0.25 mmol) was dissolved in methanol (75 mL). 10 molar equivalents of $NaPF_6$ were added and the reaction was stirred for 2 h. Precipitate formed within 0.5 h of addition of $NaPF_6$. The precipitate was separated on Büchner funnel then washed several times with water and dried with diethyl ether. Yield =0.37 g, 0.23 mmol, 91%.

^{1}H NMR (acetone, J /Hz, δ/ppm): 0.67 (t *J*=6.8, 12H, CH_3), 1.68 (m, 16H, CH_2) 1.44 (qu, *J*=6.8, 8H, CH_2), 3.06 (t, *J*=6.8, 8H, CH_2), 3.37 (br, 4H, ArCH_2Ar), 4.06 (br, 4H, ArCH_2Ar), 5.05 (s, 8H, CH_2), 5.45 (t, *J*=5.2, 4H, N**H**), 7.25 (s, 8H, Ar**H**), 7.50-7.54 (m, 8H, Py**H**), 7.91 (dd, *J*=5.2, 1.6, 4H, Py**H**), 7.97 (s, br, 4H, Py**H**).

^{1}H NMR (CD_3CN, J /Hz, δ/ppm): 0.85 (t *J*=6.8, 12H, CH_3), 1.28 (m, 16H, CH_2) 1.61 (m, CH_2), 3.16 (t, *J*=6.8, 8H, CH_2), 3.9 (br, 8H, $ArCH_2Ar$), 5.22 (s, 8H, CH_2), 5.71 (t, *J*=9.0, 4H, NH), 7.20 (s, 8H, ArH), 7.50-7.54 (m, 4H, PyH), 7.60 (dd, *J*=9.0, 6.0, 4H, PyH), 7.80 (d, *J*=4.0, 4H, PyH), 7.81 (s, 4H, PyH).

Anal: Calcd. $C_{72}H_{92}N_8O_4P_4F_{24}$: C, 50.47, H, 5.41, N, 6.76. Found C, 50.83, H, 5.36, N, 6.30.

ES$^+$-MS: m/z 426 $[M\text{-}3PF_6]^{3+}$ 283 $[M\text{-}4PF_6]^{4+}$

IR (v/cm^{-1}): 3418m (NH)

Mesityl calix[4]arene (**2.7**). [54]

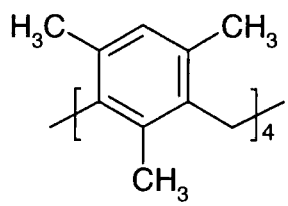

To a solution of α-chloroisodurene (5.0g, 39 mmol) in dry CH_2Cl_2 (50 mL) was added $SnCl_4$ (0.7 mL, 2.69 mmol) under a constant stream of N_2. The mixture was refluxed for 2h, resulting in a colour change to red and subsequent formation of white precipitate. The mixture was carefully hydrolyzed with water (50 mL) and then extracted with further portions of CH_2Cl_2 (25mL) each. The exracts were dried over $MgSO_4$, and the volume was reduced under pressure, resulting in the deposition of the product as a white solid. The product was recrystallised from CH_2Cl_2 and ethyl acetate. Yield =3.5 g, 6.7 mmol, 69%.

^{1}H NMR: ($CDCl_3$, δ/ppm); 1.20 (s, 12 H, $ArCH_3$), 2.36 (s, 24 H, $ArCH_3$), 3.90 (s, 8 H, $ArCH_2Ar$), 6.82 (s, 4 H, ArH).

HR ESI-MS: m/z=551.35 [M] +Na

Anal: Calcd. For $C_{40}H_{48}$: C, 90.89, H, 9.10%. Found: C, 90.94, H, 8.93%.

Tetrakis-p-bromomethylated mesityl calix[4]arene (**2.19**).

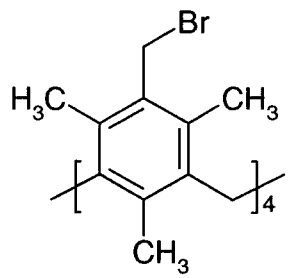

0.5 molar equivalent (to calixarene) of zinc and also HBr (45% in acetic acid) (2mL) was heated and stirred in glacial acetic acid (20 mL) until Zinc had dissolved and a colourless solution was left. Mesityl calix[4]arene (0.53g, 1.00 mmol), paraformaldehyde (1.5 g, 51.7 mmol), and HBr (45% in acetic acid) (10 mL) was added to this slowly and left for 48 h at 90°C. The resulting white suspension was filtered under suction through G3 glass frit and washed thoroughly with water, diethyl ether and again with water, then dried under suction. Yield =0.59g, 6.55 mmol, 86%.

^{1}H NMR ($CDCl_3$, J/Hz, δ/ppm): 1.01 (s, 12H $ArCH_3$), 2.37 (s, 24H, $ArCH_3$), 3.94 (s, 8H, $ArCH_2Ar$), 4.56 (s, 8H, CH_2Br).

ES+ MS: m/z=923.3 $[M+Na]^+$

Anal: Calcd. for $C_{44}H_{52}Br_4$: C, 58.69, H, 5.82%. Found: C, 58.53, H, 5.83%.

Tetra[3-(4-pentyl-benzylamino)-pyridium-mesityl]calixarene bromide salt (**2.20a**·4Br$^-$).

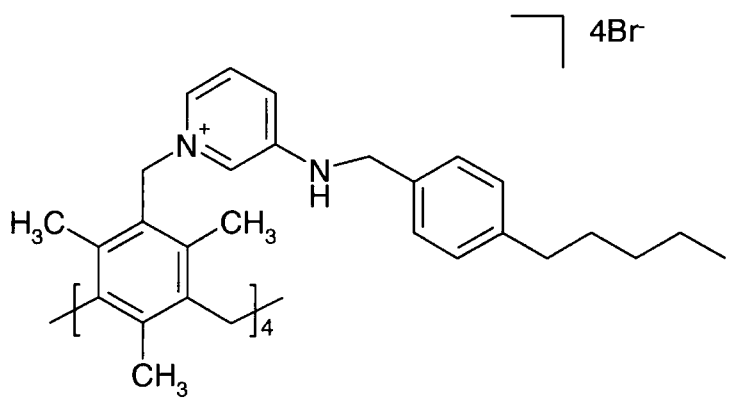

Tetrakis-p-bromomethylated mesityl calix[4]arene (0.60g, 0.66 mmol) was dissolved in CH_2Cl_2 (60 mL) and 4 equivalents of (4-Pentyl-benzyl)-pyridin-3-yl-amine (0.67g, 2.63 mmol) were added. The reaction mixture was stirred at reflux for 24h. A cream precipitate was produced. The product was filtered and washed with diethyl ether leaving a cream solid. Yield =0.95g, 0.50 mmol, 75%.

^{1}H NMR (DMSO-d_6, J/Hz, δ/ppm): 0.85 (m, 12H, CH_3-CH_2), 2.55 (br, 8H, CH_2), 4.34 (br, 8H, CH_2-Ar), 4.45 (br, 8H, CH_2-NH), 5.39 (br, 8H, CH_2-Py), 7.27-7.17 (AA' BB', *J*=7.8, ArH), 7.72 (br, 8H, 2x PyH), 7.85 (br, 4H, PyH), 7.89 (br, 4H, NH), 8.01 (br, 4H, PyH).

ES$^+$-MS: m/z= 399[M-4Br]$^{4+}$

Anal: Calcd. for $C_{112}H_{140}N_8Br_4$: C, 70.13, H, 7.35, N, 5.84%.

Anal: Calcd. for $C_{112}H_{140}N_8Br_4$ $4H_2O$: C, 67.59, H, 7.49, N, 5.63. Found: C, 67.68, H, 7.18, N, 5.56%.

Tetra[3-(4-pentyl-benzylamino)-pyridium-mesityl]calixarene hexafluorophosphate salt (**2.8a**·$4PF_6^-$).

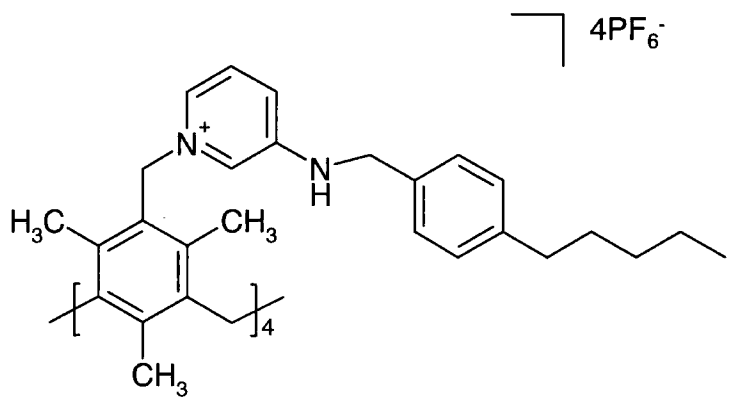

Tetra[3-(4-pentyl-benzylamino)-pyridium-mesityl]calixarene bromide salt (0.93 g, 0.48 mmol) and 10 molar equivalents of $NaPF_6$ (0.80 g, 4.81 mmol) were dissolved in methanol (100 mL) and stirred for 2h. Water was then added untill a precipitate formed and stirred for further 5 min. The precipitate was then separated on a Büchner funnel and washed several times with water and then diethyl ether. Yield = 0.85g, 0.39 mmol, 81%.

^{1}H NMR: ($CDCl_3$, J/Hz, δ/ppm): 0.87 (t, 12H, *J*=6.8, CH_3), 1.20 (s, 12H, CH_3), 1.29 (m, 16H, CH_2), 1.59 (m, 8H, CH_2), 2.24 (s, 24H, CH_3), 2.60 (t, 8H, *J*=7.6, CH_2), 4.06 (s, 8H, CH_2,), 4.31 (d, *J*=6.0, 8H, CH_2,), 5.65 (s, 8H, CH_2), 6.34 (t, 6.0, NH), 7.16, 7.19 (AA'BB', 4H, *J*=11.2, ArH), 7.49 (br, 1H, PyH), 7.56-7.65 (m, 3H, PyH).

ES$^+$-MS: m/z= 399[M-4PF_6]$^{4+}$

Anal: Calcd. for $C_{112}H_{140}N_8P_4F_{24}$; C, 61.75, H, 6.47, N, 5.14%. Found: C, 61.68, H, 6.42, N, 4.90%.

Tetra[3- (Pyren-1-ylmethylamino)pyridium-mesityl]calixarene bromide salt (**2.20e**·4Br$^-$).

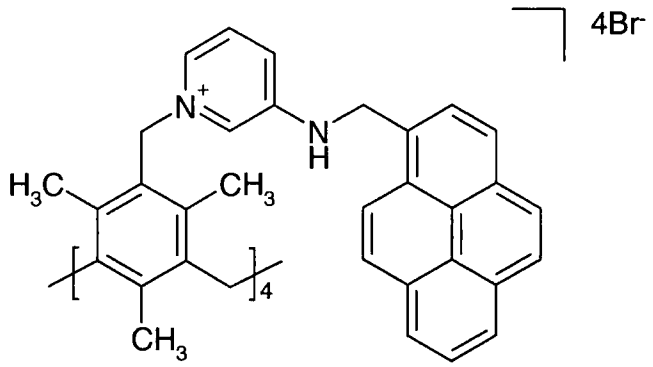

Tetrakis-p-bromomethylated mesityl calix[4]arene (0.146 g, 0.16 mmol) was dissolved in CH_2Cl_2 (50mL) and 5 equivalents (excess) of pyren-1-ylmethyl-pyridin-3-yl-amine (0.249 g, 0.81 mmol) dissolved in CH_2Cl_2 (50mL) was added. A precipitate formed within 0.5 h. The reaction was stirred at room temperature for 48 h. The precipitate was then separated on a Büchner funnel and thoroughly washed with dichloromethane followed by sonication in more fresh dichloromethane. The obtained solid was then washed with diethyl ether and dried in *vacuo*.

Yield = 0.29g, 0.14 mmol, 81%.

^{1}H NMR (DMSO-d_6, J /Hz, δ/ppm): 0.64 (s, 12H, CH_3), 2.04 (s, 24H, CH_3), 3.95 (s, 8H, ArCH_2Ar), 5,07 (br, 8H, CH_2), 5,73 (s, 8H, CH_2), 7.71(br, 4H, Py**H**), 7.75-7.79(br, Py**H**), 7.84 (br, 4H, Py**H**), 7.87 (br, 4H, N**H**), 7.96 (br, 4H, Ar**H**), 7.98 (br, 4H, Ar**H**), 8.07 (t, *J*=7.6, 2H, Ar**H**), 8.15 (s, 4H, Py**H**), 8.22 (d, *J*=8, 8H, Ar**H**), 8.256-8.35 (m, 16H, Ar**H**).

Anal: Calcd. for $C_{132}H_{116}N_8Br_4$: C, 74.29, H, 5.47, N, 5.25. Found C, 68.93, H, 5.15, N, 4.70. Analysis for C, H, N are low due to presence of excess **2.16e** which is removed in the next step (salt metathesis).

Tetra[3-(Pyren-1-ylmethylamino)pyridium-mesityl]calixarene hexafluorophosphate salt (**2.20e**·$4PF_6^-$).

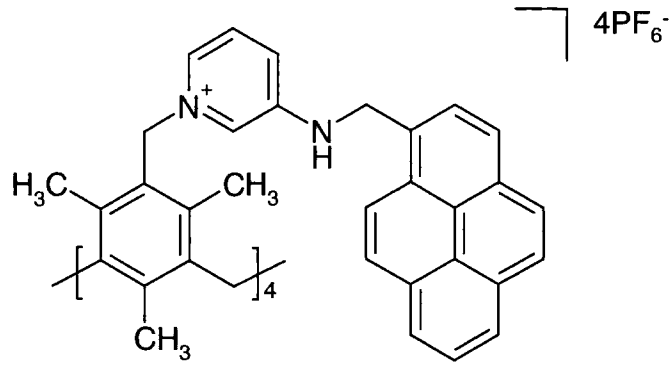

Tetra[3- (Pyren-1-ylmethylamino)pyridium-mesityl]calixarene bromide salt was dissolved in 1 : 1 acetonitrile/water mixture and 10 equivalents of $NaPF_6$ was added. The reaction mixture was stirred for 2 h. A green precipitate appeared within 0.5 h. The precipitate was separated on a Büchner funnel under suction and washed several times with diethyl ether.

^{1}H NMR (CD_3CN, J /Hz, δ/ppm): -0.001 (s, 12H, CH_3), 1.63 (s, 24H, CH_3), 2.94 (s, 8H, ArCH_2Ar), 4.93 (d, *J*=5.6, 8H, CH_2), 5.29 (s, 8H, CH_2), 6.41 (t, *J*=5.6, 4H, N**H**), 7.03 (br, s, 4H, Py**H**), 7.54 (br, 4H, Ar**H**), 7.56 (br, 4H, Ar**H**), 7.72 (d, *J*=7.6, 4H, Ar**H**), 7.74-7.77 (ddd, *J*=2, 6.4, 9.2, 4H, Py**H**), 7.91 (t, *J*=7.6, 4H, Ar**H**), 7.99 (br, 4H, Py**H**), 8.01 (d, *J*=7.6, 4H, Ar**H**), 8.08 (s, 1H, Py**H**), 8.10-8.13 (m, 16H, Ar**H**).

ES$^+$-MS: m/z=1051 $[M-2PF_6]^{2+}$, 653 $[M-3PF_6]^{3+}$, 453 $[M-4PF_6]^{4+}$

Anal: Calcd. for $C_{132}H_{116}P_4F_{24}$: C, 66.21, H, 4.88, N, 4.68.

Calcd. for $C_{132}H_{116}P_4F_{24}$ $2H_2O$: C, 65.23, H, 4.97, N, 4.61. Found: C, 65.05, H, 4.78, N, 4.30.

IR (ν/cm^{-1}): 3411s (NH)

5-[1,2]Dithiolan-3yl-pentanoic acid pyridin3-ylamide (**3.18**).

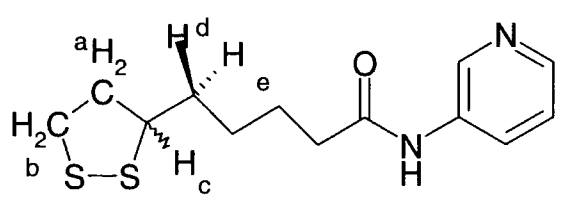

Thioctic acid (0.825 g 4.0 mmol) and (3-dimethylamino-propyl)-ethyl-carbodiimide (EDC) (0.621g, 4.0 mmol) were dissolved in dichloromethane (70 mL) and stirred for 2 h. Hydroxybenzatriazole hydrate (HoBt) (0.540 g, 4 mmol) was added followed by 3-aminopyridine (0.37g 4mmol). The reaction mixture was stirred at room temperature for 24 hours. The solvent was then removed under vacuum and the resultant oil was washed several times with water until pure.

^{1}H NMR ($CDCl_3$, J /Hz, δ/ppm): 1.38-1.44 (m, 2H, CH_2), 1.48-1.68 (m, 4H, CH_2), 1.81-1.83 (q, *J*=6.8, 1H, He), 2.34 (t, *J*=6.8, 1H, Hd), 2.36-2.41 (m, 2H, Hb), 3.00-3.12 (m, 2H, Ha), 3.47-3.51 (m, 1H, Hc), 7.21 (dd, *J*=4.8, 8.4, 1H, PyH), 8.13 (ddd, *J*=1.6, 2, 8.4, 1H, PyH), 8.25 (dd, *J*=1.6, 4.8, 1H, PyH), 8.33 (br, s, 1H, NH), 8.51 (d, *J*=2, 1H, PyH).

ES^+-MS: m/z=283$[M+H]^+$

Anal: Calc. for $C_{13}H_{18}N_2OS_2$: C, 55.28, H, 6.42, N, 9.91.

Calc. for $C_{13}H_{18}N_2OS_2{}^+0.25H_2O$: C, 53.57, H, 6.57, N, 9.61. Found: C, 53.24, H, 6.30, N, 8.96.

IR (v/cm^{-1}): 3420w (NH); 558w (S-S).

6,8-Dimercapto-octanoic acid pyridin-3-ylamide (**3.21**).

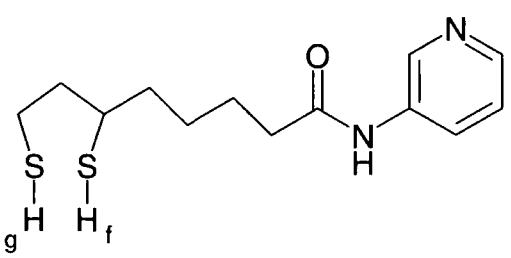

Compound **3.18** (3.83g, 10 mmol) was dissolved in 50 mL of 1:1 EtOH/water with stirring. $NaBH_4$ (416 mg, 11 mmol) was added and stirred for 60 min or until the solution became colorless. The reaction mixture was diluted with water (100 mL) and extracted with $CHCl_3$ (3 × 75 mL). The combined organic phases were dried over magnesium sulfate ($MgSO_4$), filtered, and evaporated to result in colourless oil.

^{1}H NMR ($CDCl_3$, J /Hz, δ/ppm): 1.23 (d, *J*=8, 1H, Hf), 1.29 (t, *J*=8, 1H, Hg), 1.40-1.43 (m, 2H, CH_2), 1.44-1.58 (m, 2H, CH_2), 1.58-1.68 (m, 2H, CH_2), 1.81-1.83 (q, *J*=7.6, 2H), 2.35 (t,

J=7.6, 1H), 2.58-2.68 (m, 2H), 2.84 (b,m, 1H), 7.21 (dd, *J*=4.8, 8.4, 1H, Py**H**), 8.13 (ddd, *J*=1.6, 2, 8.4, 1H, Py**H**), 8.25 (dd, *J*=1.6, 4.8, 1H, Py**H**), 8.33 (br, s, 1H, N**H**), 8.51 (d, *J*=2, 1H, Py**H**).

ES$^+$-MS: m/z=285 $[M+H]^+$

IR (v/cm^{-1}): 3420w (NH); 2536 w(S-H).

Anal: Calcd. for $C_{13}H_{20}N_2OS_2$: C, 55.28, H, 6.42, N, 9.91.

Calcd. for $C_{13}H_{18}N_2OS_2$+0.5H_2O: C, 53.20, H, 7.21, N, 9.54. Found: C, 53.62, H, 6.73, N, 9.37.

Synthesis of gold nanoparticles **3.20**.

Sodium naphthalenide was prepared by adding sodium (100 mg) to a dry solution of naphthalene (410 mg) in 35 mL of diglyme. The mixture was degassed and filled with N_2 three times in a Schlenk and then sonicated whilst under vacuum until dark green solution appeared.

$HAuCl_4$ (30 mg, 8.83 x 10^{-5} moles) was dissolved in 20 mL of dry diglyme in a Schlenk to which the sodium napthalenide reducing solution was added dropwise until the orange gold solution has turned purple. The colloidal suspension was then exposed to air atmosphere to ensure all the reducing agent is quenched and stirred for 3-4 min. Compound **3.18** (0.068 g, 0.17 mmol) was dissolved in 10 mL of diglyme and the resulting solution was added slowly to the reduced gold nanoparticle colloid and stirred for 1 h. The precipitated nanoparticles were then centrifuged and the supernatant decanted. The nanoparticles pellet was washed aided with sonication in ethanol three times to remove any remaining diglyme and **3.18**. The final pellet was resuspended in 40 mL of methanol aided by gentle sonication for 2-3 min.

Synthesis of tetraalkyl ammonium bromide protected nanoparticles. [154]

$HAuCl_4$ (0.3537 g, 0.95 mmol) was dissolved in 30 mL of H_2O. Trioctyl propyl ammonium bromide (1.9 g, 4.0 mmol) was dissolved in 80 mL of toluene. Both solutions were combined and stirred vigorously for 10 min. A solution of $NaBH_4$ (0.38 g in 25 mL of H_2O) was then added dropwise to the stirred reaction over a period of 30 min ensuring that organic and aqueous phases were being mixed together. The resulting deep red colloidal solution was stirred for further 20

min. Organic phase was extracted and washed once with diluted H_2SO_4 (for neutralization) and five times with distilled water. Organic layer was then dried with Na_2SO_4.

Synthesis of gold nanoparticles **3.22**.

To 20 mL of the tetraalkyl ammonium bromide protected nanoparticles stock solution (prepared as above) was added dodecanethiol solution in acetone (4.62×10^{-3}M) (93.6 mg in 100 mL). The reaction mixture was stirred for 2 h. It was then precipitated with methanol, centrifuged and washed several times with methanol and then ether. Nanoparticles were then redissolved in chloroform.

Synthesis of gold nanoparticles **3.23**.
Compound **3.18** (66 mg, 0.24 mmol) was dissolved in 10 mL of chloroform and added to **3.22** chloroform solution (20 mL) which contained 20 mL of the original stock solution of the tetraalkyl ammonium bromide protected nanoparticles (approx. 0.24 mmol of Au). The reaction mixture was stirred for 24 h. The nanoparticles were then precipitated with methanol, centrifuged and washed several times with methanol and then ether. Nanoparticles were then redissolved in chloroform.

Appendix 1

In the method of continuous variation, one mixes equal concentration solution of two species, A and B, in varying ratios and measures a property characteristic of the complex formed. Because the total concentration, [A] + [B], is constant in all solutions, the concentration of an AB complex will reach a maximum value when [A] = [B] and the concentration of an A_2B complex will reach a maximum value when [A] = 2[B], etc. A plot of concentration of complex as a function of the mole fraction of A in solution is constructed; the maximum amount of complex is found at the point corresponding to the mole-fraction of A in the complex. The following

derivation applies where C_i is the concentration of species I, $C_{H(0)}$ is the initial concentration of host, δ_i is the chemical shift of species I, and δ_{obs} is the observed chemical shift.

$C_H=C_{H(0)}-C_c$

$\delta_{obs}=(\delta_H C_H+ \delta_C C_C)/C_{H(0)}$

$\delta_{obs}=(\delta_H C_{H(0)}- C_C+ \delta_C C_C)/C_{H(0)}$

$\delta_{obs}=C_C(\delta_C- \delta_H)/C_{H(0)}+ \delta_H C_{H(0)}/C_{H(0)}$

$\delta_{obs}- \delta_H= C_C(\delta_C- \delta_H)/C_{H(0)}$

$C_C= (\delta_{obs}- \delta_H)C_{H(0)}/(\delta_C- \delta_H)$

Because $(\delta_C- \delta_H)$ is a constant, the concentration of the complex is proportional to $\Delta\delta$ (the observed chemical shift minus the chemical shift of the free host) times the initial concentration of host. An appropriate Job plot for our situtation would be $\Delta\delta$ times the initial concentration of host as a function of the mole fraction of host (X_H). However, because of the constraint of the method of continuous variation that the sum of the host and guest concentration are equal in all measurements, $C_{H(0)}$ in the final expression above can be replaced by the X_H in the host guest mixture. Thus plots of $\Delta\delta X_H$ as a function of the X_H are used.[175]

References

References

1. Davis, A. P.; Joos, J. B., *Coord. Chem. Rev.*, **2003,** 240, 143-156.
2. Llinares, J. M.; Powell, D.; Bowman-James, K., *Coord. Chem. Rev.*, **2003,** 240, 57-75.
3. McKee, V.; Nelson, J.; Town, R. M., *Chem. Soc. Rev.*, **2003,** 32, 309-325.
4. Gale, P. A., *Coord. Chem. Rev.*, **2003,** 240, 191-221.
5. Gale, P. A., *Coord. Chem. Rev.*, **2003,** 240, 1-1.
6. Gale, P. A., *Coord. Chem. Rev.*, **2000,** 199, 181-233.
7. Dietrich, B., *Pure & Appl. Chem.*, **1993,** 65, 1457-1464.
8. Atwood, J. L.; Holman, K. T.; Steed, J. W., *J. Chem. Soc., Chem. Commun*, **1996**, 1401-1407.
9. Hennrich, G.; Anslyn, E. V., *Chem.-Eur. J.*, **2002,** 8, 2219-2224.
10. Bondy, C. R.; Loeb, S. J., *Coord. Chem. Rev.*, **2003,** 240, 77-99.
11. Kanyo, Z. F.; Christianson, D. W., *J. Biol. Chem.*, **1991,** 266, 4264-4268.
12. Lavigne, J. J.; Anslyn, E. V., *Angew. Chem., Int. Edit.*, **2001,** 40, 3119-3130.
13. Beer, P. D.; Gale, P. A., *Angew. Chem., Int. Ed.*, **2001,** 40, 487-516.
14. Metzger, A.; Lynch, V. M.; Anslyn, E. V., *Angew. Chem., Int. Edit.*, **1997,** 36, 862-865.
15. Atwood, J. L.; Szumna, A., *Chem. Commun.*, **2003**, 940-941.
16. Schmuck, C.; Geiger, L., *J. Am. Chem. Soc.*, **2004,** 126, 8898-8899.
17. Beer, P. D.; Davis, J. J.; Drillsma-Milgrom, D. A.; Szemes, F., *Chem. Commun.*, **2002**, 1716-1717.
18. Zhang, J.; Bond, A. M.; Belcher, J.; Wallace, K. J.; Steed, J. W., *J. Phys. Chem. B,* **2003,** 107, 5777-5786.
19. Abouderbala, L. O.; Belcher, W. J.; Boutelle, M. G.; Cragg, P. J.; Steed, J. W.; Turner, D. R.; Wallace, K. J., *Proc. Nat. Acad. Sci. USA,* **2002,** 99, 5001-5006.
20. Abouderbala, L. O.; Belcher, W. J.; Boutelle, M. G.; Cragg, P. J.; Fabre, M.; Dhaliwal, J.; Steed, J. W.; Turner, D. R.; Wallace, K. J., *Chem. Commun.*, **2002**, 358-359.
21. Holman, K. T.; Halihan, M. M.; Jurisson, S. S.; Atwood, J. L.; Burkhalter, R. S.; Mitchell, A. R.; Steed, J. W., *J. Am. Chem. Soc.*, **1996,** 118, 9567-9576.

22. Holman, K. T.; Halihan, M. M.; Steed, J. W.; Jurisson, S. S.; Atwood, J. L., *J. Am. Chem. Soc.*, **1995,** 117, 7848-7849.
23. Buda, M.; Ion, A.; Moutet, J.-C.; Saint-Aman, E.; Ziessel, R., *J. Electroanal. Chem.*, **1999,** 469, 132-138.
24. Bondy, C. R.; Gale, P. A.; Loeb, S. J., *Chem. Commun.*, **2001**, 729-730.
25. Wallace, K. J.; Belcher, W. J.; Turner, D. R.; Syed, K. F.; Steed, J. W., *J. Am. Chem. Soc.*, **2003,** 125, 9699-9715.
26. Beer, P. D.; Cormode, D. P.; Davis, J. J., *Chem. Commun.*, **2004**, 414-415.
27. Gale, P. A.; Light, M. E.; McNally, B.; Navakhun, K.; Sliwinski, K. E.; Smith, B. D., *Chem. Commun.*, **2005**, 3773-3775.
28. Smith, B. D.; Lambert, T. N., *Chem. Commun.*, **2003**, 2261-2268.
29. Dietrich, B.; Hosseini, M. W.; Lehn, J. M.; Sessions, R. B., *J. Am. Chem. Soc.*, **1981,** 103, 1282-1283.
30. Snellink-Ruel, B. H. M.; Antonisse, M. M. G.; Engbersen, J. F. J.; Timmerman, P.; Reinhoudt, D. N., *Eur. J. Org. Chem.*, **2000**, 165-170.
31. Antonisse, M. M. G.; Reinhoudt, D. N., *Chem. Commun.*, **1998**, 443-448.
32. Dannenberg, J. J., *J. Mol. Struct.*, **2002,** 615, 219-226.
33. Jeffrey, G. A., *An Introduction to Hydrogen Bonding*, OUP: Oxford, 1997.
34. Schmidtchen, F. P., *Tetrahedron Lett.*, **1989,** 30, 4493-4496.
35. Galan, A.; Andreu, D.; Echavarren, A. M.; Prados, P.; De Mendoza, J., *J. Am. Chem. Soc.*, **1992,** 114, 1511-1512.
36. Ayling, A. J.; Perez-Payan, M. N.; Davis, A. P., *J. Am. Chem. Soc.*, **2001,** 123, 12716-12717.
37. Steed, J. W.; Atwood, J. L., *Supramolecular Chemistry*, J. Wiley & Sons: Chichester, 2000.
38. Ilioudis, C. A.; Tocher, D. A.; Steed, J. W., *J. Am. Chem. Soc.*, **2004,** 126, 12395-12402.
39. Hettche, F.; Reiss, P.; Hoffmann, R. W., *Chem.-Eur. J.*, **2002,** 8, 4946-4956.
40. Bai, Y.; Zhang, B.-G.; Xu, J.; Duan, C.-Y.; Dang, D.-B.; Liu, D.-J.; Meng, Q.-J., *New J. Chem.*, **2005,** 29, 777-779.
41. Beer, P. D.; Cheetham, A. G.; Drew, M. G. B.; Fox, O. D.; Hayes, E. J.; Rolls, T. D., *Dalton Trans.*, **2003**, 603-611.
42. Pratt, M. D.; Beer, P. D., *Polyhedron,* **2003,** 22, 649-653.

43. Evans, A. J.; Matthews, S. E.; Cowley, A. R.; Beer, P. D., *Dalton Trans.*, **2003**, 4644-4650.
44. Uppadine, L. H.; Keene, F. R.; Beer, P. D., *J. Chem. Soc., Dalton Trans.*, **2001**, 2188-2198.
45. Berry, N. G.; Pratt, M. D.; Fox, O. D.; Beer, P. D., *Supramol. Chem.*, **2001**, 13, 677-682.
46. Beer, P. D.; Brindley, G. D.; Fox, O. D.; Grieve, A.; Ogden, M. I.; Szemes, F.; Drew, M. G. B., *J. Chem. Soc., Dalton Trans.*, **2002**, 3101-3111.
47. Beer, P. D.; Hayes, E. J., *Coord. Chem. Rev.*, **2003**, 240, 167-189.
48. Beer, P. D.; Drew, M. G. B.; Hesek, D.; Nam, K. C., *Organometallics*, **1999**, 18, 3933-3943.
49. Beer, P. D.; Cadman, J., *Coord. Chem. Rev.*, **2000**, 205, 131-155.
50. Beer, P. D., *Acc. Chem. Res.*, **1998**, 31, 71-80.
51. Beer, P. D.; Dent, S. W.; Hobbs, G. S.; Wear, T. J., *Chem. Commun.*, **1997**, 99-100.
52. Staffilani, M.; Hancock, K. S. B.; Steed, J. W.; Holman, K. T.; Atwood, J. L.; Juneja, R. K.; Burkhalter, R. S., *J. Am. Chem. Soc.*, **1997**, 119, 6324-6335.
53. Holman, K. T.; Orr, G. W.; Steed, J. W.; Atwood, J. L., *Chem. Commun.*, **1998**, 2109-2110.
54. Staffilani, M.; Bonvicini, G.; Steed, J. W.; Holman, K. T.; Atwood, J. L.; Elsegood, M. R. J., *Organometallics*, **1998**, 17, 1732-1740.
55. Bondy, C. R.; Gale, P. A.; Loeb, S. J., *Supramol. Chem.*, **2002**, 2, 93-96.
56. Bondy, C. R.; Gale, P. A.; Loeb, S. J., *J. Am. Chem. Soc.*, **2004**, 126, 5030-5031.
57. Turner, D. R.; Hursthouse, M. B.; Light, A. E.; Steed, J. W., *Chem. Commun.*, **2004**, 1354-1355.
58. Tovilla, J. A.; Vilar, R.; White, A. J. P., *Chem. Commun.*, **2005**, 4839-4841.
59. Harding, L. P.; Jeffery, J. C.; Riis-Johannessen, T.; Rice, C. R.; Zeng, Z. T., *Dalton Trans.*, **2004**, 2396-2397.
60. Metzger, A.; Anslyn, E. V., *Angew. Chem., Int. Edit.*, **1998**, 37, 649-652.
61. Chin, J.; Walsdorff, C.; Stranix, B.; Oh, J.; Chung, H. J.; Park, S.-M.; Kim, K., *Angew. Chem., Int. Edit.*, **1999**, 38, 2756 - 2759.
62. Oh, K. S.; Lee, C. W.; Choi, H. S.; Lee, S. J.; Kim, K. S., *Org. Lett.*, **2000**, 2, 2679-2681.
63. Vacca, A.; Nativi, C.; Cacciarini, M.; Pergoli, R.; Roelens, S., *J. Am. Chem. Soc.*, **2004**, 126, 16456-16465.
64. Wallace, K. J.; Hanes, R.; Anslyn, E.; Morey, J.; Kilway, K. V.; Siegel, J., *Synthesis-Stuttgart*, **2005**, 2080-2083.

65. Sohn, Y.-S.; Goodey, A.; Anslyn, E. V.; McDevitt, J. T.; Shear, J. B.; Neikirk, D. P., *Biosens. Bioelectron.,* **2005,** 21, 303-312.

66. Wright, A. T.; Anslyn, E. V., *Chem. Soc. Rev.,* **2006,** 35, 14-28.

67. Goodey, A.; Lavigne, J. J.; Savoy, S. M.; Rodriguez, M. D.; Curey, T.; Tsao, A.; Simmons, G.; Wright, J.; Yoo, S. J.; Sohn, Y.; Anslyn, E. V.; Shear, J. B.; Neikirk, D. P.; McDevitt, J. T., *J. Am. Chem. Soc.,* **2001,** 123, 2559-2570.

68. Ihm, H.; Yun, S.; Kim, H. G.; Kim, J. K.; Kim, K. S., *Org. Lett.,* **2002,** 4, 2897-2900.

69. Schmuck, C.; Schwegmann, M., *J. Am. Chem. Soc.,* **2005,** 127, 3373-3379.

70. Christofi, A. M.; Garratt, P. J.; Hogarth, G.; Steed, J. W., *J. Chem. Soc., Dalton Trans.,* **2000**, 2137-2144.

71. Christofi, A. M.; Garratt, P. J.; Hogarth, G., *Tetrahedron,* **2001,** 57, 751-759.

72. Christofi, A. M.; Garratt, P. J.; Hogarth, G.; Ibbett, A. J.; Ng, Y. F.; Steed, J. W., *Tetrahedron,* **2002,** 58, 4543-4549.

73. Garratt, P. J.; Ibbett, A. J., *Tetrahedron,* **1998,** 54, 949-968.

74. Atwood, J. L.; Bott, S. G.; Junk, P. C.; May, M. T., *J. Coord. Chem.,* **1996,** 37, 89-105.

75. Hancock, K. S. B.; Steed, J. W., *Chem. Commun.,* **1998**, 1409-1410.

76. Walsdorff, C.; Saak, W.; Pohl, S., *J. Chem. Res. (S),* **1996**, 282 - 283.

77. Belcher, W. J.; Fabre, M.; Farhan, T.; Steed, J. W., *Org. Biomol. Chem.,* **2006,** 4, 781-786.

78. de Silva, A. P.; Gunaratne, H. Q. N.; Gunnlaugsson, T.; Huxley, A. J. M.; McCoy, C. P.; Rademacher, J. T.; Rice, T. E., *Chem. Rev.,* **1997,** 97, 1515-1566.

79. McSkimming, G.; Tucker, J. H. R.; Bouas-Laurent, H.; Desvergne, J. P., *Angew. Chem., Int. Edit.,* **2000,** 39, 2167-2169.

80. Albrecht, M.; Zauner, J.; Burgert, R.; Röttele, H.; Fröhlich, R., *Mat. Sci. Eng. C.,* **2001,** 18, 185-190.

81. Gomez, D. E.; Fabbrizzi, L.; Licchelli, M.; Monzani, E., *Org. Biomol. Chem.,* **2005,** 3, 1495-1500.

82. Boiocchi, M.; Boca, L. D.; Esteban-Gómez, D.; Fabbrizzi, L.; Licchelli, M.; Monzani, E., *Chem.- Eur. J.,* **2005,** 11, 3097-3104.

83. Turner, D. R.; Smith, B.; Goeta, A. E.; Evans, I. R.; Tocher, D. A.; Howard, J. A. K.; Steed, J. W., *Cryst. Eng. Comm.,* **2004,** 6, 633-641.

84. Turner, D. R.; Paterson, M. J.; Steed, J. W., *J. Org. Chem.,* **2006,** 71, 1598-1608.

85. Sasaki, S.; Citterio, D.; Ozawa, S.; Suzuki, K., *J. Chem. Soc., Perkin Trans. 2,* **2001**, 2309-2313.

86. Czarnik, A. W., *Acc. Chem. Res.,* **1994,** 27, 302-308.

87. Gunnlaugsson, T.; Davis, A. P.; Glynn, M., *Chem. Commun.,* **2001**, 2556-2557.

88. Kubo, Y.; Ishihara, S.; Tsukahara, M.; Tokita, S., *J. Chem. Soc., Perkin Trans. 2,* **2002,** 2, 1455-1460.

89. Bai, Y.; Zhang, B. G.; Duan, C. Y.; Dang, D. B.; Meng, Q. J., *New J. Chem.,* **2006,** 30, 266-271.

90. Gutsche, C. David; Dhawan, B.; Levine, J. A.; Hyun No, K.; Bauer, L. J., *Tetrahedron,* **1983,** 39, 409-426.

91. Kim, S. K.; Bok, J. H.; Bartsch, R. A.; Lee, J. Y.; Kim, J. S., *Org. Lett.,* **2005,** 7, 4839-4842.

92. Liu, S.-Y.; He, Y.-B.; Wu, J.-L.; Wei, L.-H.; Qin, H.-J.; Meng, L.-Z.; Hu, L., *Org. Biomol. Chem.,* **2004,** 2, 1582-1586.

93. Hirata, O.; Takeuchi, M.; Shinkai, S., *Chem. Commun.,* **2005**, 3805-3807.

94. Kubo, Y.; Ishii, Y., *J. Nonosci. Nanotechno.,* **2006,** 6, 1489-1509.

95. Matthews, S. E.; Beer, P. D., *Supramol. Chem.,* **2005,** 17, 411-435.

96. Amendola, V.; Boiocchi, M.; Fabbrizzi, L.; Palchetti, A., *Chem.-Eur. J.,* **2005,** 11, 5648-5660.

97. Vanloon, J. D.; Verboom, W.; Reinhoudt, D. N., *Org. Prep. Proced. Int.,* **1992,** 24, 437-462.

98. Gunnlaugsson, T.; Glynn, M.; Tocci, G. M.; Kruger, P. E.; Pfeffer, F. M., *Coord. Chem. Rev.,* **2002,** 250, 3094-3117.

99. Lenthall, J. T.; Steed, J. W., *Coord. Chem. Rev.,* **2007,** In Press, Corrected Proof.

100. Gutsche, C. D., *Calixarenes*, Royal Society of Chemistry: Cambridge, 1989.

101. Gutsche, C. D., *Calixarenes Revisited,* Royal Society of Chemistry: Cambridge, 1997.

102. Sansone, F.; Dudic, M.; Donofrio, G.; Rivetti, C.; Baldini, L.; Casnati, A.; Cellai, S.; Ungaro, R., *J. Am. Chem. Soc.,* **2006,** 128, 14528-14536.

103. Baklouti, L.; Harrowfield, J.; Pulpoka, B.; Vicens, J., *Mini-Rev. Org. Chem.,* **2006,** 3, 355-384.

104. Iwamoto, K.; Araki, K.; Shinkai, S., *J. Org. Chem.,* **1991,** 56, 4955-4962.

105. Beer, P. D.; Drew, M. G. B.; Hazlewood, C.; Hesek, D.; Hodacova, J.; Stokes, S. E., *J. Chem. Soc., Chem Commun.*, **1993**, 229-231.

106. Verboom, W.; Durie, A.; Egberink, R. J. M.; Asfari, Z.; Reinhoudt, D. N., *J. Org. Chem.*, **1992,** 57, 1313-1316.

107. Groenen, L. C.; Ruël, B. H. M.; Casnati, A.; Timmerman, P.; Verboom, W.; Harkema, S.; Pochini, A.; Ungaro, R.; Reinhoudt, a. D. N., *Tetrahedron Lett.*, **1991,** 32, 2675-2678.

108. Cho, E. J.; Moon, J. W.; Ko, S. W.; Lee, J. Y.; Kim, S. K.; Yoon, J.; Nam, K. C., *J. Am. Chem. Soc.*, **2003,** 125, 12376-12377.

109. Fabbrizzi, L., *Coord. Chem. Rev.*, **2006,** 250, 1209-1209.

110. Anzenbacher, P.; Jursikova, K.; Lynch, V. M.; Gale, P. A.; Sessler, J. L., *J. Am. Chem. Soc.*, **1999,** 121, 11020-11021.

111. Valeur, B.; Leray, I., *Coord. Chem. Rev.*, **2000,** 205, 3-40.

112. Birks, J. B., *Rep. Prog. Phys.*, **1975,** 38, 903-974.

113. Collins, E. M.; McKervey, M. A.; Madigan, E.; Moran, M. B.; Owens, M.; Ferguson, G.; Harris, S. J., *J. Chem. Soc. Perkin Trans. 1,* **1991**, 3137-3142.

114. Winnik, F. M., *Chem. Rev.*, **1993,** 93, 587-614.

115. Schazmann, B.; Alhashimy, N.; Diamond, D., *J. Am. Chem. Soc.*, **2006,** 128, 8607-8614.

116. Yang, J.-S.; Lin, C.-S.; Hwang, C.-Y., *Org. Lett.*, **2001,** 3, 889-892.

117. Fisher, A. C.; *Electrode Dynamics,* OUP: New York, 1996, 36-37.

118. Gutsche, C. D.; Dhawan, B.; No, H. K.; Mhthukrishnan, R. J., *J. Am. Chem. Soc.*, **1981,** 103, 3782-3792.

119. Guo, T. D.; Zheng, Q. Y.; Yang, L. M.; Huang, Z. T., *J. Incl. Phenom & Macrocycl. Chem.*, **2000,** 36, 327-333.

120. Bazzicalupi, C.; Bencini, A.; Bianchi, A.; Cecchi, M.; Escuder, B.; Fusi, V.; Garcia-Espana, E.; Giorgi, C.; Luis, S. V.; Maccagni, G.; Marcelino, V.; Paoletti, P.; Valtancoli, B., *J. Am. Chem. Soc.*, **1999,** 121, 6807-6815.

121. Sessler, J. L.; Camiolo, S.; Gale, P. A., *Coord. Chem. Rev.*, **2003,** 240, 17-55.

122. Arion, V. B.; Beer, P. D.; Drew, M. G. B.; Hopkins, P., *Polyhedron,* **1999,** 18, 451-458.

123. Klein, C.; Graf, E.; Hosseini, M. W.; De Cian, A.; Fischer, J., *Chem. Commun.*, **2000**, 239-240.

124. Klein, C.; Graf, E.; Hosseini, M. W.; De Cian, A., *New J. Chem.*, **2001,** 25, 207-209.

125. Filby, M. H.; Humphries, T. D.; Turner, D. R.; Kataky, R.; Kruusma, J.; Steed, J. W., *Chem. Commun.*, **2006**, 156-158.

126. Budka, J.; Lhotak, P.; Michlova, V.; Stibor, I., *Tetrahedron Lett.*, **2001,** 42, 1583-1586.

127. Cameron, B. R.; Loeb, S. J., *Chem. Commun.*, **1997**, 573-574.

128. Javier Catalán, C. D., *Eur. J. Org. Chem.*, **1999,** 1999, 885-891.

129. Reichardt, C., *Solvents and solvent effects in organic chemistry*, Wiley-VCH: 1988.

130. Prodi, L.; Ballardini, R.; Gandolfi, M. T.; Roversi, R., *J. Photoch. Photobio. A,* **2000,** 136, 49-52.

131. Juris, A.; Prodi, L., *New J. Chem.*, **2001,** 25, 1132-1135.

132. Binstead, R. A.

133. Koulov, A. V.; Mahoney, J. M.; Smith, B. D., *Org. Biomol. Chem.*, **2003,** 1, 27-29.

134. Atwood, J. L.; Barbour, L. J.; Heaven, M. W.; Raston, C. L., *Chem. Commun.*, **2003**, 2270-2271.

135. Steed, J. W.; Wallace, K. J., *Advances in Supramolecular Chemistry*, G. W. Gokel, Cerberus: New York, 2003, 221-262.

136. Turner, D. R.; Smith, B.; Spencer, E. C.; Goeta, A. E.; Evans, I. R.; Tocher, D. A.; Howard, J. A. K.; Steed, J. W., *New J. Chem.*, **2005,** 29, 90-98.

137. Turner, D. R.; Spencer, E. C.; Howard, J. A. K.; Tocher, D. A.; Steed, J. W., *Chem. Commun.*, **2004**, 1352-1353.

138. Russell, J. M.; Parker, A. D. M.; Radosavljevic-Evans, I.; Howard, J. A. K.; Steed, J. W., *Chem. Commun.*, **2006**, 269-271.

139. Watanabe, S.; Sonobe, M.; Arai, M.; Tazume, Y.; Matsuo, T.; Nakamura, T.; Yoshida, K., *Chem. Commun.*, **2002**, 2866-2867.

140. Chechik, V., *J. Am. Chem. Soc.*, **2004,** 126, 7780-7781.

141. Garcia, B.; Salome, M.; Lemelle, L.; Bridot, J.-L.; Gillet, P.; Perriat, P.; Roux, S.; Tillement, O., *Chem. Commun.*, **2005**, 369-371.

142. Hutchison, J. E.; Woehrle, G. H.; Brown, L. O., *J. Am. Chem. Soc.*, **2005,** 127, 2172-2183.

143. Mucic, R. C.; Storhoff, J. J.; Mirkin, C. A.; Letsinger, R. L., *J. Am. Chem. Soc.*, **1998,** 120, 12674-12675.

144. Shipway, A. N.; Katz, E.; Willner, I., *ChemPhysChem,* **2000,** 1, 18-52.

145. Labande, A.; Ruiz, J.; Astruc, D., *J. Am. Chem. Soc.*, **2002,** 124, 1782-1789.

146. Kreibig, U.; Vollmer, M., *Optical Properties of Metal Clusters*, Springer: Berlin, 1995.

147. Hutter, E.; Fendler, J. H., *Adv. Mater.*, **2004,** 16, 1685-1706.

148. Moores, A.; Goettmann, F., *New J. Chem.*, **2006,** 30, 1121-1132.

149. Mulvaney, P.; Liz-Marzan, L. M.; Giersig, M., *Langmuir,* **1996,** 12, 4329-4335.

150. Alejandro-Arellano, M.; Ung, T.; Blanco, Á.; Mulvaney, P.; Liz-Marzán, L. M., *Pure Appl. Chem.*, **2000,** 72, 257-267.

151. Frederix, F.; Friedt, J. M.; Choi, K. H.; Laureyn, W.; Campitelli, A.; Mondelaers, D.; Maes, G.; Borghs, G., *Anal. Chem.*, **2003,** 75, 6894-6900.

152. Kalyuzhny, G.; Vaskevich, A.; Ashkenasy, G.; Shanzer, A.; Rubinstein, I., *J. Phys. Chem. B,* **2000,** 104, 8238-8244.

153. Englebienne, P.; Verhas, M.; Hoonacker, A. V., *Analyst,* **2001,** 126, 1645-1651.

154. Brust, M.; Walker, M.; Bethell, D.; Schiffrin, D.; Whyman, R., *J. Chem. Soc., Chem Commun.*, **1994**, 801-802.

155. Murray, R. W.; Hostetler, M. J.; Wingate, J. E.; Zhong, C.-J.; Harris, J. E.; Vachet, R. W.; Clark, M. R.; Londono, J. D.; Green, S. J.; Stokes, J. J.; Wignall, G. D.; Glish, G. L.; Porter, M. D.; Evans, N. D., *Langmuir,* **1998,** 14, 17-30.

156. Schiffrin, D. J.; Fink, J.; Kiely, C. J.; Bethell, D., *Chem. Mater.*, **1998,** 10, 922-926.

157. Brust, M.; Fink, J.; Bethell, D.; Schiffrin, D.; Kiely, C., *J. Chem. Soc., Chem. Commun.*, **1995**, 1655-1656.

158. Lazarides, A. A.; Schatz, G. C., *J. Phys. Chem. B,* **2000,** 104, 460-467.

159. Murray, R. W.; Hostetler, M. J.; Green, S. J.; Stokes, J. J., *J. Am. Chem. Soc.*, **1996,** 118, 4212-4213.

160. Hicks, J. F.; Miles, D. T.; Murray, R. W., *J. Am. Chem. Soc.*, **2002,** 124, 13322-13328.

161. Maye, M. M.; Zhong, C.-J., *J. Mater. Chem.*, **2000,** 10, 1895-1901.

162. Whetten, R. L.; Khoury, J. T.; Alvarez, M. M.; Murthy, S.; Vezmar, I.; Wang, Z. L.; Stephens, P. W.; Cleveland, C. L.; Luedtke, W. D.; Landman, U., *Adv. Mater.*, **1996,** 8, 428-433.

163. Jimenez, V. L.; Leopold, M. C.; Mazzitelli, C.; Jorgenson, J. W.; Murray, R. W., *Anal. Chem.*, **2003,** 75, 199-206.

164. Hutchison, J. E.; Weare, W. W.; Reed, S. M.; Warner, M. G., *J. Am. Chem. Soc.*, **2000,** 122, 12890-12891.

165. Chechik, V.; Ionita, P.; Caragheorgheopol, A.; Gilbert, B. C., *J. Am. Chem. Soc.*, **2002,** 124, 9048-9049.

166. Mirkin, C. A.; Letsinger, R. L.; Elghanian, R.; Viswanadham, G., *Bioconjugate Chem.*, **2000,** 11, 289-291.

167. Mirkin, C. A.; Li, Z.; Jin, R.; Letsinger, R. L., *Nucl. Acids Res.*, **2002,** 30, 1558-1562.

168. Vance, A. L.; Willey, T. M.; Nelson, A. J.; van Buuren, T.; Bostedt, C.; Terminello, L. J.; Fox, G. A.; Engelhard, M.; Baer, D., *Langmuir,* **2002,** 18, 8123-8128.

169. Sneeden, E. Y.; Harris, H. H.; Pickering, I. J.; Prince, R. C.; Johnson, S.; Li, X.; Block, E.; George, G. N., *J. Am. Chem. Soc.*, **2004,** 126, 458-459.

170. Jansen, M.; Schulz-Dobrick, M.; Sarathy, K. V., *J. Am. Chem. Soc.*, **2005,** 127, 12816-12817.

171. Reed, L. J.; Gunsalus, I. C.; Schnakenberg, G. H. F.; Soper, Q. F.; Boaz, H. E.; Kern, S. F.; Parke, T. V., *J. Am. Chem. Soc.*, **1953,** 75, 1267-1270.

172. Beer, P. D.; Hopkins, P. K.; McKinney, J. D., *Chem. Commun.*, **1999**, 1253-1254.

173. Murray, R. W.; Templeton, A. C.; Wuelfing, W. P., *Acc. Chem. Res.*, **2000,** 33, 27-36.

174. Sheldrick, G. M. *SHELXS-97*, University of Göttingen, 1997.

175. Blanda, M. T.; Horner, J. H.; Newcomb, M., *J. Org. Chem.*, **1989,** 54, 4626-4636.